Circuit Techniques for Multiple and Wideband Beamforming

A THESIS
SUBMITTED TO THE FACULTY OF THE GRADUATE SCHOOL
OF THE UNIVERSITY OF MINNESOTA
BY

Qingrui Meng

IN PARTIAL FULFILLMENT OF THE REQUIREMENTS
FOR THE DEGREE OF
Doctor of Philosophy

PROF. RAMESH HARJANI

June, 2018

Acknowledgements

This thesis summarizes the work I have done during the years I spent in the University of Minnesota. I would like acknowledge a lot of people, who have directly or indirectly contributed to my dissertation in graduate school.

First and foremost, I would like to thank my advisor, Prof. Ramesh Harjani, for his consistent support on the research I am interested in. Without his inspiration and guidance, it would have been nearly impossible to overcome many difficulties during my research. In addition, I learned a lots of soft skills, such as how to write and present the work, which will be equally important in my future career. I also appreciate his kind support during the time I am overwhelmed with family affair.

I am thankful to Prof. Rhonda Franklin for the three microwave courses, providing me useful knowledge I used in both my research and work. I am also grateful to Prof. Chris Kim and Prof. Zhi Yang for the advice and support on my thesis. Also, I want to express my sincere thanks to Prof. Rhonda Franklin, Prof. Chris Kim and Prof. Zhi Yang to serve as my final defense committee. I also appreciate Professor Robert Sainati and Professor Hubert Lim, who have served as preliminary oral exam committee.

In Prof. Harjani's lab, I got a lot of help from my labmates accelerating my study and life. I am grateful to Xingyi Hua, from whom I have gotten lots of help. Anindya Saha gave me many useful suggestions, when I encountered questions during my work and study. Shiva Jamali generously spared out unused area for my tapeout, and added much interests to the lab life in small talks. Emily Carroll gave me advice on my English enunciation before micro-teachings for the TA class. Bosi Yang helped me to accommodate campus affairs during last few months when I am physically absent from university. I also want to thank the other labmates even though I didn't specifically mentioned, who have smoothed and enriched my lab life.

Internships are also important part during my Ph.D study. I would like to thank Texas Instruments for offering me the first internship opportunity. I had worked Mark Morgan in Kilby lab. My second internship was carried out in Skyworks Solutions, where I work with Harry Liu and Paul Andrys. These two internships provided me the opportunity working with experienced guru in RF design, and granted me the insights how to conduct successful work from the engineers' view. In addition, I also got friendship with internship peers, from whom I received the help on my research work and career even after internships are finished.

There is no doubt that my industrial high speed circuit design experience also benefits my Ph.D research. In addition to the people I have mentioned in my master and bachelor thesis, I would like to thank the following people I had learned technical knowledge after my master study: Max Lee, Karl Liu from Mstar semiconductor (now with Mediatek), Qiurong He and Shawn Kuo from Analog Devices. I wish each of them a continued career success.

Lastly, I would like to thank the following family people. Especially, I want to express my sincere thanks to my wife, who always raises me up when I am down in the life. Without her, I could not overcome many difficulties I ever met with. My parents have ensured that I receive the best education, and kept supporting my desire to pursue Ph.D, even if I had been already in the age of earning money. My parents-in-law help to take care of my daughter, and give me the courage when I face difficulties. Also, I want to thank my adorable daughter for letting me be your father. I expect you are always happy in your life as you grow up.

Dedication

To my family, parents and parents-in-law.

Abstract

This thesis presents different architectures with regard to multiple beamforming and wideband phased array transceiver. Three different designs are implemented in TSMC 65nm RF CMOS to demonstrate different solutions. The design in this thesis have included major RF blocks in state-of-art wireless transceiver: RF receiver, local oscillator, and RF transmitter.

First, a RF/analog FFT based four-channel four-beam receiver with progressive partial spatial filtering is proposed. This architecture is particularly well suited for MIMO systems where multiple beams are used to increase throughput. Like the FFT, the proposed architecture reuses computations for multi-beam systems. In particular, the proposed architecture redistributes the computations so as to maximize the reuse of the structure that already exist in a receiver chain. In many fashions the architecture is quite similar to a Butler matrix but unlike the Butler matrix it does not use large passive components at RF. Further, we exploit the normally occurring quadrature down-conversion process to implement the tap weights. In comparison to traditional MIMO architectures, that effectively duplicate each path, the distributed computations of this architecture provide partial spatial ltering before the nal stage, improving interference rejection for the blocks between the LNA and the ADC. Additionally, because of the spatial ltering prior to the ADC, a single interferer only jams a single beam allowing for continued operation though at a lower combined throughput. The four-beam receiver core prototype in 65nm CMOS implements the basic FFT based architecture but does not include an LNA or extensive IF stages. This four-channel design consumes 56mW power and occupies an active area of $0.65mm^2$ excluding pads and test circuits.

Second, a wideband phased array receiver architecture with simultaneous spectral and spatial filtering by sub-harmonic injection oscillators is presented. The design avoids using expensive delay elements by many conventional wideband phased array. Different from prior art of channelization which cannot solve beam-squinting issue among the sub-channels, we use sub-harmonic injection locking scheme, which make the center frequencies of all sub-channels point to the same spatial direction to overcome beam-squinting issue. The low frequency, low power and narrowband phase shifters are placed

at LO in comparison to conventional way of placing delay elements or phase shifters in the signal path. This avoids receiver performance degradation from delay elements or phase shifters. The simultaneous spectral and spatial filtering dictates less ADC dynamic range requirement and further reduces power. The injection locking scheme reduces the phase noise contribution from the oscillators. The two-band prototype design realized in 65nm GP CMOS is centered at 9GHz, provides 4GHz instantaneous bandwidth, reduces beam-squinting by half, consumes 31.75mW/antenna and occupies $2.7mm^2$ of chip area.

In the third work, a steerable RF/analog FFT based four-beam transmitter architecture is presented. This work is based on the idea of FFT based multiple beamforming in first work, but extended to the transmitter and make the all beams steerable. Due to the reciprocity between receiver and transmitter, decimation-in-frequency (DIF) FFT is utilized in the transmitter. All the beams are steered simultaneously by front-end phase shifters, while keep each of the beams is independent of the others. The steerability of FFT based multiple beamforming scheme makes this proposed prototype could tackle more complicated portable wireless environment.

The first and second proposed architecture have been silicon verified, and the design of the third has been finished and ready for tapeout.

Contents

List of Tables

List of Figures

Chapter 1

Introduction

Wireless technology has experienced proliferation in the last three decades. The techniques, such as cell phone, WIFI, GPS, bluetooth and NFC, etc offer unprecedented convenience in our daily lives. Integrated circuits play an important role to drive wireless technology advances. Per Moore's law, transistor channel length is decreased to be half every 1.5 years, which empower approximate fourfold characteristic frequency f_T improvement per generation. Different from wired communication where each transmission channel is virtually isolated, wireless communication uses air channel that is rich of interferences. Consider the wireless communication environment :the signals from transmitters go through various paths reflected by environment objects before arriving at the receivers. Due to path length difference, the signals from various paths have different phases. The out-of-phase signals result in reduced channel gain, which is called fading [1]. In the rich scattering environment, many paths ends up with probabilistic channel tap values, leading to Rayleigh fading. The fading degrades wireless transmission reliability. Anther highlight is the everlasting and rapidly increased data rate requirements as technique advances. Fig. 1.1 shows data rate requirements increases by orders every five years for different cell phone standards [2]. Wireless system are investigating different schemes to improve communication reliability and capacity.

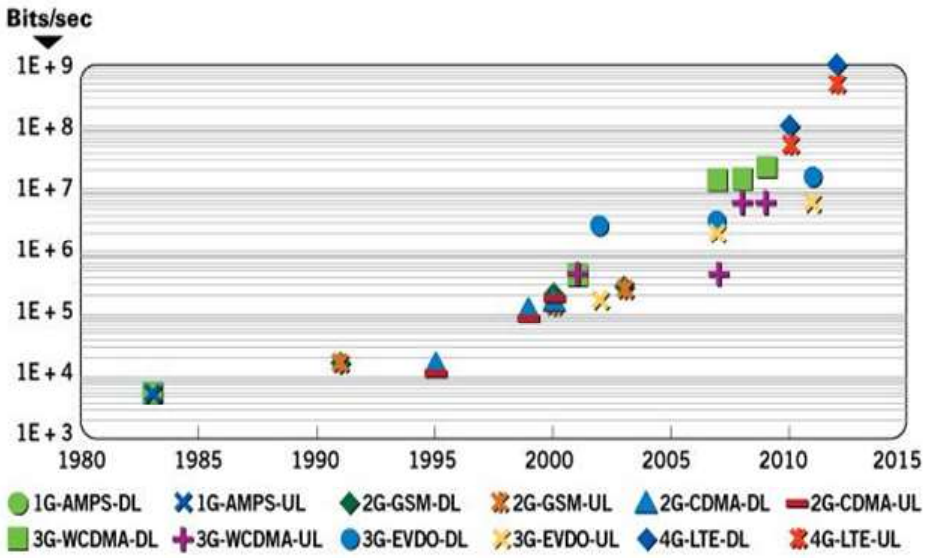

Figure 1.1: Data rate trends of cell phone standards

1.1 Degree of freedom, reliability and capacity

The reliability and capacity can be improved by increasing communication system signal to noise ratio (SNR) and/or by offering more degree of freedom (DoFs). The increase of SNR becomes more and more harder as supply voltage decreases. Investigating DoFs becomes more powerful weapon to satisfy start-of-art products requirements. The more DoFs can be obtained by providing independent paths for communication. It can be realized in time domain, frequency domain and spatial domain. Time domain DoFs yields the way that same or/and different data are communicated in different time slots, which can improves the overall throughput but decreases the data rates. Investigating more spectral and spatial domain DoFs becomes more and more significant to improve wireless communication performance. Spectral DoF can be achieved by increasing bandwidth, and Spatial DoF have been typically implemented as multi-input-multi-output (MIMO) system. Their improvement can be considered in the following two aspects.

1) Diversity gain: The channel fading can be mitigated by adding redundancy in the manner of communicating the same information through different DoF. For single DoF

system, the error probability is inversely proportional to SNR: $P_e^{Single} \propto \frac{1}{SNR}$, where P_e is the error probability. Diversity reduce the error probability in the manner of Eqn. (1.1).

$$P_e^{Div} \propto \frac{1}{SNR^L} \tag{1.1}$$

where L is the diversity order. The communication reliability is significantly improved providing more diversity.

The spectral DoF is directly associated with the ratio overall bandwidth allocated over the bandwidth for transmission one information, and spatial DoF in MIMO is related to diversity order in the following way: For $n_t \times n_r$ MIMO transceiver, where n_t if the number of transmitter antennas, and n_r is the number of receiver antennas, it can achieve maximal spatial diversity of $n_t n_r$, *if all channels are independent of each other*. The correlation among different fades decreases the diversity order and thus reduce reliability.

2) Multiplexing gain: The capacity for the single DoF system can be expressed as $C^1 = log_2(1 + SNR)$. As more degree of freedoms are available, the channels capacity becomes

$$C^M = M\dot{l}og_2(1 + SNR) \tag{1.2}$$

where M equals the number of DoF. Eqn. (1.2) indicates that the channel capacity linearly increases by the factor M. The M factor could be replaced by bandwidth (BW) for spectral DoF, as what have been shown from Shannon's theory. For spatial DoF, the multiplying factor is equal to $min(n_t, n_r$. More details on this later. The way of employing simultaneous spectral and spatial DoF can achieve $M\dot{m}in(n_t, n_r)$ times capacity improvement. Channel correlation could reduce capacity multiplying factor to be less than $min(n_t, n_r)$ [3].

1.2 Wideband

Wideband system includes the system that has instantaneous wide bandwidth, and that has a wide range of carrier frequencies with smaller instantaneous bandwidth for each. The wideband system can also be implemented in two ways: the first one is that one

transmitter or/and receiver is build to see the whole wideband spectrum. This scheme is power and area economic, but yields a high design challenge. Based on [4], the wideband can demand huge ADC power consumption. In addition, an entire spectrum wideband signal can see large number of interference, which could incur saturation, and dictate large dynamic range and power for the blocks in receiver, such as ADC before DSP [5]. As shown in Fig. 1.2, in the presence of large interference which is 40dB above desired signal power, the ADC needs 40dB more dynamic range for proper processing of the signal.

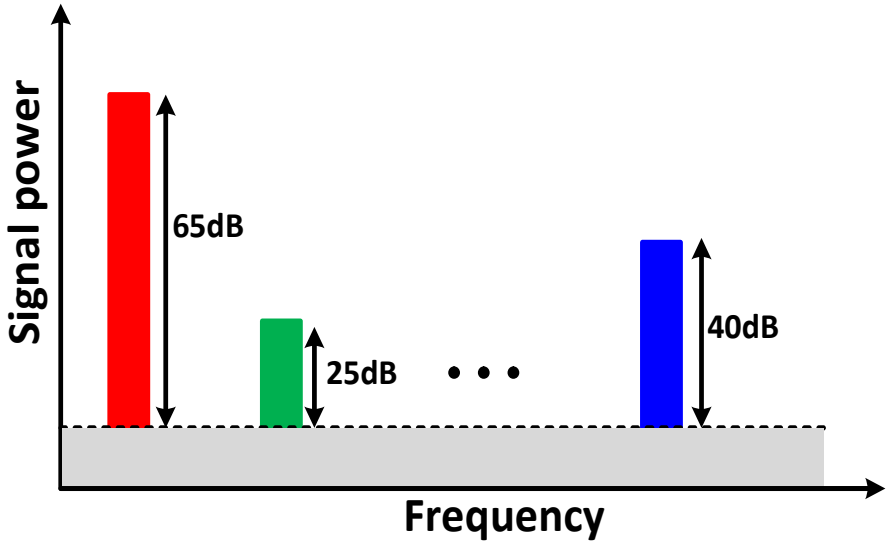

Figure 1.2: Dynamic range requirement for ADC with wide range spectrum

The second scheme is to divide the wideband spectrum into a set of sub-channels, and each channel is comparable narrowband. By doing in this way, the BB analog building blocks in each sub-channel, i.e. ADC, can also see a smaller number of interference, and dynamic range requirement (and thus power) can be significantly reduced. Fig. 1.3 shows that the BB analog blocks in the channel for desired signal can't see the large interference at other sub-channel, and the dynamic range requirement can be reduced by 40dB. This can significantly reduce the power of BB analog blocks, especially ADC.

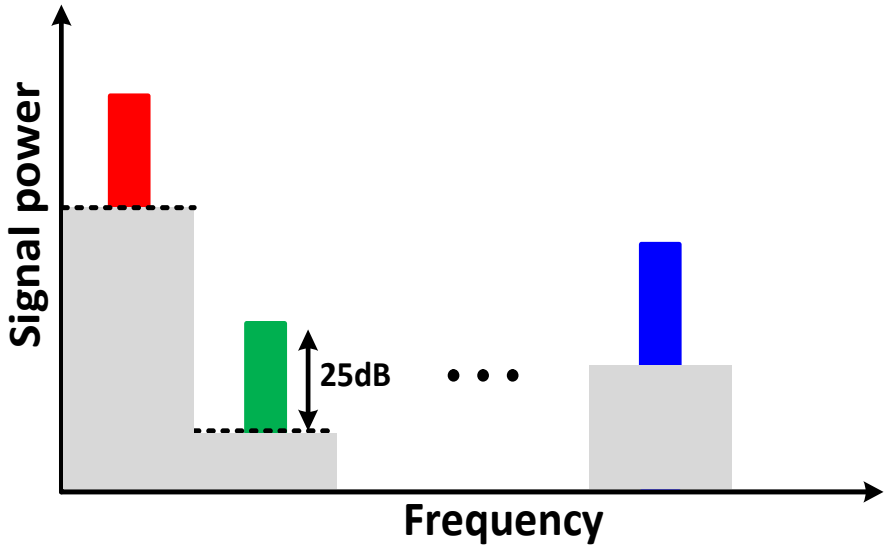

Figure 1.3: Dynamic range requirement for ADC after channelization

The basic components of this architecture includes filtering banks and frequency shifting. After dividing the wideband spectrum into sub-channels, the center frequency of sub-channels are located at different frequencies. Frequency shifting to DC of center frequencies can save the overall system power. Depending on frequency shifting scheme, channelized received can be categorized into two methods: down-sampling based or LO-based.

Fig. 1.4 shows the example of down sampling based channelized receiver [6, 7]. In this architecture, the wideband signal is first sampled and channelized by filter banks, where the center frequencies of each banks are different from each other. The followed down-sampling shifts the center frequency of each filter to DC. The advantage of this architecture is that all operations are located at IF, which can be very low power and low area. However, there is the high speed sampler needed at front-end, which could see the whole wideband spectrum. Based on Nyquist theory, it's hard to achieve instantaneous wide bandwidth due to limited sampler speed at decent performance. In addition, extra handshake circuits are needed to guarantee proper timing control between front-end sampler and following down-sampling circuit, posing more design complexities.

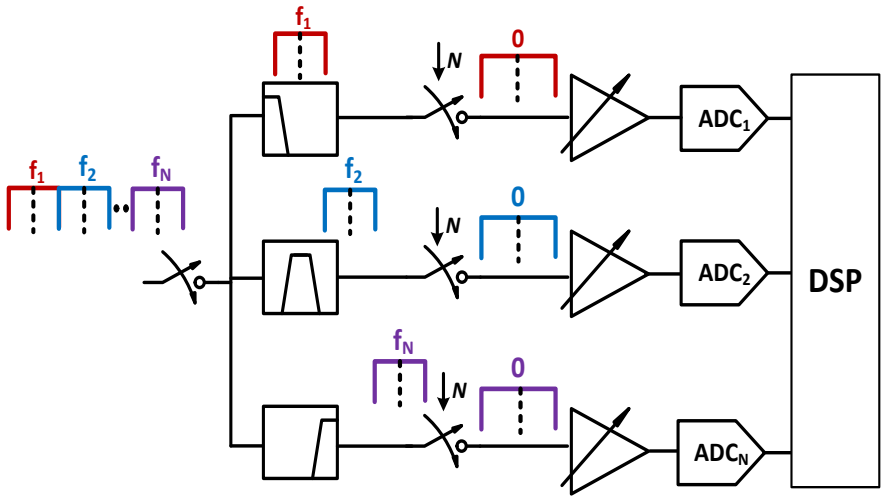

Figure 1.4: Down sampling based channelized wideband receiver

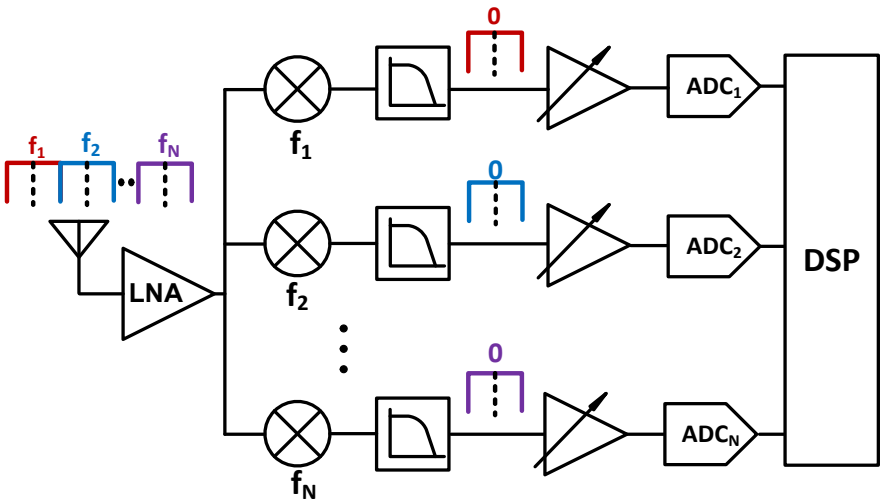

Figure 1.5: LO based channelized wideband receiver

Another architecture, as exemplified in Fig. 1.5, is LO based channelized receiver [8, 9]. The input wideband signal is first frequency shifted by different frequeny LOs at mixers, and then filtered by low pass filters (LPFs) with desired sub-channel bandwidth. The mixer based channelized scheme, on the contrary, implement all the operations in continuous-time domain, are more feasible in wide instantaneous bandwidth, as what exactly more data rate requires.

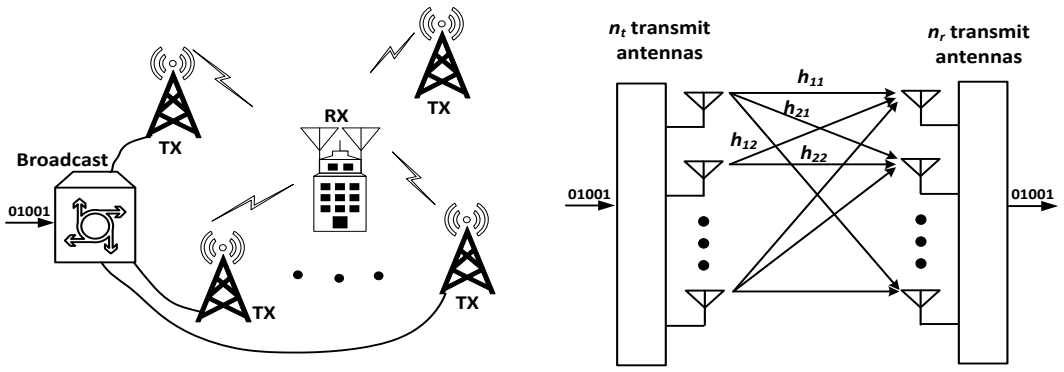

(a) (b)

Figure 1.6: (a) Wireless MIMO environment; (b) MIMO from channel perspective

1.3 MIMO

MIMO system shown in Fig. 1.6 is the architecture that exploit spatial degree of freedom to improve wireless system performance. It is an antenna technology for wireless communication system where multiple antennas are used at both the source (transmitter) and the destination (receiver). In other words, MIMO is defined from channel perspective. As evident in Fig. 1.6b, an $n_t \times n_r$ MIMO consists n_t transmitter and n_r receivers. The received information vector y can be expressed by the product of channel matrix H and input transmission vector x, in addition to noise vetor n as Eqn. (1.3).

$$y = Hx + n \tag{1.3}$$

where the vectors can be written as

$$y = \begin{bmatrix} y_1 \\ y_2 \\ \cdot \\ \cdot \\ y_{n_r} \end{bmatrix}, \qquad H = \begin{bmatrix} h_{11}h_{12} \cdots h_{1n_t} \\ h_{21}h_{22} \cdots h_{2n_t} \\ \cdots \\ \cdots \\ h_{n_r}h_{n_r2} \cdots h_{n_rn_t} \end{bmatrix}, \qquad x = \begin{bmatrix} x_1 \\ x_2 \\ \cdot \\ \cdot \\ x_{n_r} \end{bmatrix}, \qquad \text{and } n = \begin{bmatrix} n_1 \\ n_2 \\ \cdot \\ \cdot \\ n_{n_r} \end{bmatrix}$$

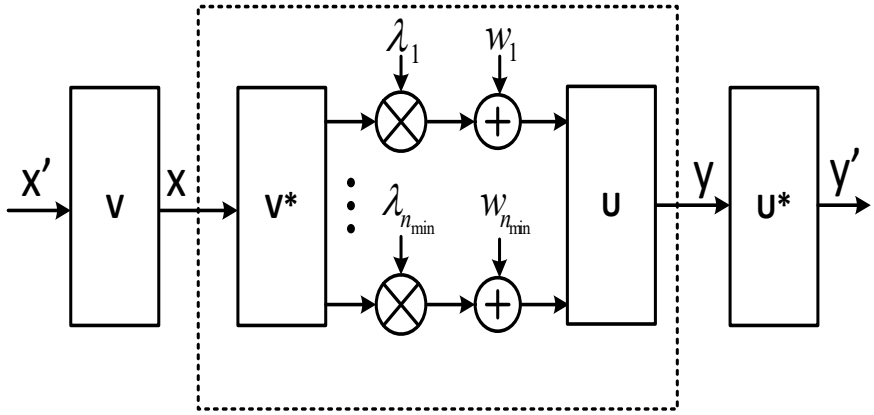

Figure 1.7: SVD based MIMO transceiver model

To get diversity gain in spatial domain, as exemplified in Fig. 1.8 for the transmitter, the same information is transmitted through n_t antenna. Each of the n_r antennas at receiver can receive the n_t of the same information. So the total diversity gain (or diversity order) that can be achieved for $n_t \times n_r$ is $n_t \times n_r$.

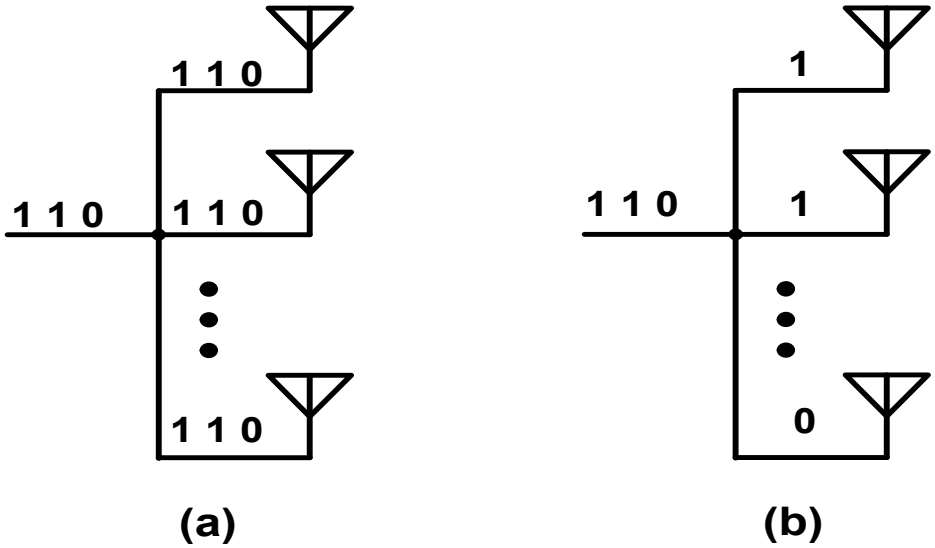

Figure 1.8: Multiple antennas system: (a)diversity gain, (b) multiplexing gain

Multiplexing gain is achieved in a another way, where different information will be transmitter through different antennas. The MIMO channel matrix H could be converted into a set of parallel channels through singular value decomposition (SVD)

which is

$$H = U \wedge V \tag{1.4}$$

where U and V are unitary matrices and $\wedge$ is a diagonal matrix whose diagonal elements are non-negative numbers and off-diagonal elements are all zeros. The diagonal elements are called as singular value, and the number of singular values equals the rank of H, which could be $min(n_t, n_r)$. The overall transceiver system is Fig. 1.4, from which we can conclude there are $min(n_t, n_r)$ sub-channels (or diversity gain) in total maximally.

1.4 Organization

This thesis proposes beamforming solutions to exploit spatial and spectral degree of freedom. After briefly review phased array basics, we proposed a new FFT based multi-beam generation receiver that exploit the full spatial DoF for MIMO. We also present a novel channelization based wideband phased array architecture, which beam squinting can also be mitigated, to obtain simultaneous spectral and spatial DoF. Lastly, we extend our proposed FFT based multip-beam architecture to transmitter design and introduce a new steerability scheme, facilitating its practical application in MIMO.

The detail organization of the thesis are summarized below.

- Chapter 1 introduces the application background with regard to this thesis. The details include the basic concept of degree of freedom, wideband communication system, and multiple-antenna MIMO system.
- Chapter 2 briefly reviews the phased array basics. Different phased array receiver and transmitter architectures, including RF, LO, and IF phase shifting based, are presented. Different types of phase delay elements are overviewed.
- In Chapter 3, the proposed FFT based multiple beamforming receiver architecture is presented. The core part is based decimation-in-time FFT architecture. Both the system and circuit details are elaborated. Comparison with its counterpart, Butler matrix, are detailed. Its an scheme that exploit the full spatial DoF to improve wireless system performance.

- Chapter 4 describes the proposed a sub-harmonic ILO based channelized wide-band phased array receiver. The scheme proposed here solves beam squinting issue without using large passive delay elements. This channelization architecture features simultaneous spectral and spatial filtering, mitigate ADC dynamic range requirement. It's an approach that can exploit both spectral and spatial DoF.

- Chapter 5 presents the proposed steerable FFT based multi-beam transmitter. This is an extended work of proposed receiver architecture. We use decimation-in-frequency, other than decimation-in-time, to implement the transmitter. A new beam-steering scheme is presented to further facilitate the FFT based architecture application in MIMO.

- Chapter 6 concludes thesis by summarizing the research contribution.

Chapter 2

Phased Array Basics

2.1 Operation Principles

Phased array is a type of multiple-antenna system that can electronically steer the direction of transmission and reception of electromagnetic waves. In order to accomplish this, there is steerable delay element at each antenna signal path to compensate the incident wave difference. The progressive delay difference can be changed according to desired signal direction. Fig. 2.1 shows the basic diagram of N-antenna phased array receiver. Assuming adjacent antenna distance is d, the spatial angle referenced to broadside is θ. The progressive delay difference at each antenna is

$$\Delta t = dsin(\theta)/c \tag{2.1}$$

where c is the speed of light in free space. For sinesoidal signal with amplitude of V_o and frequency of ω, the input wave at the k_{th} antenna can be expressed as

$$S_k(t) = V_o cos(\omega t - (k-1)d\sin(\theta)/c + \phi) \tag{2.2}$$

To compensate input delay difference arriving at each antenna, the reverse progressed variable delay elements are included in the signal path of antennas. That means the delay element associated with k_{th} antenna signal path is $(N-k+1)\tau$. The output signal after delay element for k_{th} path can be written as

$$S_{k,\tau}(t) = V_o cos(\omega t - (k-1)d\sin(\theta)/c - (N-k+1)\tau + \phi) \tag{2.3}$$

The combiner followed by delay elements of signal paths yields output as

$$S_{sum}(t) = \sum_{i=0}^{N-1} V_o cos(\omega t - (k-1)d\sin(\theta)/c - (N-k+1)\tau + \phi) \tag{2.4}$$

The array factor (AF) (or the gain) of phased array is defined by the ratio of the power gain for N-antenna array over the power gain for single antenna. Taking the ratio of $S_{sum}(t)$ over $S_0(t)$ gives AF expressed as

$$AF = (\frac{\sin(\frac{N(\omega\tau - \omega d\sin\theta/c)}{2})}{\sin\frac{\omega\tau - \omega d\sin\theta/c}{2}})^2 \tag{2.5}$$

The above equation yields sinc function from input to the output. At the desired signal direction where all input signals are added coherently, there is N^2 times peak gain, improving the system power gain. After counting N times uncorrelated noise addition, the overall SNR improvement is N.

Fig. 2.2 shows AF plots corresponding to different $\tau's$ in terms of direction angles.

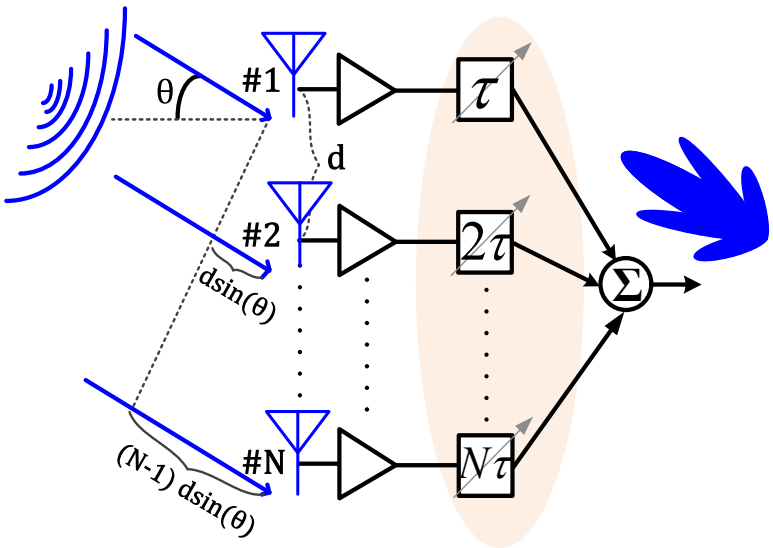

Figure 2.1: Generic phased array diagram

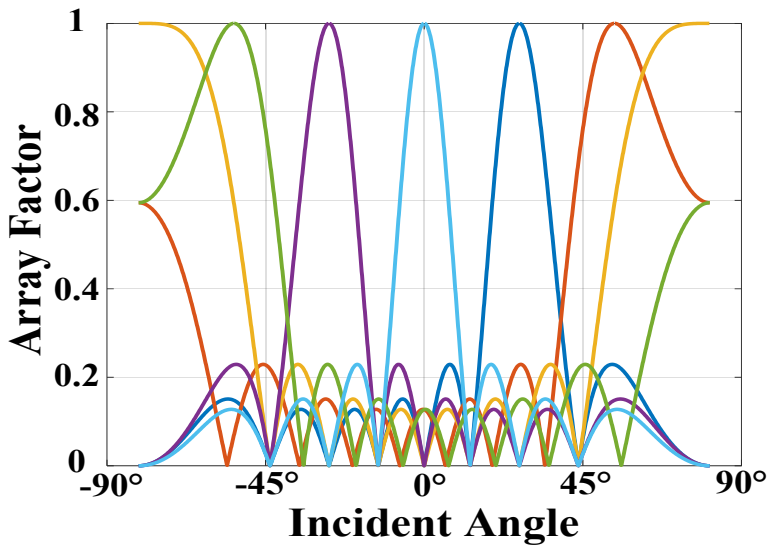

Figure 2.2: Array factor at different spatial angles for 8-element

2.2 Spatial filter

In addition to the main lobe, there are directions that make signal vanish, which are called nulls. The nulls can be placed at undesired signal directions, and knock down interference. The whole phased array behaves as filtering property in spatial domain, which provides the gain for desired signal direction and create nulls for interference directions, and thus can be thought as spatial filter.

The overall transfer function from inputs to output is formed in the way of sinc in terms of spatial direction β. There are high gain beam pointing to desired signal direction, and nullings to rejection interference.

2.2.1 Directivity

The directivity of the ability to focus the gain in the particular direction. It can be calculated by normalizing the peak gain by the average gain over the sphere, which can be expressed by

$$D = \frac{4\pi|F|^2}{\int_0^{2\pi}\int_{-\pi/2}^{\pi/2}|F(\theta,\phi)|^2 cos\theta d\theta d\phi} \tag{2.6}$$

Its has to be noticed that the gain (or array factor) is maximal for specific angle,

but the directivity changes with spatial angle. For example, for the linear broadside array, the array factor provides additional N^2 gain compared to single elements, but the directivity is given by

$$D = \frac{N^2}{N + 2\sum_{n=1}^{N-1}(N-n)sinc(nkd)} \tag{2.7}$$

2.2.2 Beamwidth

The beamwidth is the width of spatial pattern, defined by

$$Beamwidth = \frac{\lambda}{D} \tag{2.8}$$

Where λ is the wavelength, and D is the directivity. Higher directivity indicates smaller beamwidth. If adjacent antenna distance is $\lambda/2$, the beam width can be approximated as

$$Beamwidth = \frac{\lambda}{(N-1)\lambda/2} \tag{2.9}$$

Similar as directivity, the beamwidth is also dependent on spatial angel, where broadside exhibits narrowest beamwidth and endfire widest.

2.2.3 Sidelobes

While the main lobe comes from the direction that all the N-paths signals are summed in phase. There are also the directions that sub-set of the paths are combined in phase, yielding sidelobes, which present less gain compared to the main lobe. The sidelobes can receive the interference from undesired directions, and thus have to be avoided. The first sidelobe for uniform lineary array is -13dB lower compared to the main lobe.

2.2.4 Weighting

The normalized gain of the path i can be set as w_i, and the overall weighting factor is $w = [w_1 w_2 ... w_N]$. Different weighting factors exhibit different array pattern, and thus varied beamwidth and sidelobes.

When $w = [11...1]$, the phased array is called as uniform linear array. The associated array pattern yields narrowest beamwidth, but highest sidelobes. Triangle weighting approach, for which larger gain in the middle and smaller gain at two ends, yields lower sidelobes and wider beamwidth. The contents in page 418 in [10] presents more weighting examples for weighting effect of phased array.

2.2.5 Grating lobes

If the adjacent antenna distance is larger than $\lambda/2$, there are more spatial directions that all paths signals are coherently added. The additional lobes, pointing to undesired interference directions, are called as grating lobes. They have the same gain as the main lobe at desired signal spatial angle, and thus are more harming than sidelobes.

2.3 Bandwith, Time Delay or Phase Shift

As what described previously, time delays are expected in multiple antenna receivers to compensate input wave difference. However, integrated time delay blocks are hard to implement in practice. For example, for transmission medium with dielectric constant of 3.5, and the maximum operating frequency of the band is 8GHz, then total length needed for full spatial span is 20mm. Compared to the time delay elements, phase shifters are easier to implement. For narrowband systems when then frequency band can be approximated as a single center frequency f_c, phase shifters can be adopted to replace with time delays to facilitate easier implementation. However, as shown in Fig. 2.3 , the phase errors increase as in-band signal frequency f_{sig} is away from the center, which is expressed as

$$\Delta\phi = 2\pi(f_{sig} - f_c)\tau_d \tag{2.10}$$

where τ_d is the desired delay value. This error in turn induce the change of beam directions. These yield that the beam directions associated with the in-band frequencies are different. This phenomenon is called as beam squinting, which is one of the problems that have to be resolved for wideband phased array.

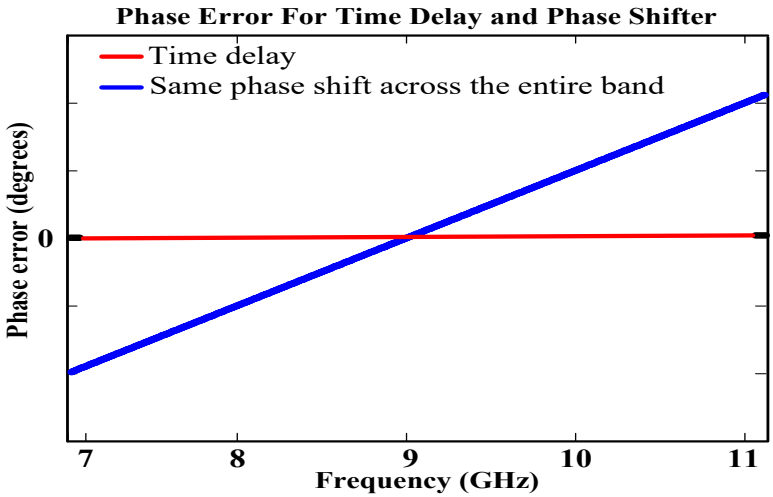

Figure 2.3: Array factor at different spatial angles

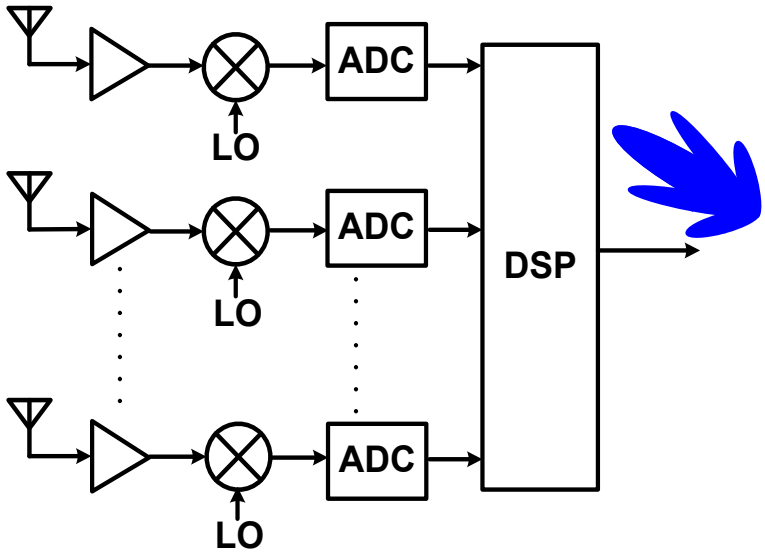

Figure 2.4: Digital phase shifting architecture

2.4 Architecture

The phased array architecture can be categorized by the position of phases shifters or delay elements. They can be either implemented in digital or analog domain, referred to as digital phase shifting or RF/analog phase shifting. RF/analog phased array includes

RF phase shifting, LO phase shifting and IF phase shifting. In this section, the detail architectures and design trade-offs are depicted.

2.4.1 Digital Phase Shifting

Fig. 2.4 exhibits N-antenna digital phase shifting architecture, where each block before DSP in the single-path receiver is replicated to N-path. This architecture attains attention because of it's the most versatile topology compared to the ones detailed below. Owning to advantages of integration of CMOS technology, digital phase shifting architecture have more capability to control amplitude and delay to perform different array patterns, such as tracking the desired signal of arrival by main lobe with the beamwidth in specification, and pointing the nulls under expected sidelobe rejection ratio (SRR) to the interferes. Moreover, this architecture facilitate digital calibration to correct array pattern error due to mismatch and couplings among different channels.

The main disadvantage is that it dictates more power and size. Due to multiplication of single-path receiver before DSP, the total power and size are multiplied by N to retain the same dynamic range requirement for all the blocks in duplication. The power overflow is more significant for ADC as its dynamic range requirement is increased, making it surpass power budget of electronic devices.

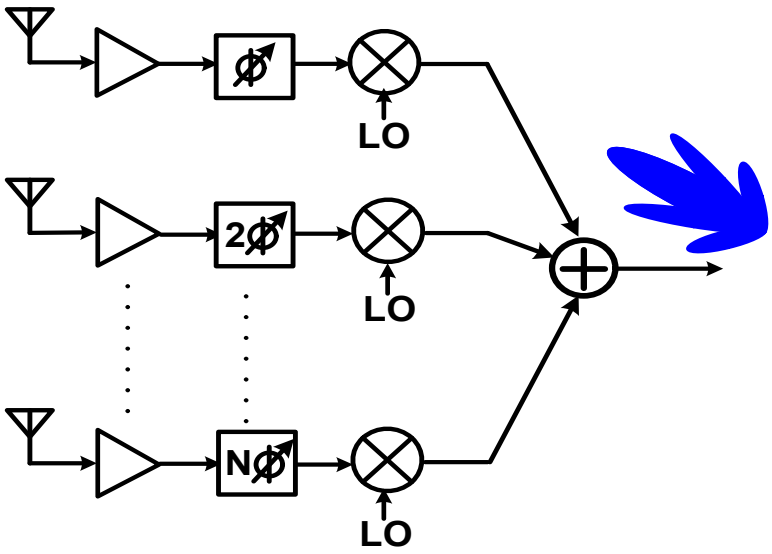

Figure 2.5: RF phase shifting architecture

2.4.2 RF Phase Shifting

Fig. 2.5 shows RF phase shifting architecture [?, ?]. In this architecture, RF phase shifters or delay elements are located at RF signal paths. The signals received by the antenna are phase shifted or delayed at RF and then followed by combination. After these, the generic down conversion approaches single-path receiver, such as heterodyne, homodyne, and image rejection low-IF, etc., can be readily employed to form the whole architecture. The RF phase-shifting architecture has gained more popularity because of the following reasons: First, there are fewer components required to construct the whole architecture. Note: for N-antenna phased array receiver as example, N parallel components are needed before the combination, while only single-path receiver components are needed after it. RF phase shifting architecture places combination before down-conversion, so only single-path LO, mixer and BB stages are required. Second, RF phase shifting has better linearity. The combination occurs before downconversion, so the spatial filtering is constructed before down-conversion. Suppose a desired signal and a strong interference are incident at antenna array input, the interference can be nulled out before downconversion if placed at nulling direction because of spatial filtering. The linearity requirements for mixer and following blocks can be mitigated.

The main drawback of RF phase shifting architecture is that it needs RF phase shifters to build beamforming. As what will be detailed later in this chapter, RF phase shifters, either passive or active, are hard to design. The reasons are not only that high frequency phase shifters tends to be physically bulky or/and power hungry, but also they are located at signal path, thus their inherent merits, such as noise, linearity, gain and bandwidth, etc., can impact, or even balance out, the advantages of array gain and spatial filtering. In addition, it's more expensive to do array pattern engineering, since RF front-end VGAs are needed.

2.4.3 LO Phase Shifting

Fig. 2.6 demonstrates LO phase shifting architecture, where phase shifters are placed at LO paths, and the combination occurs at IF after downconversion [11, 12] . This architecture is based on the fact that the downconversion of RF signal with LO signal ends up to subtraction of their phases. Similar as RF phase shifting architecture, LO phase

shifting also need high frequency phase shifting scheme, which necessarily demands large size or/and high power. Different from RF phase shifting scheme, the phase shifters in LO-based architecture are not placed at signal path. Therefore, they don't have direct impacts on system performance such as noise, linearity, gain and bandwidth, etc. This benefit makes the design of LO phase shifters much easier compared to RF based architecture. What's more, LO phase shifting architecture can fully and partially utilize readily available LO based multiple phase generation schemes. For example, ref utilize ring oscillators at LO to provide multiple phases needed for phase shifting. ref implement weighed vector modulator for phase shifting at LO, where quadrature generation block is bypassed, because quadrature phases is available for conventional quadrature downconversion. Last, the variable-gain-amplifiers for array pattern engineering can be implemented at IF before combination. This dictates less power and size.

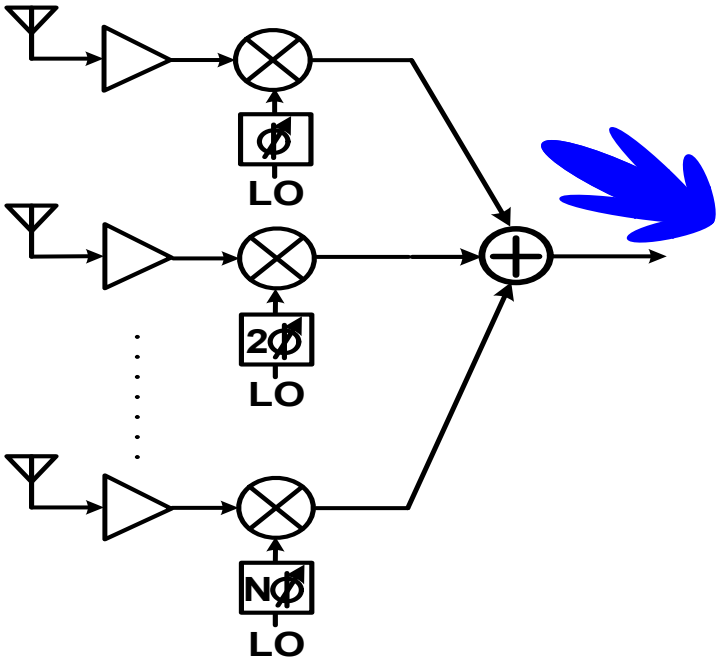

Figure 2.6: LO phase shifting architecture

It should not be surprising that LO phase shifting architecture also suffers drawbacks compared to RF based counterpart: first, it needs N mixers and LO paths for beamforming before IF combination. Second, mixers dictate more linearity requirement, since the spatial filtering of phased array can't null out interference before IF combination.

Third, LO phase shifting architecture is hard to achieve beam-squinting-less wideband phased array. LO phase shifting architecture have phase shifters in the LO path other than signal path, which alleviate the bandwidth reduction by phase shifters non-ideality. However, LO is a single tone (or one frequency) signal, which indicates inherent delay-phase approximation after mixing. This prohibits progressive delay compensation for wideband signal for wideband phased array.

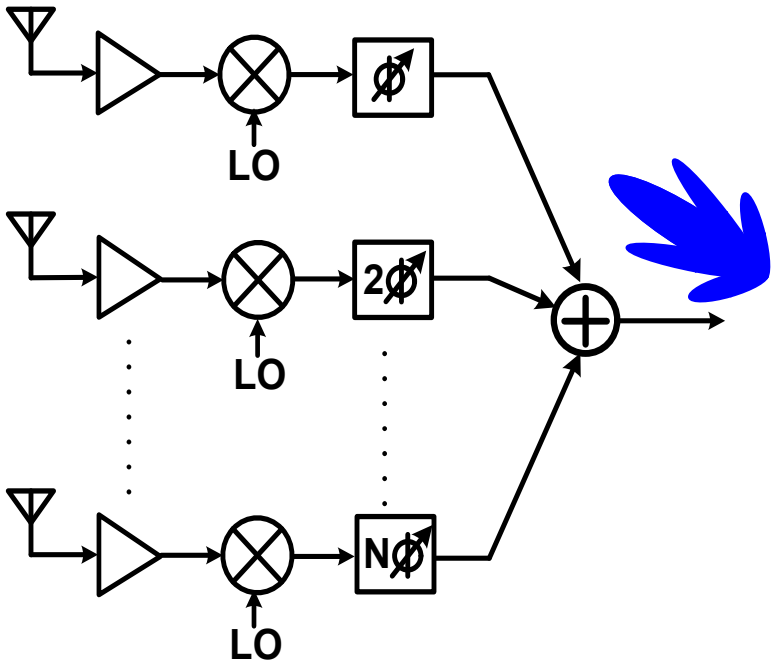

Figure 2.7: IF phase shifting architecture

2.4.4 IF Phase Shifting

Another typical beamforming architecture is IF phase shifting as shown in Fig. 2.8 . In addition to IF combination, this architecture implements phase shifters after down-conversion at IF, implying comparable easier design, and lower power and size. Similar side benefit as LO phase shifting over RF phase shifting, quadrature phases are available after downconversion.

However, as phase shifters move towards to the later stages of the receiver, there are fewer unshared blocks demanding more power and size. Furthermore, The unshared receiver blocks before combination experience the same SINR, so they need to be the

same dynamic range requirements as those in single-antenna receiver. This indicates more power.

2.5 Phase Delay

The phase delay element, either phase shifter or time delay, is the most featured and basic building block in the phased array. They can be implemented in active or passive way. There are specifications to characterize the features of the phase delay element.

- Range: the minimum to maximum phase or delay change. This directly impact the total spatial coverage of the beam. For -180° 180° phase ranges yields the full spatial coverage of the beam from broadside to endfire.
- resolution: the minimum change of the phase or delay step. The quantization step is typically controlled by the discrete signal, such as DAC. The resolution of phase shifter or time delay translates to the beam spatial resolution.
- Linearity: the phase delay elements are placed before the combination, so linearity is critical. Passive implementation have better linearity.
- Power: the passive phase delay elements have zero power consumption. But the active ones consume the power to attain precise phase resolution and moderate gain.
- Insertion loss or gain: the passive architecture experience insertion loss due to conductive and dielectric loss. The issue can be addressed by active implementation.
- Physical size: the passive phase delay elements are physically bulky, especially for low frequency implementation. The issue can be alleviated in active way.

2.5.1 Time Delay

The variable time delay can be implemented as by transmission line. The transmission delay of electromagnetic wave can be controlled by the travel distance or/and wave velocity.

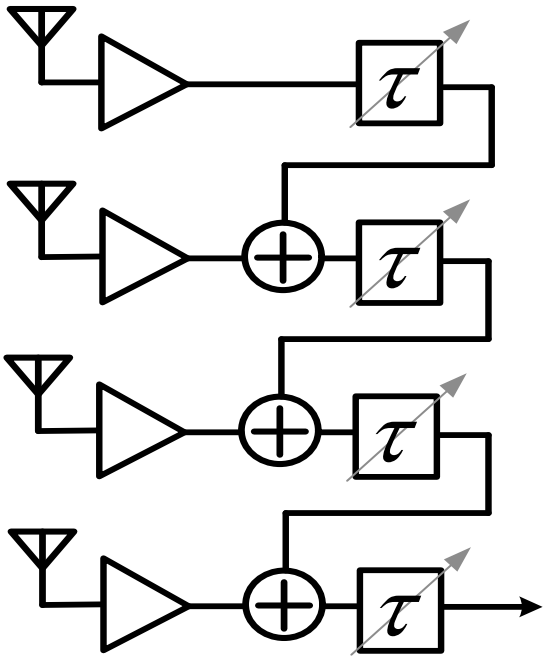

Figure 2.8: Path sharing architecture

Trombone line is one typical way to implement variable time delay, where the signal delay can be changed by travel distance. In addition, where the wave velocity can be adjusted by varying separation between signal and ground, or changing the dielectric material nature. However, direct transmission line implementation of time delay takes large physical size. For example, for material with dielectric constant of 3.5 and operating frequency of 8GHz, the total length of transmission line for full spatial span is 20mm per channel! To reduce the chip size, the transmission line can be implemented by synthesized architecture. Moreover, it's expected to be the change of the progressive delay instead of individual path delay, the path sharing technique as exhibited in Fig. **??** has been proposed [13]. In this architecture, each path is delayed by the trombone line, and then combined with adjacent channel. The delay requirement for each trombone line is reduced to be a factor of N.

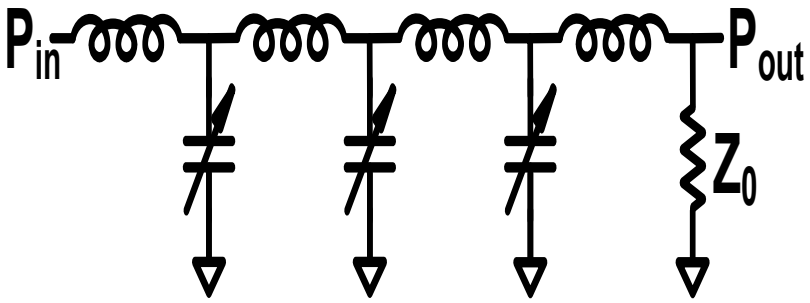

Figure 2.9: Varactor loaded transmission line

Varactor loaded transmission line as shown in Fig. 2.9 demonstrates another kind of implementation [14]. Based on velocity equation $v_p = \frac{1}{\sqrt{LC}}$, the delay can be changed with different capacitance value of the varactor. One problem of this architecture is that characteristic impedance of transmission line is also varied with varactor according to $Z_0 = \sqrt{\frac{L}{C}}$, yielding undesired changeable insertion loss over delay range.

Solutions have been reported to compensate characteristic impedance variation over delay range. One approach is to add one varactor in series with the inductor of the π-network, and the equivalent inductance value can be adjusted by changing the bias of the varactor. However, this is necessarily with limited bandwidth due to series inductor-varactor tank, negating the benefit of time delay for wideband phased array. Another work to implement variable inductance is performed in the way of adding or subtracting from primary flux by routing different secondary current using transformers and switches. However, this prototype only incorporates three inductance values: L, L+M and L-M.

The third type is approximating delay g_m- (R)C all pass filter (APF) in an active way. Consider the transfer function of all pass filter

$$H(j\omega) = \frac{1 - j\omega RC}{1 + j\omega RC} = 1 \cdot \angle 2actan(\omega RC) \tag{2.11}$$

When $\omega \ll 1/RC$, the phase change can be expressed as $\angle 2actan(\omega RC) \approx 2\omega RC$, yielding a constant group delay. Thus, the unit gain g_m- (R)C APF can be thought as active delay element.

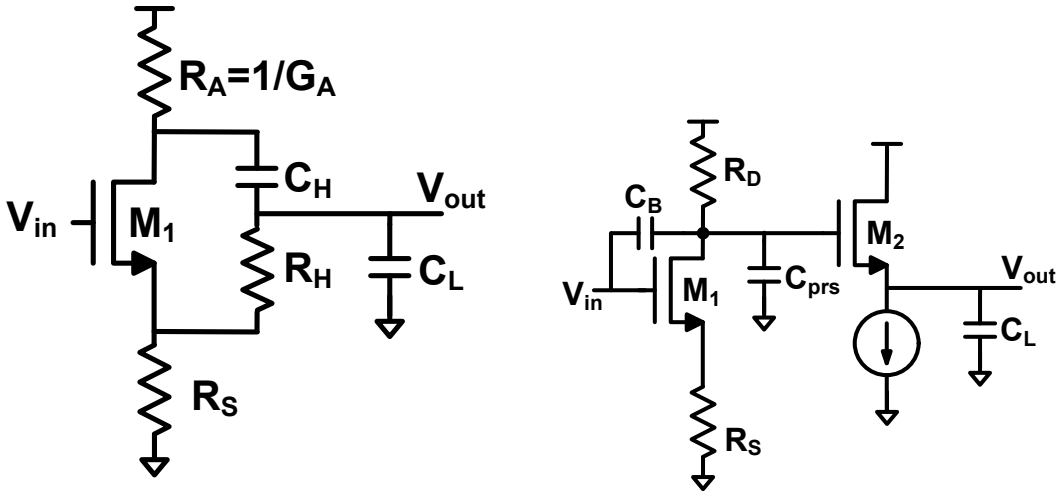

(a) (b)

Figure 2.10: (a)Classic,and (b)alternate analog all pass filter based delay cell

Fig. 2.10a shows one typical APF based active delay element [15]. The associated approximate transfer function is expressed as Eqn. (2.12)

$$\frac{V_{out}}{V_{in}} \approx \frac{g_m}{g_m + G_A} \frac{1 - R_H C_H s}{1 + (R_H + \frac{2}{g_m + G_A})(C_H + C_{in} + C_L)s} \tag{2.12}$$

To make it attain the form of Eqn. (2.11), the following two conditions have to be satisfied:

1. $\frac{g_m}{g_m + G_A} = 1$
2. $(R_H + \frac{2}{g_m + G_A})(C_H + C_{in} + C_L) \approx R_H C_H$

Another delay element topology is exhibited in Fig. 2.10b [16], and the associated transfer function is

$$\frac{V_{out}}{V_{in}} \approx -\frac{R_D}{\frac{1}{g_{m1}} + R_s} \frac{1 - \frac{1 + g_{m1} R_s}{g_{m1}} C_B s}{1 + R_D C_B (1 + \frac{2}{R_D g_{m2}})(1 + \frac{\frac{C_{prs}}{C_B} + \frac{C_L}{C_B} \frac{1}{R_D g_{m2}}}{1 + \frac{2}{R_D g_{m2}}})s} \tag{2.13}$$

The "-" sign in the right side indicates -180_{circ} phase shift, which can be removed by swapping outputs of differential circuit. Similarly, to ensure Eqn. (2.13) with the same APF form, the following two conditions have to be met:

1. $\frac{R_D}{\frac{1}{g_{m1}}+R_s} = 1$
2. $\frac{1+g_{m1}R_s}{g_{m1}}C_B = R_D C_B(1+\frac{2}{R_D g_{m2}})(1+\frac{\frac{C_{prs}}{C_B}+\frac{C_L}{C_B}\frac{1}{R_D g_{m2}}}{1+\frac{2}{R_D g_{m2}}})$

Comparing above topology, g_m- (R)C APF exhibits the smallest area, but the worst linearity due to active implementation. Varactor loaded transmission line presents the best linearity because of pure passive implementation. However, the requirement to maintain constant insertion loss over phase shift range demands tunablity of inductance value, inducing other sacrifices. The trombone line delay element presents good linearity performance, but is limited by the active buffers.

2.5.2 Phase Shifter

The phase shifters can be adopted in narrowband phased array. Depending on the practical situations, they can be used in RF, LO or IF phase shifting architecture.

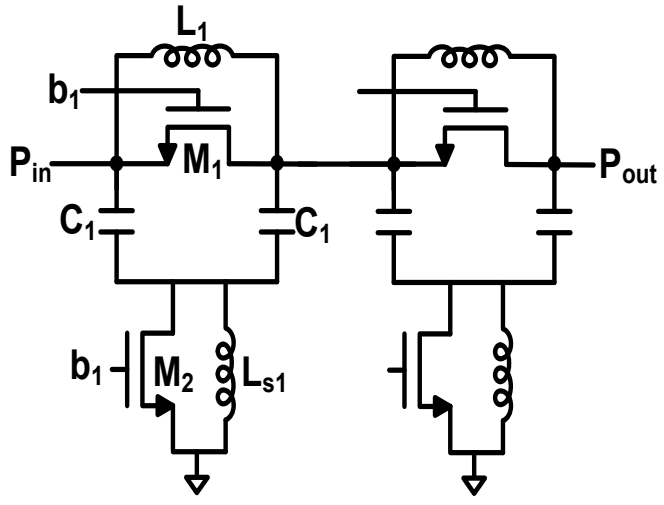

Figure 2.11: Switched transmission line phase shifter

The first prototype is switched transmission line, which consists of a series of transmission line sections with different phase shifts and MOSFET switches [17]. Each section

can be either π or T type. Discrete phase shifts can be achieved by configuring switches states. Considering π section as exemplified in Fig. 2.11 , L' and C' value in each section are decided by characteristic impedance value of $Z_0 = \sqrt{\frac{L'}{2C'}}$, and expected phase shift of $\phi_d = \omega\sqrt{2L'C'}$, where ϕ_d is 180^{circ} for the first section, and 90^{circ} for the second. The π section can be either switched in or bypassed. When control bit b1 is high, switch M1 is open and M2 is closed, the first section takes effect. When b1 is low, switch M1 is closed and M2 is open, the first section is bypassed. The component L_{s1} is used to resonate out parasitic capacitance of M2, forming parallel LC tank, or high impedance path, for the signal transmitted.

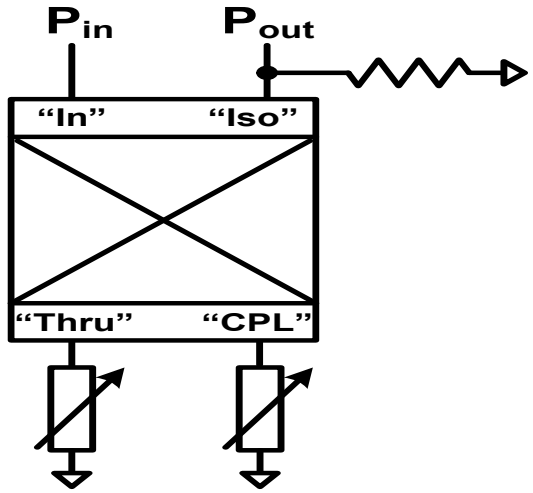

Figure 2.12: Reflection type phase shifter

The second kind of phase shifter is reflection-type phase shifter (RTPS) [18, 19]. Fig. 2.12 shows the prototype that employs one 90^{circ} hybrid and two purely reactive loads connecting to through port and coupled port respectively. When the signal is incident at input port, then the reflection coefficient for through and coupled port can be expressed as $\Gamma_L = \frac{jX_L - Z_0}{jX_L + Z_0}$, where $|\Gamma_L| = \sqrt{\frac{X_L^2 - Z_0^2}{X_L^2 + Z_0^2}}$, and $\angle\Gamma_L = -2actan\frac{X_L}{Z_0}$ The signal at the isolated port, actually the output port of RTRS, is the sum of the two phase shifted signals, which is $S_{out} = 1\angle(-\frac{\pi}{2} - 2actan\frac{X_L}{Z_0})$. When the reactive load is implemented by either inductor and capacitor (or varactor), to achieve -180^{circ} phase shift, the range of the value of either inductor and capacitor has to be fromm 0 to inf, which is impractical. Therefore, cascaded multi-section RTPS or high order reactive

terminations, such as series LC tank, have been proposed to extend phase shift range. The methods of cascade RTPS is simple, but it increase the insertion loss, especially the number of stages is large. High order resonant load increase phase shift range by adding more poles and zeros to the reactive loads as exemplified in ref.

The passive implementation attain the benefit of good linearity, but suffers insertion loss and large physical size. The active negative resistance can be added to optimize the insertion loss of RTPS for differential design. However, it degrades the noise and linearity performance. Other than branch-line hybrid, much research work on lumped transformer based hybrid with inductive and capacitive coupling, which is fundamentally coupled line, have been investigated to reduce the area.

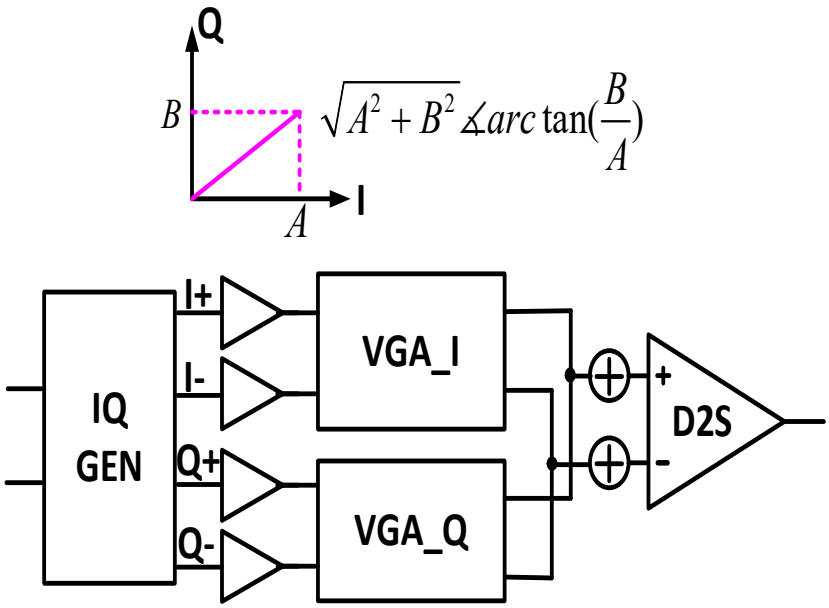

Figure 2.13: Vector modulated phase shifter

Another common phase shifter architecture is called as vector modulated phase shifter (VMPS) [20] , as illustrated in Fig. 2.13 The input signal is first splitted into two paths by quadrature phase generation (QPG): I and Q, followed by two variable-gain-amplifiers connecting to I and Q path respectively, and then the summation. The two variable-gain-amplifiers modulate the weights of I and Q paths by different gain of A_1 and A_2, and then the output signal phase is $actan\frac{A_2}{A_1}$. Regarding QPG, it can be implemented as poly-phase filter (PPF), quadrature all-pass filter (QAF), or 90^{circ}

hybrid as the one utilized for RTPS. PPF can generate 90^{circ} phase difference signals at two outputs over a wide frequency range through low-pass and high-pass network. But the amplitudes of the two outputs are equal only at one frequency, but with -3dB amplitude degradation ideally. Multi-stage PPF can be carried out to mitigate amplitude imbalance with more reduced gain. Instead of using passive RC-CR, QAF proposed by Rebeize uses LC-CL to generate quadrature phases. The architecture is benefit from improved gain due to LC resonance with increased Q, but takes large area because the inductors are used. Both PPF and QAF transfer the signal in the way of "voltage" instead of "power", which assumes zero input impedance and inf output impedance. The discrepancies, such as capacitive load from next stage, can reduce voltage gain and limit amplitude and phase balance of the quadrature outputs. In comparison, lumped transformer based 90^{circ} hybrid is according to power transfer that assumes $Z_0 = \frac{L'}{C'}$ impedance terminations, while capacitive parasitics from adjacent stage may be absorbed into lumped transformer model. Each variable-gain-amplifier is implemented as Gilbert quad to achieve 360^{circ} phase shift. The variable gain can be achieved either by varying the tail current through the DAC or changing the number of unit cells. The variable-gain-amplifiers are employed in an active way, limiting the linearity performance, and large dynamic range requirement necessarily demands high power consumption.

VMPS has been widely used for RF, LO and IF phase shifting architecture. When it's used in RF phase shifting architecture, VMPS usually takes smaller size due to active implementation.When the VMPS is implemented in IF phase shifting architecture, the expensive quadrature generation block can be avoided, because the I and Q signals are readily available for conventional quadrature down-conversion receiver. Only low frequency and low power variable-gain-amplifiers are needed. This advantage make VMPS very popular for IF phase shifting architecture. Fig. 2.14 shows the typical complex IF phase rotation architecture.

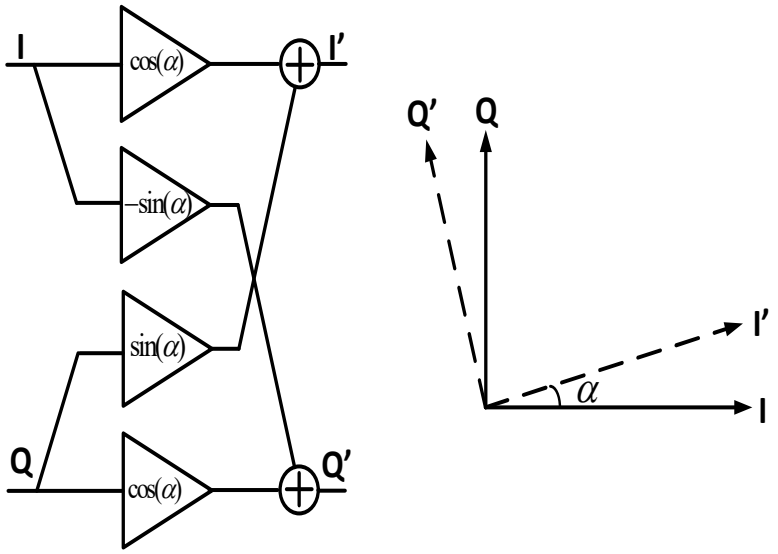

Figure 2.14: Complex IF phase rotation

The are two variants to resolve different problems for attention. First, output DC voltage varies when changing the gain, either by varying tail current or the number of the unit cells. Hua's architecture in [21] can solve the problem, but with increased area and the output parasitics, because the additional Gilbert quad is needed for each unit cell. Second, conventional VMPS can cover full amplitude and full phase range by sweeping I and Q control bits of variable-gain-amplifiers. However, full amplitude range is not necessarily needed, since phase shifter ideally only need constant amplitude. g_m sharing technique in ref has been proposed to reduce redundant g_m cells for generating full amplitude range. Therefore, the power and size are saved.

There are phase shifting scheme that can be used in LO based architecture. The first scheme is to use multi-phase ring oscillator and multiplexer at LO to feed phase shift. The ring oscillator consists of a couple of g_m stages, while each g_m stage introduce identical phase shift. The g_m stages are typically implemented in the differential way. For the N-stage differential ring oscillator, the g_m stages are connected in series, and a phase inversion is performed before closing of the ring. Each stage introduce $\frac{180^{circ}}{N}$ phase shift. It deserves awareness that different g_m stage outputs sustain different phases, and each differential outputs can provide one phase and its inverse. Thus, $2N$ phases can be generated in total. The challenge of this architecture is how to route

LO phases to different antenna mixer in physical layout, since the ring oscillator are typically far away from the mixers at signal paths. The approaches to symmetrically route multi-phase LO signals to each signal path to critical for array performance, while they normally need large power and area to realize.

Another multi-phase generation method specifically associated with LO phase shifting architecture is utilizing injection locking scheme. The basic theory is originally invented by Robert Adler, which states that when an external signal with frequency of ω_{inj} inject into oscillator whose free-running frequency is ω_0, where ω_{inj} is close to ω_0, the oscillator frequency will be synchronized to ω_{inj} as external signal. Whether oscillator can be synchronized with external injection signal depends whether the frequency offset $|\omega_{inj} - \omega_0|$ is smaller than the locking range of $\omega_L = \frac{\omega_0 I_{inj}}{2QI_0}$, where I_{inj} is the tail current of external differential pair, I_0 is the tail current of oscillator core and Q is the quality factor of oscillator LC tank. The phase difference between the injected locked oscillator and the injected signal can be expressed as

$$\delta\phi = acsin(\frac{\omega_{inj} - \omega_0}{\omega_L}) \tag{2.14}$$

When $\omega_{inj} \neg \omega_0$, then $\delta\phi \neg 0$. It means that there is the phase difference when the injected signal frequency is different from free-running oscillator frequency. The maximum phase shift of 90^{circ} can be obtained when $\omega_{inj} = \omega_0 \pm \omega_L$, yielding 180^{circ} phase shift range in total. The first example based on this principle is in ref., where each oscillator associated with each antenna is resonated at different free-running frequencies, but injected locked by common reference source. The desired phase shift of each oscillator is configured by changing free-running frequency. The second example is called as coupled oscillator array (COA). N free-running oscillators are placed in a linear array and each oscillator is injected by its nearest neighbors. When N-2 oscillators in the middle are tuned to resonate at ω_0, and the edge two oscillators are tuned to be $\omega_0 + \delta\omega$ and $\omega_0 - \delta\omega$ respectively, then all the oscillator outputs exhibit the same locked oscillation frequency of ω_0 and progressive phase difference.

2.6 Phased Array Transmitter

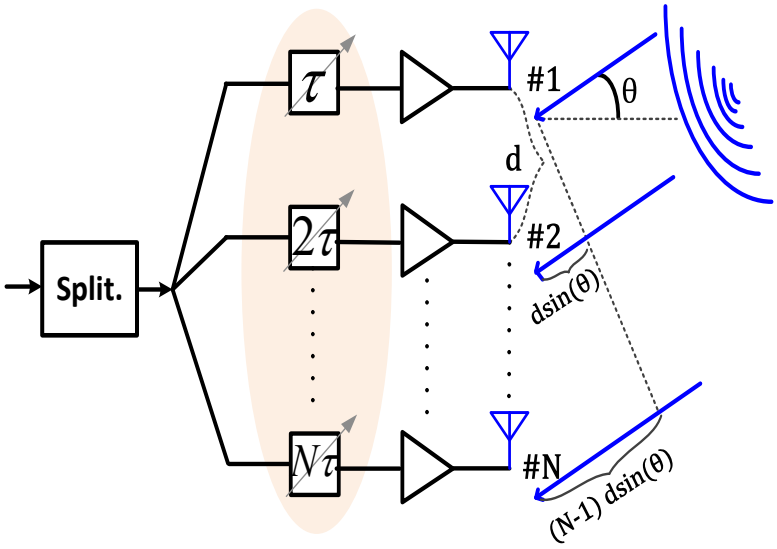

Figure 2.15: Phased array transmitter

The operation principle of phased array transmitter is similar as the receiver. As shown in Fig. 2.15, the signal is firstly splitted or replicated into M paths. Each is delayed or phase shifted, and then followed by combination. This also results in coherent addition in the desired direction(s), and incoherent addition in other directions. In the way of spatial filtering, the transmitter radiates less power at receivers that are not targeted, further reducing interference impact on the wireless link, in addition to the spatial filtering effect of the receiver. Second, the power gain by phased array transmitter increase the effective isotropic radiated power (EIRP) by M^2. This indicates the power that has to be generated in phased array transmitter is only $\frac{1}{M^2}$ of that in an isotropic transmitter, assuming a given power at the receiver. The improvement originates from the coherent addition of the electromagnetic waves in the desired signal direction. (To be more specific, M times improvement comes from spatial directivity, and another M times is from power addition). In addition to the N times improvement of SNR from the receive, the total improvement in system is M^2N, comparing to single antenna transceiver.

The phased array transmitter architecture can also be categorized as RF phase

shifting, LO phase shifting, IF phase shifting and digital phase shifting, depending on where the phase shifters are located. There is less power consumption and smaller size if the phase shifters are closer to the antennas due to more components reuse. Oppositely, when the phase shifters are closer to baseband, phase shifters are easier to design, but more power and area are needed because of less components reuse.

2.7 Phased Array Receiver

When delay elements are set to be with progressive delay difference of $\tau = dsin(\theta)/c$, the N^2 power gain is achieved at signal direction of θ, which is also called as main lobe.

2.8 Multi-beam Antenna arrays

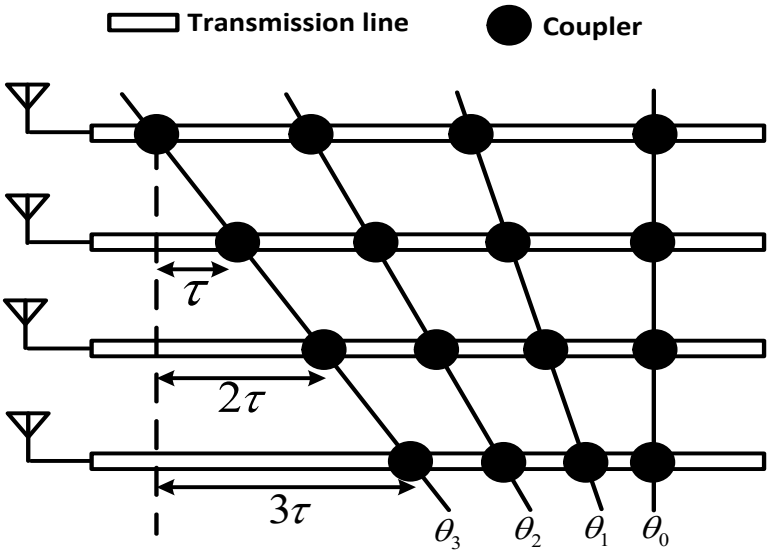

Figure 2.16: Blass matrix for multiple beams

Multi-beam antenna arrays are needed when it's desired to track multiple targets simultaneously for radar. As frequency spectrum is more crowded, it's also desired to employ multi-beam antenna array architecture to exploit spatial resources, increasing wireless communication reliability and throughput. One typical example is cellular 5G communication, where MIMO is adopted. The straightforward approach for multi-beam

generation is to replicate multiple phased array architecture, which however, increase system complexity and thus power-area hungry. This section overviews the prior art of multi-beam architecture, including Blass matrix, Chu's and Butler matrix architecture. Blass matrix and Chu's architecture employ the true time delay , which can be adopted for wideband phased array,while Butler matrix is narrowband. All of them can generate fixed multiple beams and are based on the passive implementations.

The Blass matrix employs different lengths of transmission lines to provide different progressive delay difference and passive directional couplers to feed signals from one transmission line to another. Fig. 2.16 shows one example, where black thick lines represent transmission lines and the circles are directional couplers to combine the signal. The ports $\theta_i's$ are the combination outputs, and each is pointing to one spatial direction. For example, θ_0 is the broadside direction, where the delay length for all signal paths are equal, and θ_4 is the spatial direction that progressive delay difference is τ.

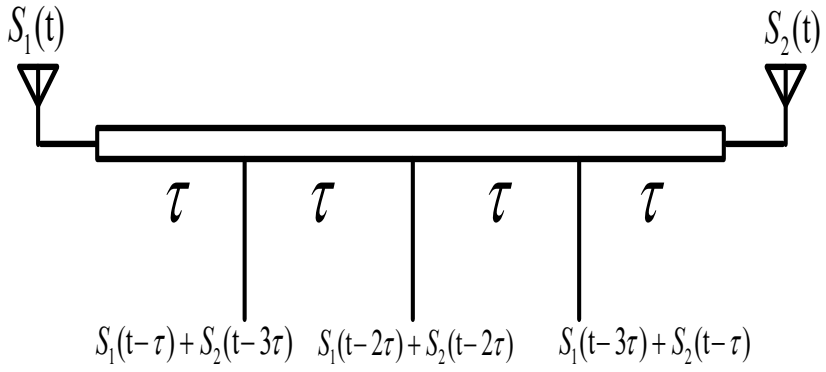

Figure 2.17: Chu's architecture for multiple beams

The Chu's architecture further reduces the number of transmission lines to facilitate single-chip integration in the way of two antennas sharing a single transmission line. Consider 1-dimensional (1-D) architecture consisting where two antennas are connected to two ends of a transmission line. The middle tap point generates the beam at the broadside direction, because the signals from two antennas experience the same delays on transmission line before arriving at combination. Other tap points are the combinations that create the beams at other spatial angles, depending on their progressive delay differences. The architecture can be extended to 2L 2L antennas and K K simultaneous

beams. For example, ref reports 2 x 2 antennas with 7 x 7 simultaneous beams.

The third typical multi-beam architecture is Butler matrix, which employs -3dB quadrature hybrids and phase shifters to generate the multiple beams. As elaborated more in next chapter, this architecture employs divide-and-conquer algorithm to save the power and size, generating simultaneous and independent multiple beams.

2.9 Summary

In this chapter, we introduce the basic operation principle and characteristics of phased array. Then various architectures are elaborated and compared. Different phase delay elements, including time delay for wideband and phase shifter for narrowband, are exhibited. Finally, multi-beam antenna arrays are briefly described.

Chapter 3

FFT based multi-channel multi-beam receiver

3.1 Introduction

Multipath interference results in fading and inter-symbol interference (ISI), imparing wireless system reliability and capacity. Multiple input and multiple output (MIMO) systems have gained attention because it provides additional spatial degrees (along with time and frequency) of freedom to improve wireless system performance. The improvements can be classified as diversity gain and multiplexing gain [22]. Diversity gain is achieved by sending or receiving the information redundantly to improve communication reliability. Compared to SISO systems, a $n_t \times n_r$ MIMO system, where n_t if the number of transmitter antennas and n_r is the number of receiver antennas, can achieve up to $n_t n_r$ times more spatial diversity. MIMO systems can also improve multiplexing gain by $min(n_t, n_r)$ times to improve the system capacity based on singular value decomposition (SVD) of communication channel. Correlation between the multiple channels can decrease both diversity and multiplexing gain [3].

In order to maximize diversity and multiplexing gain, we need to know how many spatial degree of freedoms can be obtained by antenna array, and how to generate independent channel fades. Let's look at the first question and consider the receiver only, the parameter $1/L_r$ can be considered as the criteria of resolvability in the spatial domain [22], where $L_r = n_r d_r$ is the normalized receiver array length and d_r is the

normalized adjacent receiver antenna distance. If incident angular difference of the two signals $\Phi_s << 1/L_r$, then these two signals can NOT be resolved by the receive antenna array and thus lumped into one single degree of freedom. When $d_r = \lambda/2$, the total number of degree of freedoms in receiver is $2L_r$ or equivalently n_r. The n_r degree of freedom can be implemented by generating independent multiple beams, where the progressive phase difference of incident wave for each beam satisfies

$$\theta_i = \alpha + i360^\circ/n_r, i = 1, 2, ..., n_r \tag{3.1}$$

where θ_i is the progressive phase difference of incident wave for ith beam, and α is any angle number with the range of $[0^\circ, 360^\circ)$. Similarly, the maximum degree of freedoms can be exploited for transmitter is n_t. So $n_t \times n_r$ MIMO system can partition spatial domain into $n_t n_r$ bins and thus provides maximal spatial degree of freedom of (n_t, n_r)[1]

.

There are a couple of ways to generate independent channel fades. The first is to space the antennas far apart enough. This approach works well if the system physical spaces are large enough, such as wireless base station. The second approach is to design antennas with different polarization or different radiation patterns, where each polarization mode or radiation pattern is independent of the others. The third way is to employ beamforming, such as phased array and Butler matrix, etc. On top of creating independent channels, beamforming has additional power gain, which increase effective isotropic radiated power (EIRP) by n_t for transmitter and improve output SNR by n_r for receiver. This additional benefit can further improve wireless link reliability and capacity performance based on Eqn. (1.1) and (1.2). Especially, for many power limited system where the operating SINR is typically very low, like IS-95 CDMA cellular system, Eqn. (1.2) can be approximated as $C \approx SNR \cdot log_2 e$, capacity is linearly increases with SNR that has similar effect as adding antenna numbers. From wireless link budget perspective, the improved output SNR in receiver reduces the system noise figure and sensitivity by n_r to n_r^2, depending on the noise and gain stage distribution of the system [24].

This chapter describes a FFT based RF/analog four-channel four-beam receiver that *more efficiently exploits existing receiver components for simultaneous multi-beam*

[1] These results actually hold for $d_r \geq \lambda/2$, and there are fewer spatial degree of freedoms if $d_r < \lambda/2$ [22, 23]

generation. A subset of the work has been presented in [25]. This paper is the extension of the work [25] to demonstrate advantage of FFT based multiple beamforming for MIMO compared to conventional phased array and Butler matrix. The rest of the paper is organized as follows. Section II reviews prior work for multiple beam generation. Section III shows similarity between DFT, FFT, phased array and Butler matrix, and the connection between spectral and spatial channelization. Section IV presents the system architecture. Section V describes the circuit designs and Section VI shows the measurement results. Section VII discusses the work for future investigation. Section VIII concludes the paper.

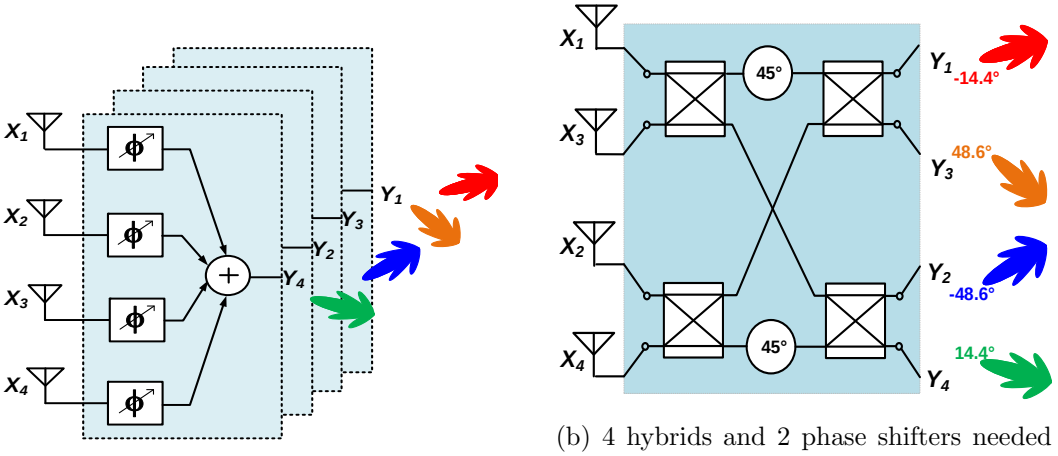

(a) 16 phase shifters needed for 4 beams

(b) 4 hybrids and 2 phase shifters needed for 4 beams

Figure 3.1: Comparison between (a) phased array and (b) Butler matrix

3.2 Prior art

This section discusses the techniques used in literature for multiple beamforming. Beamforming can be created in either digital or RF/analog domain. Digital beamforming offers more flexibility for array pattern engineering and calibration [26]. However, because absence of spatial filtering before ADC, it dictates larger ADC dynamic range and power. RF/analog beamforming implements combination for spatial filtering before ADC to reduce its dynamic range requiement. State-of-art RF/analog multiple beamforming can be classified into two broad categories: RF/analog phased array and

Butler matrix. For N-antenna RF/analog phased array, in order to get M simultaneous beams, there are MN phase shifters needed [27, 28]. The system rapidly becomes complex when the number of the beams is increased. The Butler matrix uses hybrids and RF phase shifters to efficiently provide multiple fixed beams [29] by sharing common computations. Take Fig. 3.1 as example, which shows architectures of simultaneous four-beam generation by four-antenna phased array and four-way Butler matrix. This former needs sixteen phase shifters in total, but the latter only needs four hybrids and two 45° phase shifters. The savings increase as the number of beams and antennas increase.

Conventional passive Butler matrix suffers from passive insertion loss, physical large size especially at low frequency, and limited bandwidth. The passive insertion loss at RF front-end degrades system gain and noise figure, limiting overall sensitivity. To address this issue, except for using expensive technology [30], people normally put gain stage before Butler matrix to reduce NF degradation by the passive loss [31, 32]. For instance, in [31] the Butler matrix is placed right after the LNAs, and the spatially filtered RF outputs (All outputs have sufficient spatial separation and independent of each other) are then down-converted by mixers. In addition, the quadrature phases of hybrid, either for branch-line type or coupled line, are based on quarter-wavelength transmission line. This not only occupies large size, but also adds additional factor to limit system bandwidth on top of main circuit in receiver. Direct quarter-wavelength transmission lines take large area and is rarely implemented in the integrated circuit environment [33, 34]. For example, assume operation frequency is 8GHz, and dielectric constant is about 4, then the quarter wavelength is about 4.7 millimeter. In order to reduce size, [35, 36] used lumped elements to synthesize branch-line hybrids and 45° phase shifters. Low-pass or high-pass section for transmission line synthesis places additional pole or zero to further limit the bandwidth. What's more, even though the chip size become smaller after synthesis, large passive inductor are still needed. [37, 38, 39, 40] employed transformer based hybrid with reactive load to reduce size.This architecture can be considered as coupler based on synthesized transmission line, and inherit the drawback of previous one.

3.3 DFT/FFT, Phased Array and Butler matrix

Discrete Fourier transforms (DFT) and Fast Fourier transform (FFT) are conventionally used to transform the signal from time domain to frequency domain for a different representation. IDFT and IFFT are inverse-IDFT and inverse-FFT respectively, which transform the signal representation from frequency domain to time domain. Eqn. (3.4) and (3.5) represent N-point DFT and IDFT respectively.

$$DFT : Y_k = \sum_{n=1}^{N} X_n \mathrm{e}^{i2\pi kn/N}, k = 1, 2, ..., N \tag{3.2}$$

$$IDFT : X_k = \sum_{n=1}^{N} Y_n \mathrm{e}^{-i2\pi kn/N}, n = 1, 2, ..., N \tag{3.3}$$

Phased array and Butler matrix, as previously described, are classic architectures for beamforming. They use phase shifting components to compensate for incident wave phase difference among different antennas, and create high gain beams at desired signal direction and nullings to reject inteferences.

This section will show similarity and property among DFT, FFT, phased array and Butler matrix. They are complex finite impulse response (FIR) filter, and can function as spectral or spatial filter to improve wireless system performance.

3.3.1 DFT vs. Phased array

DFT and phased array are equivalent in paradigm model as shown in Fig.3.2. Their basic operations are called "delay, phase shift and combination". The difference is how to create delay copies of input signals, either by sampler or spatial propagation. At the beginning let's look at N-point DFT architecture as shown in Fig. 3.2a. The sampler creates the delayed copies of the input signal, X_1, X_2 ,..., and X_N, then progressively phase shifted with coefficient of $\mathrm{e}^{j\frac{2\pi}{N}k}$, where $k = 0, 1, ..., N-1$, and then combined into Y_1 at final. Phased array behaves in a similar fashion: spatial propagation creates the delayed copies of the input signal from far-end, then phase shifted by the coefficient of $\mathrm{e}^{j\frac{2\pi}{N}k}$, and then combined as Y_1. Both DFT and phased array can be explained as one complex finite impulse response (FIR) filter with N coefficients of $\mathrm{e}^{j\frac{2\pi}{N}k}$, for $k = 0, 1, ..., N-1$.

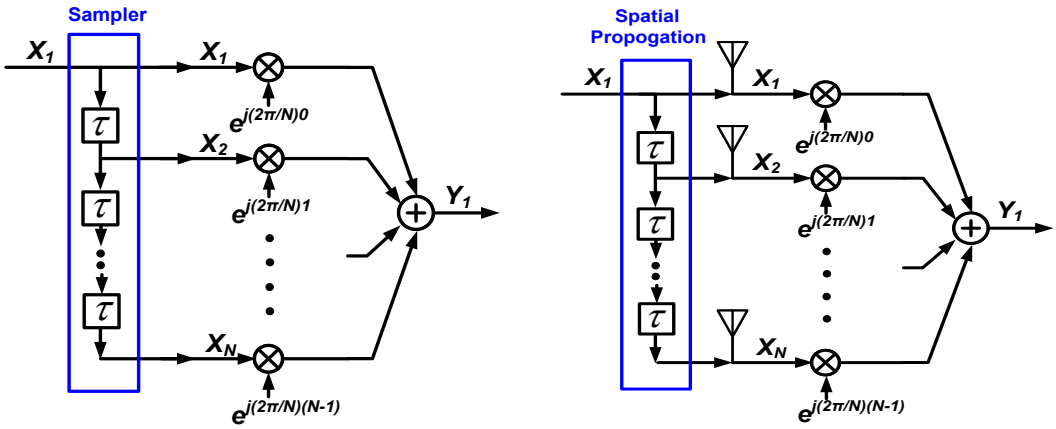

(a) (b)

Figure 3.2: Abstract model equivalence of (a) DFT: delay by sampler, and (b) phased array: delay by spatial propagation

In order to get N outputs, we need additional $N-1$ similar FIR filters with coefficients satisfying Eqn 3.1. Since the N filters are independent of each other, they can be used as spectral or spatial channelization. However, power and area are increased significantly when N is large, since the number of computations becomes more and more.

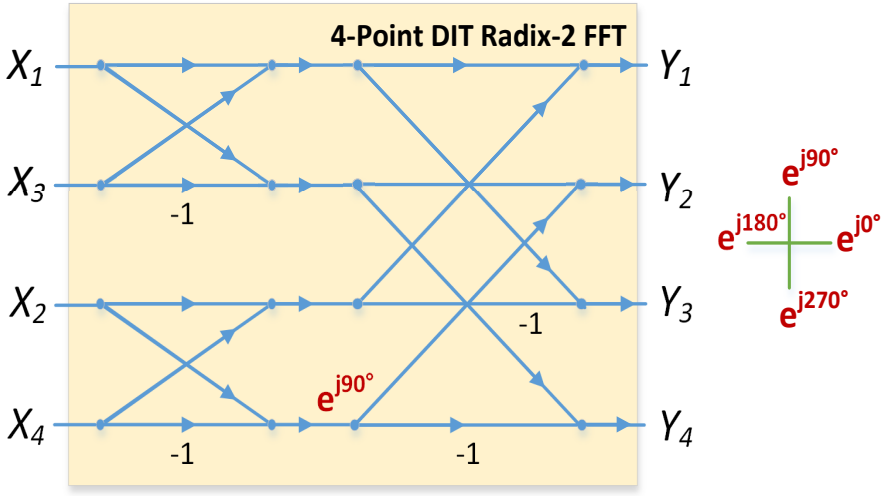

Figure 3.3: Decimation-in-time 4-point FFT

3.3.2 FFT vs. Butler matrix

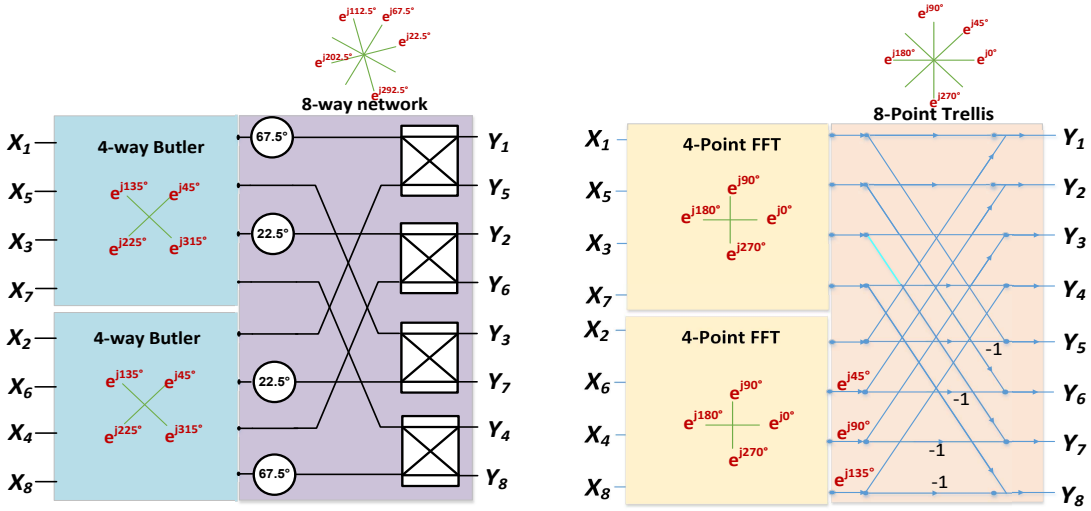

(a) 8-channel Butler matrix = two 4-channel Butler matrices + 8-port network

(b) 8-point FFT = two 4-point FFTs + 8-point trellis

Figure 3.4: Modularity of (a) 8-channel Butler matrix, and (b) 8-point FFT

FFT and Butler matrix are thus proposed to overcome the complexity issue of DFT and phased array by computation sharing based on divide-and-conquer algorithm [41].

The similarity between FFT and Butler matrix were pointed out once Butler matrix invented [42] and refined below: 1) They both have 2^m inputs and 2^m outputs; 2) Outputs are Fourier transforms of inputs; 3) They reduce the complexity order from $o(N^2)$ to $o(Nlog_2(N))$. The only minor difference between them is the progressive phase difference for Butler matrix is 45° phased rotated compared to FFT. Map this to Eqn. 3.1, FFT corresponds to $\alpha = 0°$ and Butler matrix corresponds to $\alpha = -45°$. This means even though FFT and Butler matrix generate beams pointing to different directions, the multiple beams for either of them are independent of each other to exploit the full degree of freedom in space. Fig. 3.9 shows the spatial angles and independence among the beams for FFT and Butler matrix.

Modularity: Divide-and-conquer paradigm results in modularity for FFT and Butler matrix. That means higher order architectures can be recursively constructed by

smaller designs by adding additional finer phase resolution trellises. For example, the 8-way Butler matrix shown in Fig.3.4a is basically made up with two parallel 4-way Butler matrices and additional 8-way network. The 8-way network requires $360°/16 = 22.5°$ phase step. Similarly, the 8-point FFT shown in Fig. 3.4b consists of two parallel 4-point FFTs that is followed by an 8-point trellis. The 8-point trellis requires $360°/8 = 45°$ phase resolution. FFT can uses coarser phase resolution compared to Butler matrix, and is thus easier to implement in real system.

3.3.3 Spectral vs. Spatial Channelization

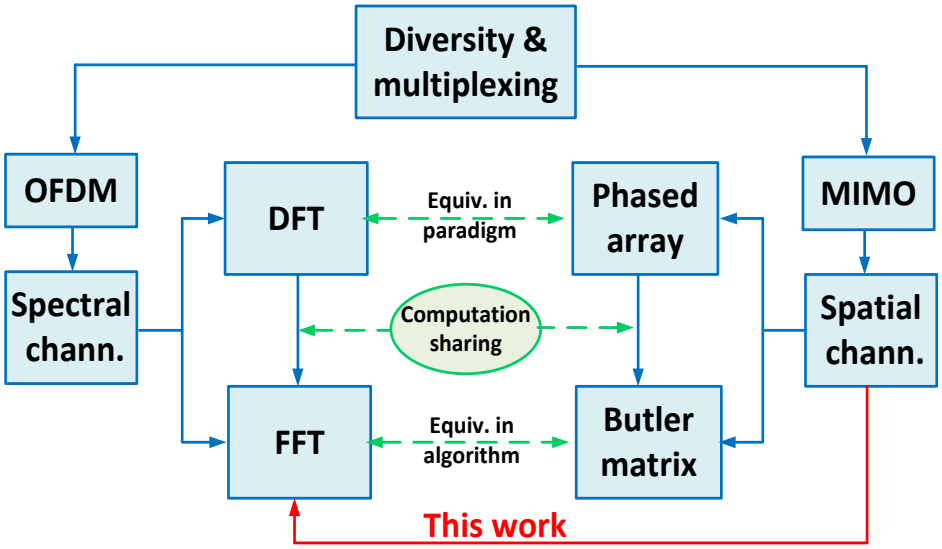

Figure 3.5: RF/analog spectral and spatial channelization

Because of architecture equivalence, either of four architectures can be used for spectral or spatial channelization. Let's look at two prior work and see the link between them.

(1) *DFT/FFT based spectral channelization*: In standard orthogonal frequency division multiplxing (OFDM) system, the independent data symbols in frequency domain are rotated by IDFT/IFFT into time domain vector at transmitter, and the received vector is rotated through DFT/FFT into frequency symbol. The transformations are conventionally implemented in digital domain. Recent years, people investigate to move DFT/FFT from digital to analog circuit in receiver [43, 44]. This is because DFT/FFT is not only a transformation of signals from time domain to frequency domain, but also

a bank of complex FIR filters as previously explained. The wideband signal is then divided into sub-bands. The carriers of the sub-bands are independent of each other, configured by sampling frequency. The ADC dynamic range requirement is reduced because less interference shown in each sub-band after spectral channelization.

(2) *Phased array and Butler matrix based spatial channelization*: In the MIMO system, the independent data symbols from far-end original signal sources are transformed by IDFT/IFFT in the way of spatial propagation: the spatial propagation from one far-end signal source to receiver antenna array can be interpreted as one equation of IDFT. N independent far-end signal sources yield N IDFT equations. People have been using RF/analog phased array and Butler matrix before ADC to retrieve original data symbols, in a analogous manner to DFT/FFT in spectral channelization. The difference is also the delay copies of original signal are created by spatial propagation instead of sampling.

Fig. 3.5 summarize the contents discussed in this section. Now we can expect to use FFT based independent multiple beamforming to overcome issues met by conventional phased array and Butler matrix in MIMO system.

3.4 System Overview

This section presents the proposed explicit-shifter-less four-channel and concurrent four-beam receiver architecture. This architecture generates independent four beams as required by MIMO to exploit full degree of spatial degree of freedom. The proposed receiver has virtually zero additional size and power cost since multiple beams are created by re-using pre-existing receiver components. The partial spatial filtering before final stage combination mitigates RF front-end circuit linearity requirement. The architecture can be extended to more beams generation due to modularity of FFT.

3.4.1 Proposed explicit-shifter-less four-channel four-beam receiver

Before we consider the actual architecture let us look at the set of four DFT equations, Eqns (3.4)-(3.7). The corresponding FFT flow diagram is shown in Fig. 3.3

$$Y_1 = X_1 e^{j0^\circ} + X_2 e^{j0^\circ} + X_3 e^{j0^\circ} + X_4 e^{j0^\circ} \quad (3.4)$$

$$Y_2 = X_1 e^{j0^\circ} + X_2 e^{j90^\circ} + X_3 e^{j180^\circ} + X_4 e^{j270^\circ} \quad (3.5)$$

$$Y_3 = X_1 e^{j0^\circ} + X_2 e^{j180^\circ} + X_3 e^{j0^\circ} + X_4 e^{j180^\circ} \quad (3.6)$$

$$Y_4 = X_1 e^{j0^\circ} + X_2 e^{j270^\circ} + X_3 e^{j180^\circ} + X_4 e^{j90^\circ} \quad (3.7)$$

The output quantities Y_1, Y_2, Y_3 and Y_4 are equal to the sum of four-channel inputs, (X_1, X_2, X_3 and X_4) phased rotated by 0°, 90°, 180° and 270° respectively. The associated Decimation-in-time FFT signal flow is shown in Fig. 3.3, where we need three different kinds of computation: (1:1) combination (or 0° phase rotation), (1:-1) combination (or 180° phase rotation) and 90° phase rotation. (1:1) combination can be thought of 2-channel broadside sub-array, and (1:-1) combination can be seen to be 2-channel endfire sub-array.

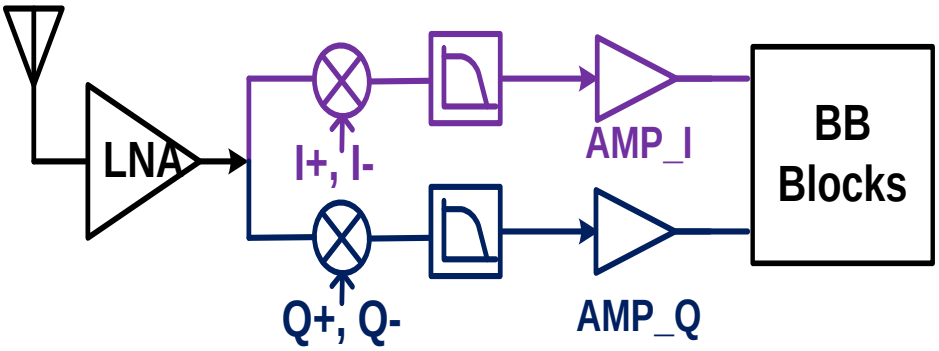

Figure 3.6: Conventional quadrature down-conversion receiver

Fig. 3.6 shows a standard receiver architecture, which consists of LNA, quadrature mixer driven by in-phase(I) and quadrature phase(Q) LO signals, IF amplifier that increases signal swing to full-scale for ADC quantization and other baseband blocks. Our target is to implement FFT architecture in Fig. 3.3 with minimum additional power and size by reusing existing receiver components in Fig. 3.6.

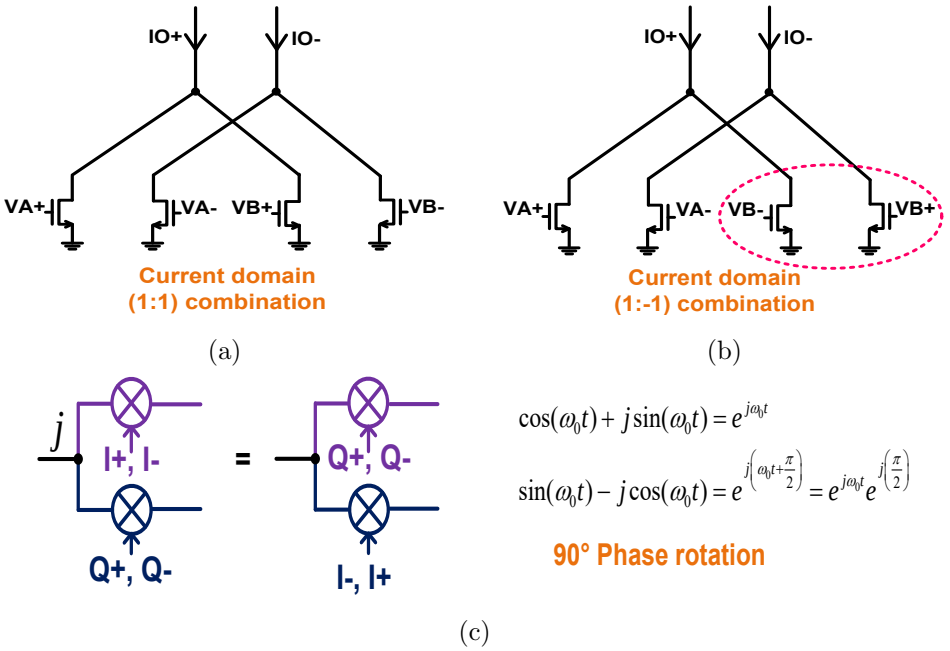

Figure 3.7: Explicit shifter-less operations for four-beam generation

Fig. 3.7 shows the explicit-shifter-less implementation scheme based on conventional receiver architecture in Fig. 3.6. We note (1:1) combination can be easily done in the current domain for common source differential pairs, and (1:-1) combination can be achieved similarly with swapped differential pairs for the second channel inputs. We also note that a normal quadrature down-conversion receiver has in(I)-phase and quadrature(Q)-phase channels: mixer in I channel driven by I phase LO signal and mixer in Q channel driven by Q phase LO. To implement 90° phase rotation, we instead use Q phase LO to drive I channel mixer and -I phase LO to drive Q channel mixer.

The proposed four-channel, four-beam receiver is shown in Fig. 4.5. The four antenna inputs are fed through external LNAs, then these signals are pairwise $(1 : \pm 1)$ combined [added (0°) or subtracted (180°)] in the current domain before down-conversion. In particular, at RF the channels associated with X_1 and X_3 form a pair, and X_2 and X_4 form the second pair using the reverse binary for a decimation-in-time FFT. The RF signals are then down-converted to IF where the final stage of signal combination is done. Considering Y_1 and Y_3 as examples, Y_1 uses the sum of mixer outputs associated with X_1 and X_2, and Y_3 uses the difference of the mixer outputs associated with X_1

and X_2. Note that for only the 4^{th} channel the I+I- and Q+Q- are replaced by Q+Q- and I-I+ for 90° phase rotations. The additions and subtractions at IF are also easily accomplished in the current domain. All the computations discussed directly utilize pre-existing components of a receiver (other than signal swapping and signal routing) without adding additional stages.

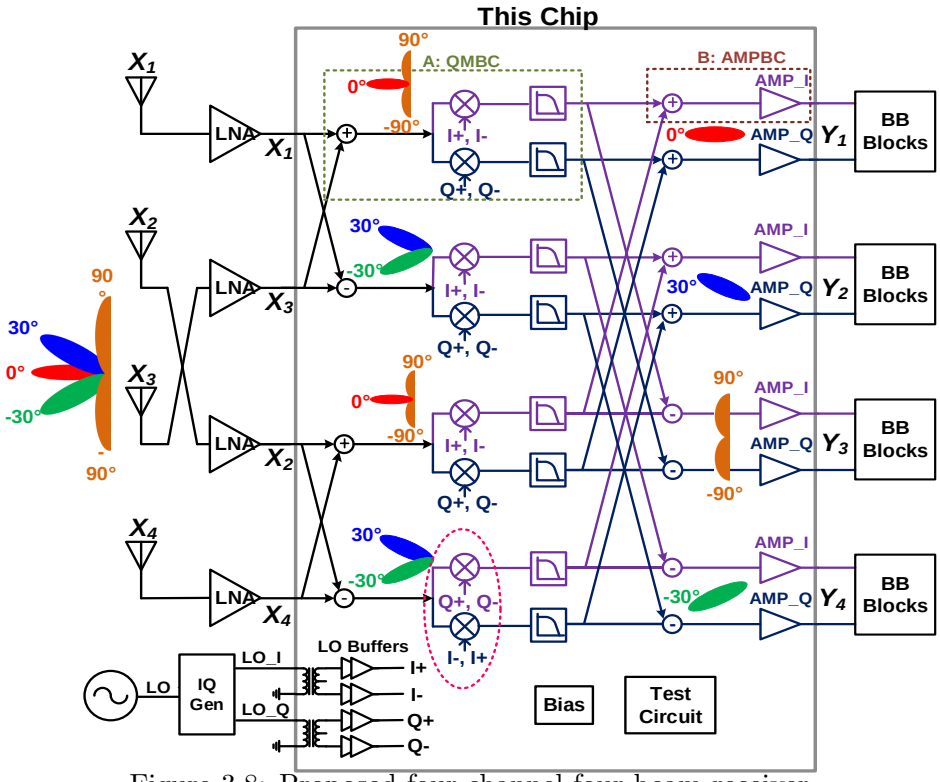

Figure 3.8: Proposed four-channel four-beam receiver

Table 3.1 summarizes the phase rotation relationship between the outputs and inputs, and their corresponding beam directions for the proposed architecture of Fig. 4.5. Each value for a conventional Butler matrix is bracketed in the table for comparison. The input phase rotation of 0°, 90°, 180° and 270° indicated by Eqns (3.4)-(3.7) yield 0°, +30°, ±90° and −30° spatial beam directions as shown in Fig. 4.5, in comparison to the −14.4°, −48.6°, 48.6° and 14.4° beam directions for a Butler matrix, using a $\lambda/2$ antenna distance. Fig. 3.9a shows the four beams generated by our proposed architecture are independent of each other(the peak of each beam corresponds to nullings of the others),in a similar fashion as Butler matrix.

	P_1	P_2	P_3	P_4	**Phase Diff.**	**Beam Direction**
P_5	0°	0°	0°	0°	0°	0°
	(315°)	(270°)	(225°)	(180°)	(315°)	(−14.4°)
P_6	0°	90°	180°	270°	90°	30°
	(270°)	(135°)	(0°)	(225°)	(225°)	(−48.6°)
P_7	0°	180°	0°	180°	180°	±90°
	(225°)	(0°)	(135°)	(270°)	(135°)	(48.6°)
P_8	0°	270°	180°	90°	270°	−30°
	(180°)	(225°)	(270°)	(315°)	(45°)	(14.4°)

Table 3.1: Phase rotation relationship

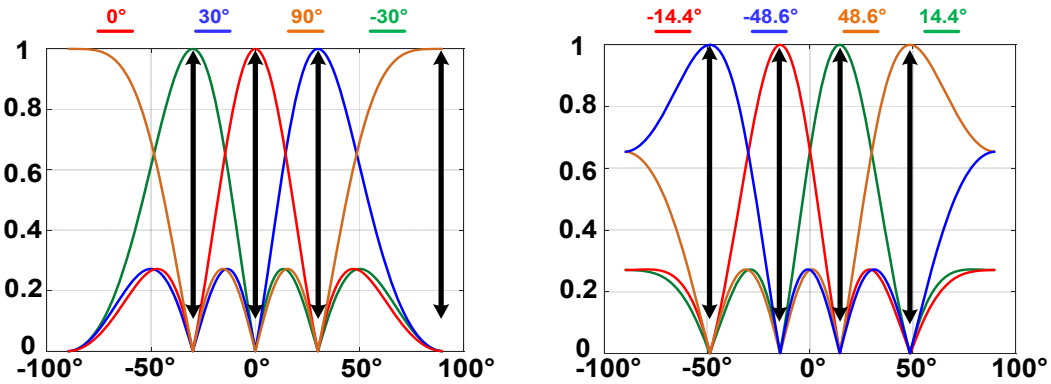

(a) FFT (b) Butler matrix

Figure 3.9: Array pattern of (a) FFT and (b) Butler matrix shows 4-channel independence: the peak of each beam corresponds to nulling of the other three

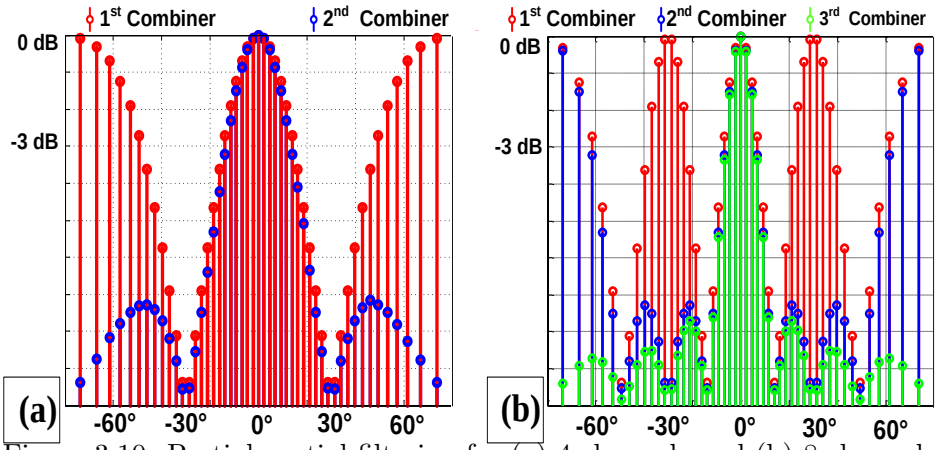

Figure 3.10: Partial spatial filtering for (a) 4-channels and (b) 8-channels

3.4.2 Partial spatial filtering

Because some of spatial filtering is done at RF our design inherits properties of both RF beamforming and IF beamforming without the difficulty of realizing all the beams at RF. Signal addition (0°), subtraction (180°) and (90°) and (270°) phase shifting could in theory all be accomplished in the baseband [43]. However, it would not provide the partial spatial filtering shown in Fig. 4.5. Note, the beam-width is given by $\lambda/(Nd)$, where N is the number of antennas, and d is the distance between adjacent antennas [45]. In our design, there are $\log_2(4) = 2$ combining stages. The first signal combining at the mixer input forms a two-channel phased array with an adjacent antenna distance of λ. In this case two grating-lobes show up due to the λ spacing. The RF signal combining provides "partial spatial filtering" of interference close to the main-lobe and improves the jammer rejection for all the blocks that follow it. The broadside array patterns for a 4-channel is shown in Fig. 3.10 (a). The red lines show the "partial spatial filtering" after the RF combiner and the blue dots show the final beam. The main lobe remains the same and only parasitic grating-lobes show up due to the larger antenna spacing.

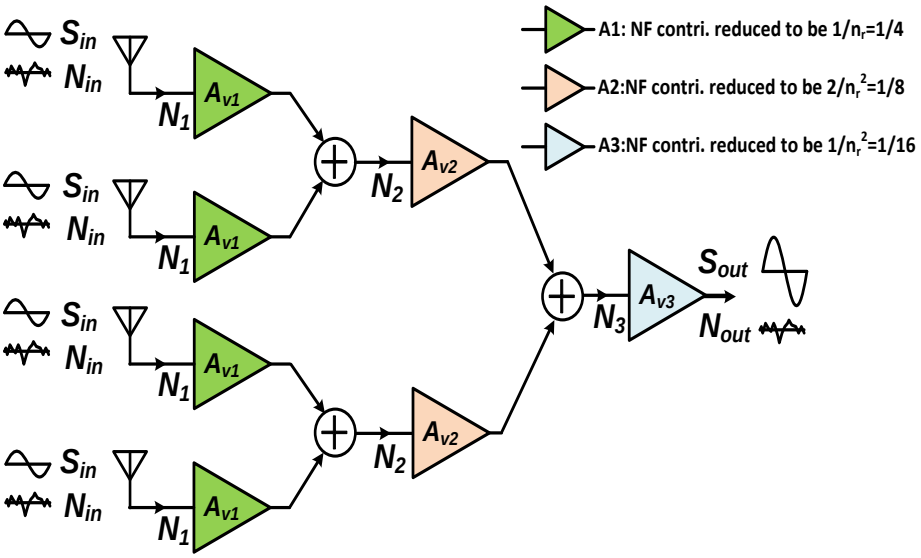

Figure 3.11: Progressive SNR improvement

3.4.3 Progressive power gain and SNR improvement

In addition to progressive spatial filtering described above, distributed computation leads to progressive SNR improvement. Consider the abstract model for anyone beamforming as shown in Fig.3.10. let $S_{in} = v_{s,in}^2$ and S_{out} be the input and output power respectively, and $N_{in} = v_{n,in}^2$ and $N_i = v_{n,i}^2$ are the noise power at antenna input and input referred noise of three gain stages. Then the output signal power is $S_{out} = v_{s,in}^2 A_{v1}^2 A_{v2}^2 A_{v3}^2$, where A_{v1}, A_{v2} and A_{v3} are the voltage gain of three stages. The output SNR for single channel and $n_r = 4$ channels receiver can be expressed as Eqn. (3.8) and (3.9) respectively.

$$SNR_{out,1} = \frac{S_{in} A_{v1}^2 A_{v2}^2 A_{v3}^2}{(N_{in} + N_1) A_{v1}^2 A_{v2}^2 A_{v3}^2 + N_2 A_{v2}^2 A_{v3}^2 + N_3 A_{v3}^2} \tag{3.8}$$

$$SNR_{out,n_r} = \frac{n_r^2 S_{in} A_{v1}^2 A_{v2}^2 A_{v3}^2}{n_r (N_{in} + N_1) A_{v1}^2 A_{v2}^2 A_{v3}^2 + \frac{n_r}{2} N_2 A_{v2}^2 A_{v3}^2 + N_3 A_{v3}^2} \tag{3.9}$$

Comparing Eqn. (3.8) with (3.9), we can see SNR improvement ranges from n_r to n_r^2, depending on gain and noise contribution from different stage components. The NF contribution by A1 and A3 are reduced to be $1/n_r = 1/4$ and $1/n_r^2 = 1/16$ respectively, and NF contribution by A2 is partially reduced to be $1/(2n_r) = 1/8$. In other words, if the noise contribution is dominated by components before any combination (N_{in}

or N_1), the output SNR is improved by n_r; if the noise contribution is dominated by components after final combination (N_3), the output SNR is improved by n_r^2. The SNR improvement is $2n_r$ times if noise contribution is dominant by components between two stage combinations of N_2. This yields progressive SNR improvement for RX because of distributed computations.

Till now we can see: NF from later stage components is attenuated not only by gain of components from early states, but also the progressive partial power gain by the array. The power gain for each component is decided by the number of combination stages before it. This provides additional freedom to trade-off NF contribution among different components along the receiver chain.

3.4.4 Increasing the number of channels and beams

As stated in Section 3.3.2, higher order architectures can be recursively constructed from low order ones by adding additional finer phase resolution trellises which are much easier to implement at IF with I and Q signals after quadrature downconversion. For example, $360°/8 = 45°$ phase resolution required by 8-point trellis in Fig. 3.4b can be implemented by cartesian combination of equal values of I and Q signals at IF.

		IF phased array		**Our architecture**	
♯ of Combiners	IF	$8 \times 2 = 16$	8 inputs	$16 \times 2 = 32$	2 inputs
	RF	–		$4 \times 2 = 8$	2 inputs
♯ of Rotators		$8 \times 7 \times 2 = 112$		$3 \times 2 = 6$	

Table 3.2: Computations comparison

The 8-point trellis differs from a fixed multi-beam IF phased array. In particular, not unlike in an FFT, the 8-point trellis reuses computations to generate the simultaneous eight beams in comparison to an IF phased array. Table 3.2 shows a comparison of computations required for a fixed IF phased-array and our architecture. (Note: the phase rotator design is more complicated for a steerable array.)

Partial spatial filtering is present in higher number of channels as well. The main-lobe remains the same while the grating-lobes get progressively smaller as we get closer to the ADC. The 8-channel case is shown in Fig. 3.10 (b) where the second combiner,

in blue, does not have the lobes at ±30° that were present for the first combiner, in red. The final narrow beam is shown in green.

Progressive SNR boosting is also inherited when increasing number of channels. The output SNR for $n_r = 2^k$ channels receiver is given by Eqn. (3.10), where k is the number of combination stages. The second term in the denominator indicates the noise contribution for components among combination are progressively attenuated by power gain of the array.

$$SNR_{out,n_r} = \frac{n_r^2 S_{in} A_{v1}^2 A_{v2}^2 A_{v3}^2}{n_r N_{in} + \sum_{i=1}^{k} \frac{n_r}{2^{i-1}} N_i A_{vi}^2 A_{v(i+1)}^2 \cdots A_{v(k+1)}^2 + N_{k+1} A_{v(k+1)}^2} \tag{3.10}$$

3.5 Circuit

All circuit implementations for beamforming are fully differential but only simplified versions are shown for clarity. Four single-ended RF signals are introduced on-chip using GSGSG probes and differential versions are generated using on-chip baluns. The baluns may not be needed if the LNA outputs are differential.[2] In a similar fashion differential versions of LO-I and LO-Q are generated using on-chip baluns.The binary tree structure is used to deliver differential quadrature phases symmetrically to different channels. LVDS buffers are placed four-channel outputs for receiver measurement.

3.5.1 Balun

The square symmetric bi-filar balun in Fig. 3.12 are used for single-ended to differential conversion [46]. Two interwound top layer thick metals are divided along symmetrical lines horizontally and vertically. The center-tap of secondary is precisely located at mid-point of the winding for high Q and better phase balance. Metal layer M8 and M7 are used for crossover. The physical layout is implemented to make all terminals at outside edges for easier connection to other circuit blocks. The ground shield by bottom layer metal M1 is placed underneath the balun to reduce the silicon substrate loss at the cost of low additional capacitance [47].

[2] The baluns are primarily to test our prototype, but can be one building block when LNA output are single-ended.

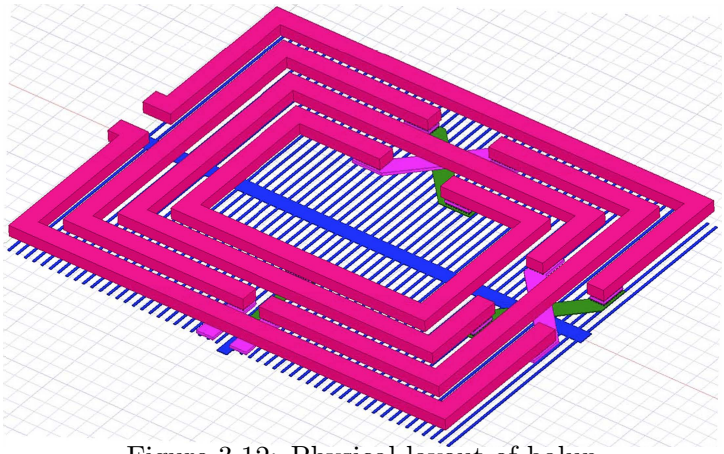

Figure 3.12: Physical layout of balun

3.5.2 Quadrature mixer with built-in combiner (QMBC)

The quadrature mixer with built-in combiner (QMBC) is based on a traditional double-balanced Gilbert cell topology and is shown in Fig. 3.13. The RF signal $(1:1)$ combination (or addition) is realized using RF tail transistors with differential signals $VRFA\pm$ and $VRFB\pm$ from the two channels. The output current is then evenly distributed between the I and Q paths, and down-converted and low pass filtered to $VIF\_I\mp$ and $VIF\_Q\mp$. In a similar fashion, the negative QMBC output is generated by interchanging the input connection to $VRFB+$ and $VRFB-$ to achieve $(1:-1)$ combination (or subtraction). The LO switches have minimum lengths to reduce loading of the LO drivers. The composite PMOS and resistor output load was sized to provide good noise performance. Note, that the RF tail transistor is split into two for each channel and the total mixer current remains the same as would have been for completely separate channels.

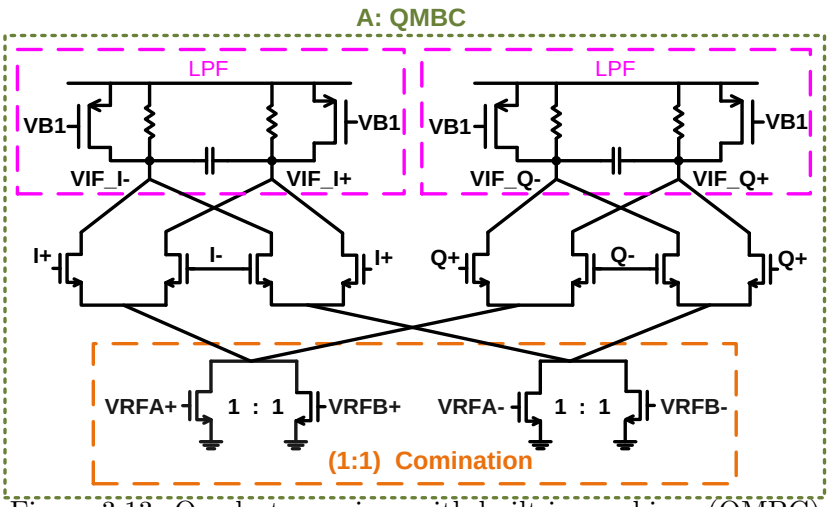

Figure 3.13: Quadrature mixer with built-in combiner (QMBC)

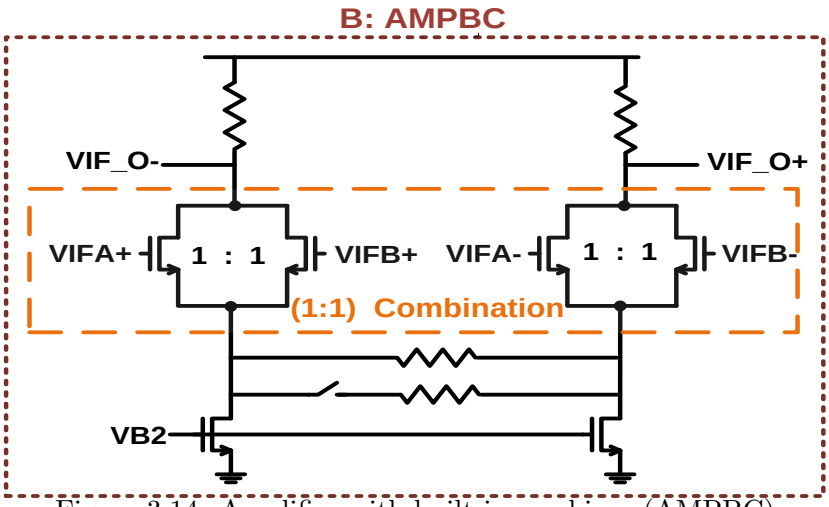

Figure 3.14: Amplifier with built-in combiner (AMPBC)

3.5.3 Amplifier with built-in combination(AMPBC)

Similarly, the $(1:1)$ combination can be implemented directly at the IF amplifier inputs, where differential signals from two channel $VIFA\pm$ and $VIFB\pm$ are combined as shown in Fig. 3.14. This circuit is based on a source degenerated common source amplifier optimized for linearity and phase accuracy. The $(1:-1)$ combination is realized by switching connections between $VIFB+$ and $VIFB-$. The length of the combination transistors are sized larger to reduce the phase error, since its loading effect at IF is less

critical. No additional current is used here either.

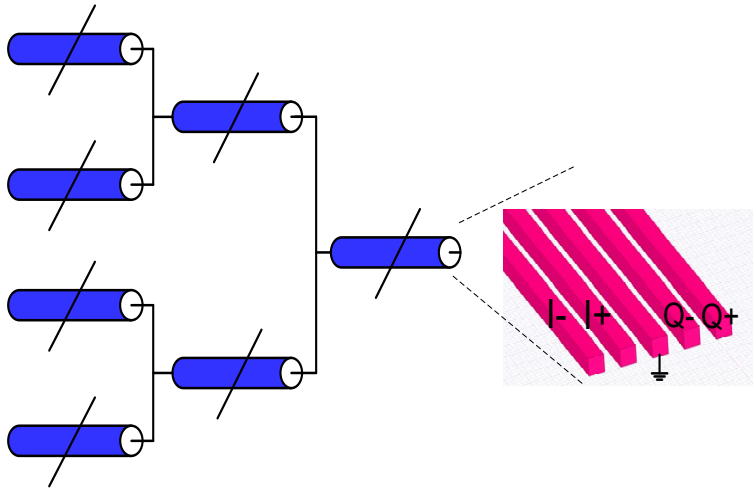

(a) Binary global LO wires routing

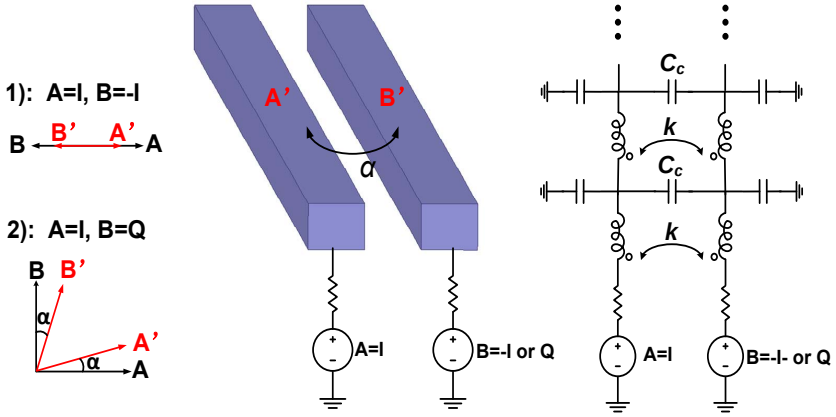

(b) Adjacent LO wires coupling

Figure 3.15: Global routing and placement for LO wires

3.5.4 LO phases distribution

Identical and precise LO waveform is expected to distribute from LO generator to four channel receivers, which impacts array characteristic. Binary tree structure shown in Fig. 3.15a is utilized for global routing to ensure identical length to four channel receivers. In addition, phase sequence of routing wires have to be properly planed. In our case, adjacent wires have either 90° or 180° phase difference. Magnetic and

capacitive coupling between two wires impact phase and magnitude property. As shown in Fig.3.15b, Let $I = \cos\omega_{LO}t$ and $Q = \sin\omega_{LO}t$ be the signal on wire A and B without coupling, and α be the coupling factor of adjacent two wires. Consider the following two cases, and The other cases can be derived similarly.

1. A=I and B=-I: then A'=$(1-\alpha)\cos\omega_{LO}t$ and B'=-$(1-\alpha)\cos\omega_{LO}t$
2. A=I and B=Q: then A'=$\sqrt{1+\alpha^2}\cos(\omega_{LO}t-\varphi)$[3] and B'=$\sqrt{1+\alpha^2}\sin(\omega_{LO}t+\varphi)$

Where A' and B' are signals on wire A and B after coupling included, and $\varphi = \arctan(\alpha)$. The results in case 1) gives reduced magnitude by factor of $(1-\alpha)$ but precise phase. The results in case 2) yields increased amplitude by $\sqrt{\alpha}$ with phase error of 2φ. To maintain good phase accuracy, the placement of wires are shown in dotted circle of Fig. 3.15a. The middle ground line is for isolation between quadrature differential wires.

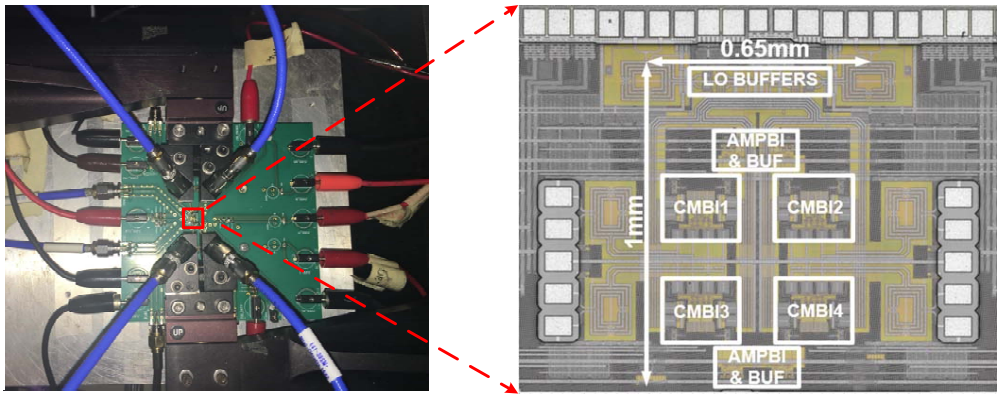

(a) (b)

Figure 3.16: (a) Printed circuit board (PCB), and (b) chip micrograph

[3] $P\sin(\omega_{LO}t)+Q\cos(\omega_{LO}t)=\sqrt{(P^2+Q^2)}\sin(\omega_{LO}t+\varphi), \varphi=\arctan\frac{Q}{P}$

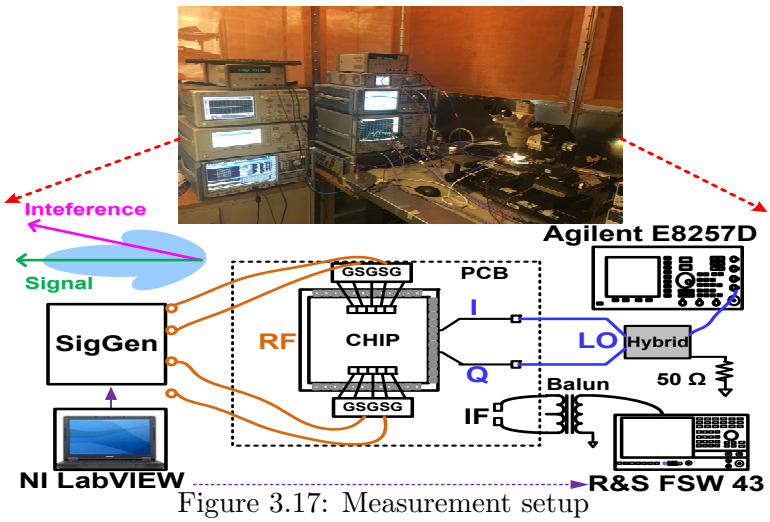

Figure 3.17: Measurement setup

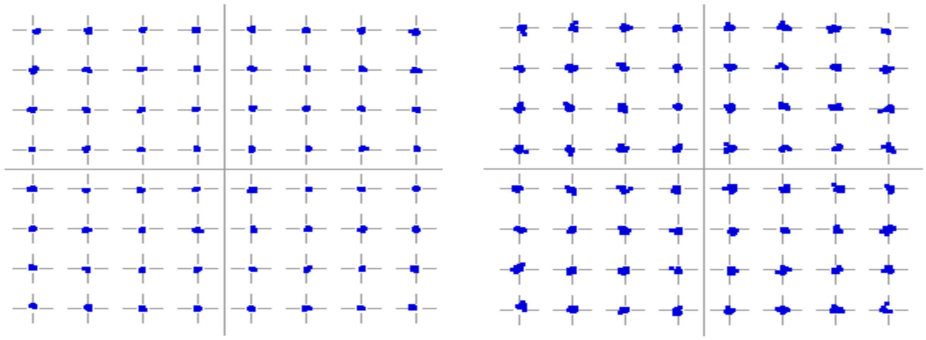

(a) EVM = 1.12%

(b) EVM = 2.08%

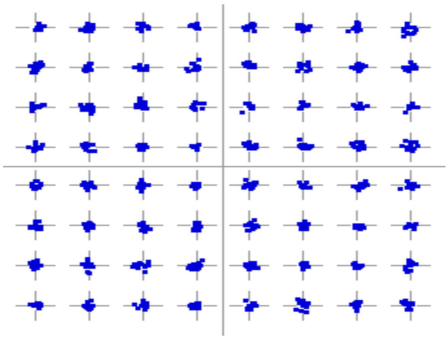

(c) EVM = 2.79%

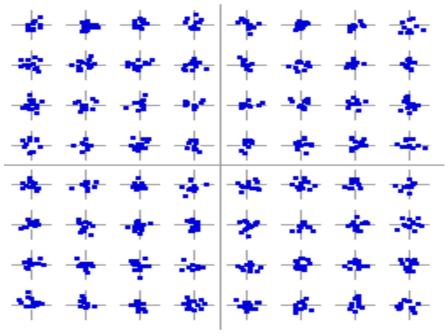

(d) EVM = 4.21%

Figure 3.18: Measured constellations for 64QAM at symbol rate of (a) 1MS/s, (b) 3MS/s, (c) 5MS/s and (d) 10MS/s

3.6 Measurements

For this first prototype a complete receiver chain was not realized to limit risk while illustrating the design principles. We did not include an LNA or extensive IF stages. However, the critical differential beamforming blocks for the proposed architecture was implement by slightly modifying pre-existing receiver components. The micrograph for the chip fabricated in TSMC's 65nm GP CMOS process is shown in Fig. 4.13. The active area (excluding test circuits) is $0.65mm^2$. The four channel receiver draws 55mA current from a 1V power supply, and the LO buffers consume 23mA.

The measurement setup for array characterization is shown in Fig. 3.17. For initial testing 4-channel CW signals were generated by Labview control of a 4-port Rohde&Schwarz ZVA 67 network analyzer. The four channel signals are input to the chip via two GS-GSG probes. On-chip 50Ω resistors are placed at RF inputs to provide termination and to convert the signals from single-ended to differential. The 7.78GHz LO signal is provided by an Agilent E8257D, power-split into I and Q by an off-chip hybrid, and fed via bond wires to the chip. A balun converts the LO signals into differential. The four-channel IF outputs are connected to a Rohde&Schwarz FSW43 Spectrum Analyzer via an off-chip balun to measure the signal power at Y_1, Y_2, Y_3 and Y_4. For array pattern measurement, the ZVA was set up in coherence mode. The measured normalized array patterns with 5° measurement steps, for the four-channel outputs at different input phases are shown in Fig. 4.19. Consider the output at Y_1 as an example: here a broadside beam at 0° is constructed, while signals at spatial angle of +30°, ±90° and −30° are nulled out. The measured null-depths for 30°, −30° and ±90° spatial angles are 24.5dB, 26.2dB and 23.4dB respectively. The other beams at spatial angle of 30°, −30° and ±90° have similar results. The measured null-depths is always better than 19dB, is limited by the phase balance of the off-chip hybrid. Measured RF bandwidth is 2.5GHz centered at 7.8GHz. Single channel noise figure for this design does not translate easily for multi-beam designs.

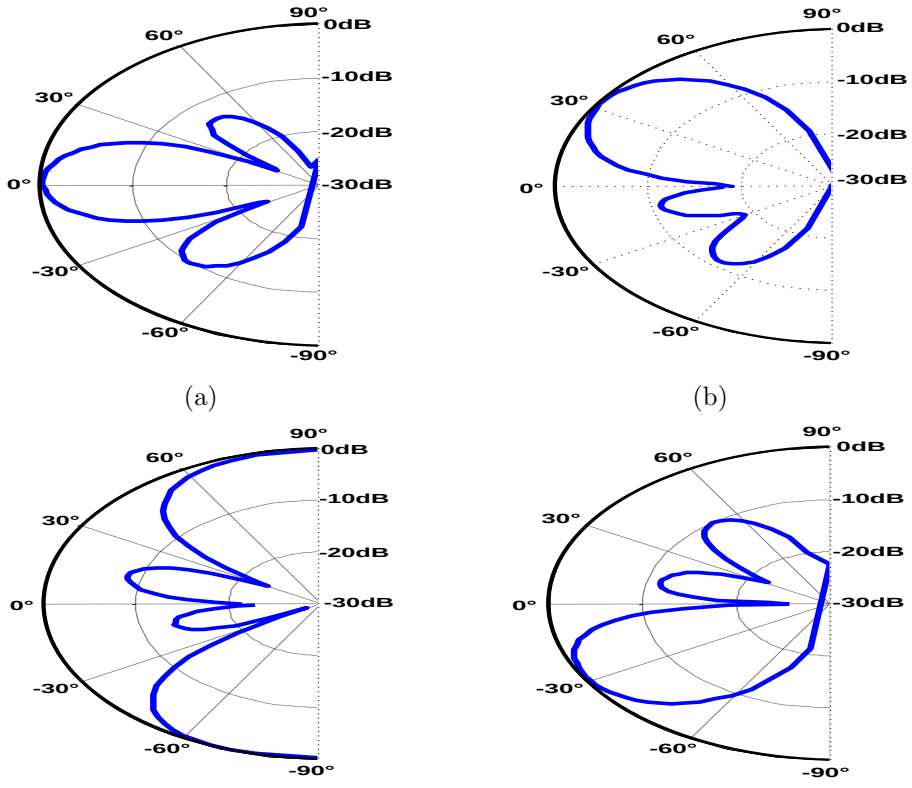

Figure 3.19: Measured normalized array patterns for the receiver at (a) P_5, broadside, (b) P_6, $+30°$, (c) P_7, end-fire, and (d) P_8, $-30°$

Next, we measure receiver EVM for different symbol rates. The setup remains the same except we send single modulated signal for all four channels. The 7.8GHz modulated signal is generated via a Rohde&Schwarz SMW vector signal generator. The power splitters divide modulated signal equally to the inputs of the four-channel receiver. The measured EVM by FSW43 is 1.12%, 2.08%, 2.79% and 4.21% for symbol rate of 1MS/s, 3MS/s, 5MS/s and 10MS/s respectively.

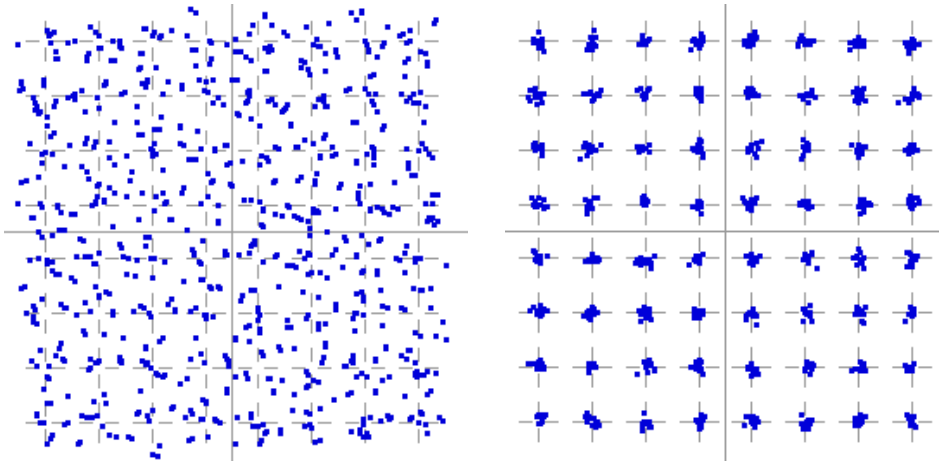

(a) EVM=11.15% (b) EVM=3.17%

Figure 3.20: Measured constellations (a) without and (b) with interference nulling

Third, we test the system EVM with and without interference nulling. Now we send composite signals for all four channels. The desired modulated signal, generated via a one port of SWM, is provided broadside at 7.8GHz. The interference signal, generated via the another port of the SMW, is provided once at broadside and once at 30°. The measured EVM for the 64QAM 1MS/s broadside beam, i.e., without interference nulling, at Y_1 is 11.15% as shown in Fig. 3.20a. While the measured EVM for the same beam when the interference is at 30° is 3.17% showing the benefit of interference nulling.

In a normal MIMO system we use the information from all four antennas. Our design, that has spatial filtering is also capable of supporting a full MIMO system as the original 4 antenna signals can be reconstructed after RF/analog beamforming. However, the proposed design has a significant advantage over four independent antennas. In the case of four independent antennas a single interference would overload all four receivers. This design also mitigates RF/analog overload by interference to improve MIMO performance.

The performance comparison is summarized in Table 4.1. A direct comparison with other designs is not straightforward, as Butler matrix publications typically remain at RF. In addition, other publications use explicit Butler matrix to create beamforming (that means they need more power and size for other RX or TX components), but ours implements beamforming implicitly by reusing existing receiver components. References [31, 36] do not specify null-depths, but was estimated from the array patterns

and is limited to 20dB worst case. The closest comparison [31] implements a full MIMO system based on a Butler matrix. We have developed an easily extendable design with partial spatial filtering.

Ref. No.	**Tech.**	**Beam No.**	**Topology**	**Area (mm^2)**	**Cent. Freq. (GHz)**	**Pass. Loss (dB)**	**Null-depth (dB)**
[31]	90 nm	4	TRX + Butler	14.28[1]	25	>2-4[2]	—[3]
[32]	32 nm	4	Butler only	0.64	11	>5	—
[36]	130 nm	8	Butler only	4.75	5.5	3.5[4]	—[3]
[39]	65 nm	4	Butler only	0.072[5]	63	2.77	>17
[40]	130 nm	4	Butler only	0.71	2	1.1	>15
This work	**65 nm**	**4**	**RX w/ built-in FFT**	**0.65**	**7.8**	—	**>19**[6]

[1] Butler matrix occupies approximate 1/4 of the total size. [2]The hybrid loss is 1-2dB[48]. [3] 15-20dB from array factor, but not directly specified. [4]By simulation. [5]Higher operation frequency. [6]Can be improved by calibration.

Table 3.3: Performance comparison of FFT based receiver

3.7 Future Investigation:Extension for spectral channelization

The prototype proposed is used for spatial channelization. Due to the similarity between spatial and spectral filtering, our proposed prototype and the distributed computation concept can also be used for spectral channelization. The left work is how to configure the center frequencies of sub-channels. Due to the difficulties of RF sampling and continuous operation mode of our prototype, we can use other types of tunable delay elements to config the center frequency of each subband, such as tunable transmission lines [49, 50], or controllable active analog delay [51, 52]. Different from previously reported analog FFT based spectral channelization, the extension of our prototype start partial spatial filtering earlier at RF before down-conversion to improve system linearity.

3.8 Conclusions

In this work, a new FFT-based four-channel four-beam receiver architecture for independent beams generation for MIMO is reported. The beamforming is implemented in

the way of *explicitly shifter-less by reusing by reusing existing blocks* in receiver. Analogous to an FFT, the design utilizes shared computations to generate four simultaneous beams with improved performance, including: a) Removal of large passive components to realize the multiple beams; b) Utilizing distributed computations (including signal combinations and phase shifting) resulting in partial spatial filtering from RF to IF resulting in better interference tolerance in comparison to IF beam forming; c) Uses larger phase steps than a Butler matrix. For example, a four-beam Butler matrix needs 45° phase resolution, while our design needs 90° resolution. The connection between Butler matrix, FFT and phased arrays are well know. However, we have exploited the architecture of integrated receivers to reduce the number and complexity of phase rotators and combiners. Higher order beams can be formed by combining multiple lower order systems. The savings increase as the number of channels increase. The proposed prototype can be extended for transmitter and spectral filtering as well.

Chapter 4

ILO Based channelized wideband phased array receiver

4.1 Introduction

As the data rate goes up every year in wretched wireless communication environment, it's critical to improve wireless communication reliability and capacity. This can be achieved by increasing diversity gain and multiplexing gain when time, frequency and spatial degree of freedoms available. To improve the communication reliability, the information has to communicated in a redundant way either in time, frequency or spatial domain to increase the diversity gain. Redundant communication in time domain decreases data rate, contradicting data rate requirement and stressing the importance of degree of freedom in spectral and spatial domain. More capacity can be achieved in the way of more multiplexing gain by utilizing frequency and spatial degree of freedoms. Wideband and multi-antenna-multi-beam system become more and more important, because they provide additional degree of freedoms in spectral and spatial domain respectively to improve reliability and capacity.

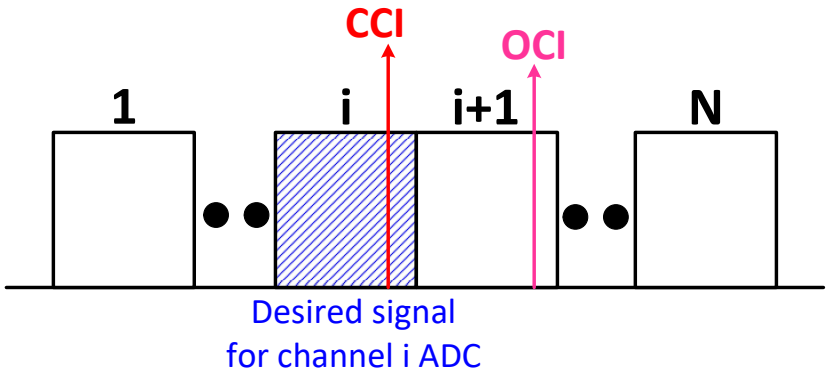

Figure 4.1: OCI and CCI for wideband signal

Interference limits wireless system performance. There are two types of interference for wireless transceiver as exemplified in Fig. 4.1: one is co-channel interference (CCI) which locates in the same channel as desired signal, and the other is out-of-channel interference (OCI) that is outside the desired signal channel. Out-of-channel interference can be mitigated by spectral filters, such as channelized receiver [53, 54]. Co-channel interference can be reduced by spatial filters, such as phased array. In Fig. 4.1,after simultaneous spectral and spatial filtering, both CCI and OCI are filtered out, and only narrow band signal shown as blue shape is feed into ADC. This reduces ADC dynamic range requirement and power [55, 56]. It becomes increasingly important for multicarrier radar systems that use instantaneous wide bandwidths multifunction (imaging and communication) systems [57].

There have been a couple of ways to achieve wideband phased array. The first one is using transmission line based delay elements to compensate input wave delay difference [49]. This way is straightforward and attain most publication focus, but it takes a large chip size. The second one is adopting analog delay circuit to implement delays along different paths [52]. This architecture is limited to be used in low frequency applications, since phase and frequency relationship deviates from linearity as frequency goes higher. The third one is based on spectral channelization [58]. It divides a wideband spectrum into a wide range of carrier frequencies with smaller instantaneous bandwidth for each. The additional advantage of this architecture is it has simultaneous spectral and spatial filtering to remove the interference. However, even though the beam squinting for each sub-channel has been resolved by smaller fractional bandwidth, the beam

squinting among sub-channels (or sub-carriers) has not been resolved. This means the beams associated sub-carriers point to different spatial directions. This drawback hinders the architecture being used in many wireless communication systems. For example, in point-to-point communication, the beams (for all sub-carriers) from transmitter and receiver have to be aligned to accommodate high path loss and make information secure in wireless environment. In addition, To the author's best knowledge, all the existing wideband schemes place delay elements or phase shifters at the signal path, which directly impact wireless receiver performance, such as noise figure, gain, and bandwidth, negating performance improvement by phased array.

This chapter describes sub-harmonic injection locked oscillators (ILO) based channelized wideband phased array, which not only get rid of delay elements and phase shifters in the signal path as conventional narrowband LO based phased array, but also address the beam squinting issues among sub-carriers. Section II presents the new system architecture. Section III describes the circuit designs and Section IV shows the measurement results. Section V concludes the paper.

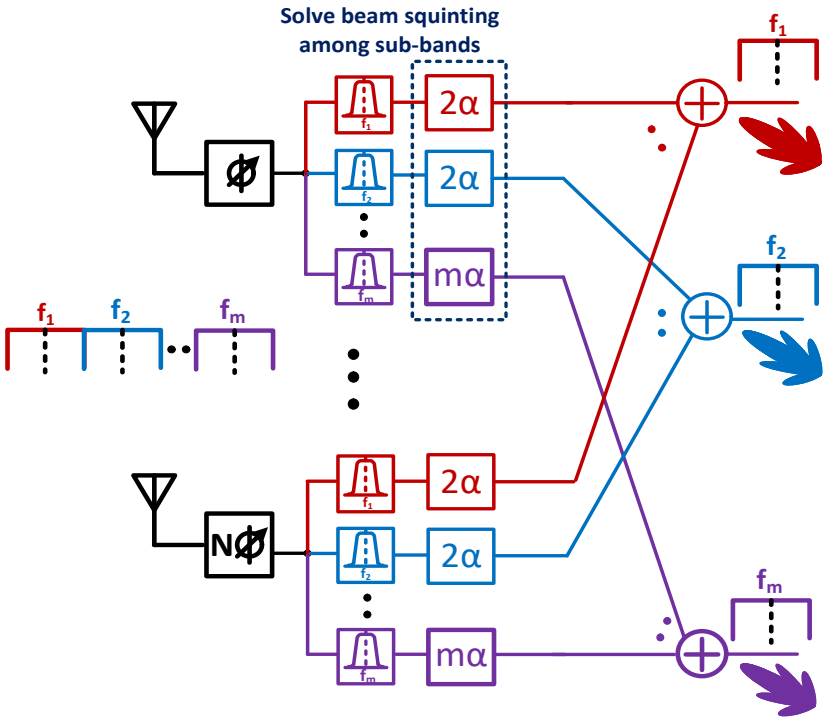

Figure 4.2: Conceptual scheme to compensate beam squinting among sub-bands

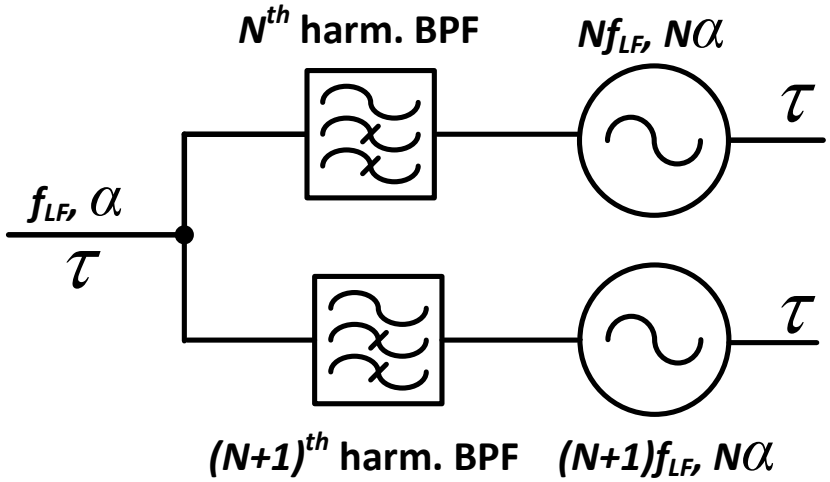

Figure 4.3: Proposed LO scheme to overcome beam squinting

4.2 Solutions for beam squinting

Realizing wideband arrays using traditional phase compensation techniques has limitations due to the beam-squinting problems associated with the difference between phase and delay. A beam direction delay can be compensated at a given frequency by a fixed delay. However, the amount of phase compensation required changes with frequency and causes beam-squinting.

Before we consider actual architecture, let's looks at the possible schemes to solve the beam squinting issue by frequency channelization. We can see that by spectral channelization, the beams squinting issue can be mitigated for each sub-band due to decreased fractional bandwidth. However, the beam squinting issue among sub-bands still exist. In order to resolve this, as shown in Fig. 4.2, we have to add one more phase shifter for each sub-band, with the phase difference value of $\alpha = \Delta f \tau$, where the Δf is the frequency difference of sub-carriers of two adjacent sub-bands. This compensation consequently makes center frequencies of all sub-bands experience the same delay difference. However, direct implementation of the additional phase shifters results in more system complexity and design effort. Fig. 4.3 illustrates input-outputs frequency and phase relationship for sub-harmonic ILO. For ILO input with frequency f_{LF} and phase α, by sub-harmonic injection locking, the output frequency and phase for two path become Nf_{LF} and $N\alpha$ after N_{th} harmonic, and $(N+1)f_{LF}$ and $(N+1)\alpha$

after $(N+1)_{th}$ harmonic. The phase difference between two-channel frequency outputs, α, can be used to resolve the beam squinting issue among sub-bands. In other words, the different frequency ILO outputs equivalently provide the same delay, other than the same phase, for sub-bands to resolve beam-squinting issues among them.

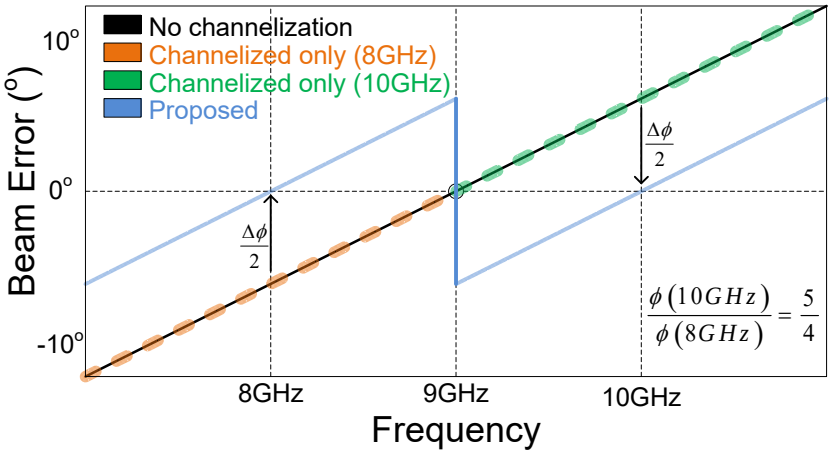

Figure 4.4: Phase error vs. frequency for wideband phased array

The squint angle for a wideband phased array is given by Eqn (4.1), where Θ_0 is the desired beam angle, $\phi(\Theta_0, f_0)$ is the necessary phase compensation required at the band center, f is the frequency of operation, c is the speed of light and d is the inter-antenna spacing.

$$\Delta\Theta = \arcsin\left[\frac{\phi(\Theta_0, f_0)\cdot c}{2\pi f \cdot d}\right] - \Theta_0 \tag{4.1}$$

The beam error vs. frequency for three different cases is shown in Fig. 4.4. Case 1, shown with the black line is the case when no channelization is done. Case 2, shown in orange (center at 8GHz) and green (center at 10GHz) is shown for the case when the total bandwidth is broken up into two bands. We note that the beam error remains the same. This is because there is an extra phase delta necessary to compensate for the sub-band center frequencies of 10GHz and 8GHz. In our architecture we injection lock to the 4^{th} and the 5^{th} harmonic of the 2GHz input. Note, in Fig. 4.5 that the progressive phase per antenna (ϕ and 2ϕ) is included before frequency multiplication. The frequency multiplication process multiplies the total phase such that the phase offset for the 5^{th} harmonic at 10GHz is greater than for the 4^{th} harmonic at 8GHz. This

extra phase is exactly what is needed to offset the band center frequency phases such that we get the blue proposed line in Fig. 4.4. Note, we show straight lines for simplicity in Fig. 4.4. However, the actual lines are somewhat curved due to the arcsin.

The proposed channelization method reduces the beam error by N times, where N is the number of frequency channelization. For example, for our prototype design, the numerical values for the worst case beam error in the non-channelized design for a desired beam direction of -36^o from broadside is 13.1^o, while the worst case beam error for our two band design is 7.7^o. Additional channelization could be used to reduce beam error even further.

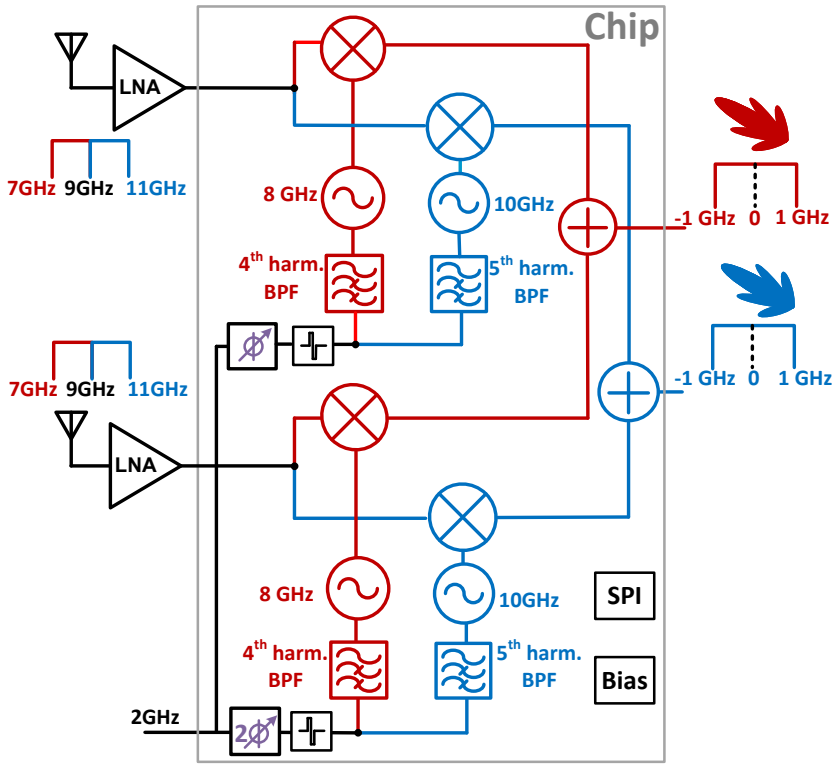

Figure 4.5: Proposed low squint wideband phased array architecture using sub-harmonic ILO based channelization

4.3 System architecture

The proposed system architecture is shown in Fig. 4.5. The design of this chip is 2-antenna wideband phased array receivers. For each antenna receiver, a wide-band LNA (WBLNA) receive 7GHz to 11GHz wideband signal, and then down-converted into two sub-bands by two different LO paths of 8GHz and 10GHz. Each sub-band has 2GHz instantaneous bandwidth at baseband. This process provides spectral channelization.

The LO path consists of phase shifters, pulse-slimmers, band-pass filters (BPFs), and ILOs. Driven by common LO input, the phase shifters provide 2GHz LO signal with phase difference of ϕ. The pulse slimmer created a reduced duty cycle of this signal that is harmonic rich in the 4th and 5th harmonics. In the 8GHz path, a BPF is tuned to select 4th harmonic and suppress the other undesired ones. A ILO tuned at self-resonance of 8 GHz is placed after BPF, and injection locked by BPF output, generating 8GHz LO with phase difference of 4ϕ for downconversion mixer. In a similar way, for 10 GHz LO chain, the tuned BPF selects 5th harmonic of the same pulse slimmer output, followed by a 10 GHz self-resonated ILO, generating 10GHz LO with phase difference of 5ϕ for downconversion mixer. Now we can see the LOs not only provide different LO frequencies required by frequency sub-bands in spectral channelization, but also generate different phase differences for frequency sub-bands. We can also see the ratio of phase difference for two frequency sub-bands, that is $5\phi/4\phi$, is the same as the ratio of LO frequencies, which is 10/8. As what we discussed before, this is equivalent to use the same delay difference of $\tau = \phi/2G$ for each frequency sub-band to overcome beam-squinting issue among two-sub-bands.

For phase shifting of each antenna receiver, there is only one narrow-band and low frequency phase shifter at LO. Different from signal path requiring bandwidth, the LO is a single tone, and thus the phase shifter dictates less power and size. The other parts for each antenna are similar as conventional wideband receiver. The beam squinting issue among sub-bands are solved together with spectral channelization requirement of wideband receiver.

We can see in an analogous way to channelized wideband phased array, our ILO based approach can also mitigate beam-squinting for each sub-channel by reducing fractional bandwidth, and achieve simultaneous spectral and spatial filtering to reduce

ADC dynamic range requirements. Different from conventional implementation, our proposed design achieve beam squinting less among sub-bands by injecting LO signals with the same progressive delay for sub-bands, making channelization wideband phased array feasible. Each antenna receiver is similar as conventional ILO based wideband phased array. A narrow band and low frequency phase shifter for each antenna receiver is placed at LO to achieve wide band phased array. Both the number of antennas and frequency bands can be extended to arbitrary numbers to facilitate practical system requirements.

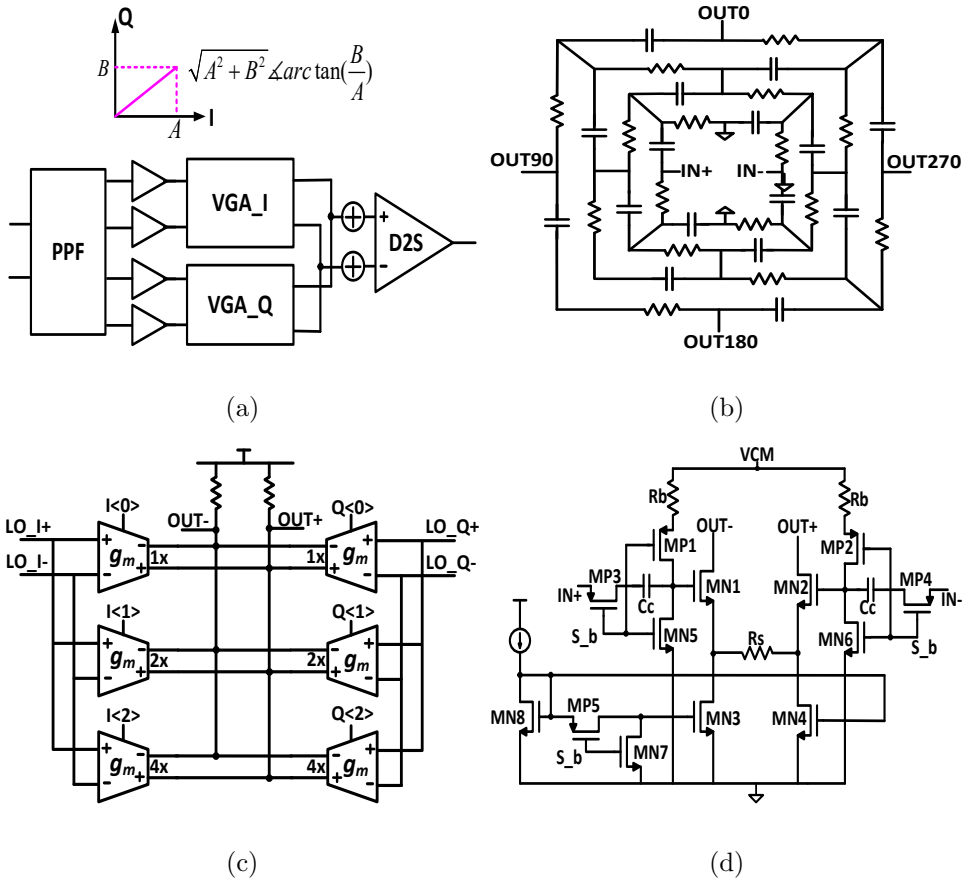

Figure 4.6: (a) Phase shifter, (b) PPF, (c) I and Q interpolator, and (d) g_m cell

4.4 Circuit design

The circuit details are explained and shown in this section.

4.4.1 Phase shifter

The phase shifter as shown in Fig. 4.6a is implemented as weighed vector modulator. It consist of four stage poly-phase-filter (PPF) that generate quadrature signals, variable gain amplifier (VGA) with the I/Q weights controlled by digital, and differential to single-ended conversion (D2S). Different output phases are controlled by digital codes of VGA.

PPF: The role of PPF in Fig. 4.6b is to generate differential quadrature signals. Theoretically PPF only has to be narrow band. We extend the bandwidth by implementing four stage to tolerate process variation.

VGA: The VGA architecture is shown in Fig. 4.6c. It starts with 3 bits Gm-cells for I and Q LO paths. The interpolated output current go through load resistors, generating desired phase. The different phases can be configured by the ratio of "on-state" Gm-cells number of I and Q LO paths.

The Gm-cell in Fig.4.6d is constructed based on source degenerated differential pair, consisting of MN1-MN4 and Rs, where MN1/2 are input differential pair, and MN3/4 provide tail current.

Two capacitors Cc at inputs provide AC coupling for input signals, and two resistors Rb and VCM give bias for input pair. All the others are switches that control the "on" and "off" states of the cell: when s_b is zero, MP1-MP5 are closed, and MN5-MN7 are open, then the cell is in "on" state. when s_b is one, MN5-MN7 are closed, and MP1-MP5 are open, then the cell is in "off" state.

It should be noticed that sub-harmonic injection scheme can extend phase range. Our design uses 4th and 5th harmonics, so only 90° other than 360° phase shift is needed to cover full spatial range. The swapping devices for reversing phase in conventional phase shifter can be removed, simplifying phase shifter design.

D2S: The D2S at backend not only converts differential signal into single-ended, but also amplify the signal into full swing for the pulse slimmer.

4.4.2 Pulse slimmer

The function of pulse slimmer is to maximize the 4th and 5th harmonics and suppress the other unwanted harmonics by changing duty cycle [54] . As shown in Fig.4.7, two-stage semidigital circuit is designed to achieve this: duty cycle adjustment (DCA) stage and differential to single-ended conversion (S2D).

The DCA is implemented by NANDing two paths. Compared to upper path, the lower path has one more inverter and R-C delay. The value of resistor R, implemented by MOS transmission gate, are controlled externally. The duty cycle of inputs of DCA is nearly 50%, and output is about 14%, the value of which maximize the 4th and 5th harmonics, and suppress all the other unwanted ones. The following S2D plays two roles: one is to further shape spectrum to highlight 4th and 5th harmonics. The other is to generate differential signals needed for BPF and ILO.

4.4.3 BPF

The role of BPF is to increase the amplitude of desired harmonics, and to decrease the amplitude of the undesired ones. The lower order undesired harmonics have larger amplitude, which potentially saturate the input g_m stage and desensitize it regarding desired harmonics.

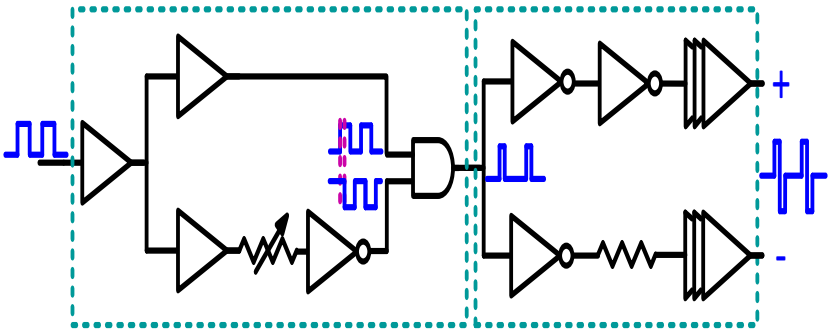

Figure 4.7: Pulse Slimmer

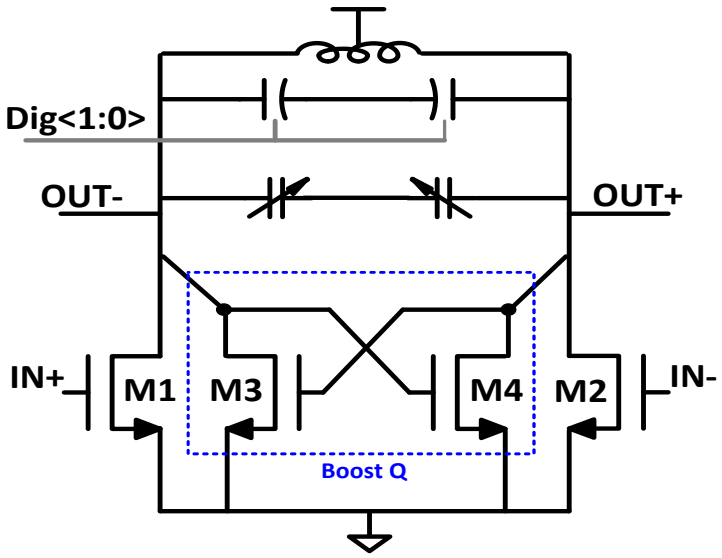

Figure 4.8: Band pass filter

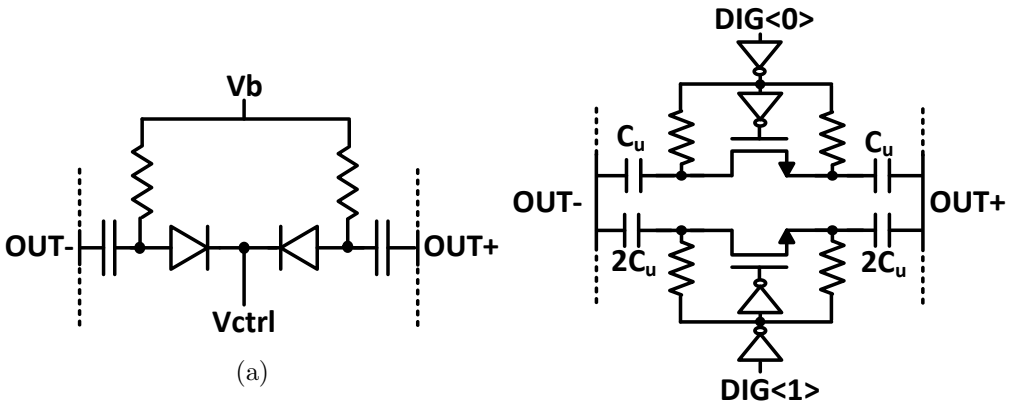

Figure 4.9: BPF Bias details for (a) varactor, and (b) capacitor bank

The BPF in Fig. 4.8 is based on injection locking scheme. It consists of one differential input pair, one cross-coupled pair (X-pair), and L-C tank. Here The X-pair pair has smaller size compared to input differential pair. The X-pair pair offers increased Q of the L-C tank. This not only increases the gain for desired 4th and 5th harmonics, but also rejects undesired harmonics by f_u/f_L, where f_u is the offset frequency at undesired harmonic and f_L is the frequency at single-sided lock range. L-C tank has one

symmetrical differential inductor, 2 bits capacitor tank for discrete tuning, and varactor for continuous tuning. Two designs are implemented at 8GHz and 10GHz for two sub-bands, where the size of capaitor and varactor are the same, but the inductor value is changed to accommodate different frequencies.

The bias detail for varactor is shown in Fig. 4.9 (a), where V_{ctrl} can be adjusted from 0 to VDD. For the 2 bits capacitor bank bias, it exploits the differential operation of oscillator, and reduces switch size to half, mitigating its parasitic impact on frequency tuning range. The inverters are minimal-size devices. In addition, when the switches are turned off, the drain and source are pulled up to Vdd, which further improves the off-state resistance by body-effect. The bias schemes here are applied to ILO either.

4.4.4 ILO

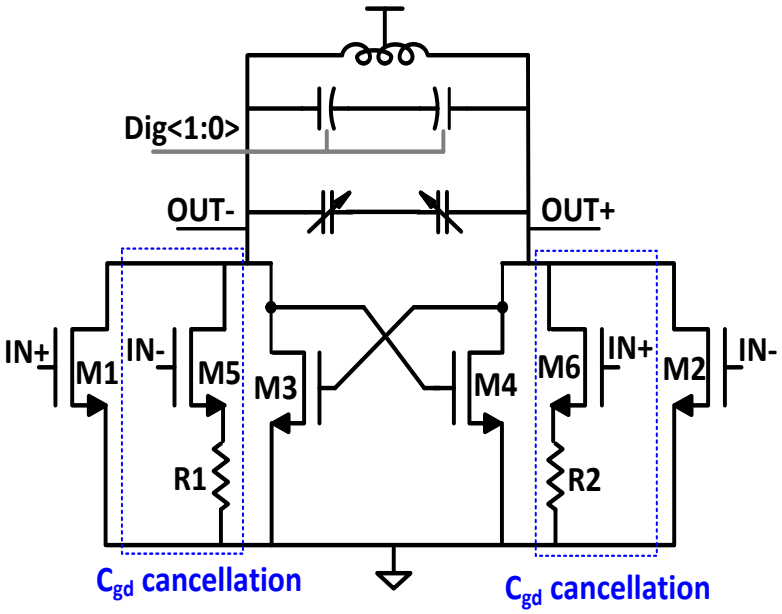

Figure 4.10: Injection locked oscillator

ILOs attains the similar topoloty as BPFs. The difference is that along with primary X-pair maded by M3 and M4 needed for oscillation, we add another auxiliary X-pair consisting of M5, M6, R1 and R2. M5 and M6 have the same aspect ratio as M1 and M2, and R1 and R2 are large resistors to make current through M5/M6 less than 1/10 of that though M1/M2. The drain of M5/M6 is connected to that of M1/M2, but

the gate is M5/M6 is connected to that of M2/M1. The equivalent circuit is shown in Fig. The $C_{gd}{}'s$ of M5/M6 play neutral capacitor for $C_{gd}{}'s$ of M1/M2. This auxiliary X-pair has two main functions: one is providing isolation between LC-tanks of ILO and BPF to avoid high order modes oscillation. The other is reducing the parasitic capacitance added by injection circuits, which decreases the frequency tuning rage of oscillator. Compared to the folded-cascode scheme in [59] where cascode clamps the drain of injection transistor, our proposed method is much more power efficient because of push-pull class-AB operation in simulation.

4.4.5 Balun

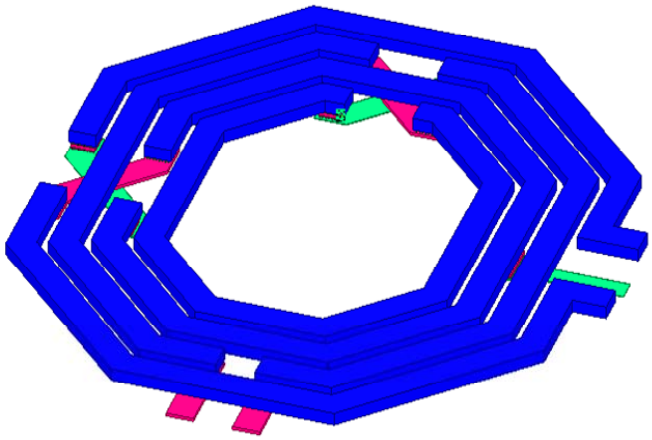

Figure 4.11: Balun for the wideband phased array receiver

The octagon symmetric balun in Fig. 4.11 are implemented for single-ended to differential conversion [46] and input impedance match. To ensure proper amplitude and phase balance, the top layer metals are interwound symetrically along horizontal and vertical directions. The secondary topmost layer is used for crossover. The secondary center-tap is placed at mid-point.The primary and secondary has 90° angle rotation for top layout connection with other blocks.

4.4.6 Mixer

The active Gilbert mixer is implemented for down-conversion. The bias current is provided in the way of current mirror instead of at common source to accommodate voltage headroom requirement. Regarding the mixer load, a single larger resistor load yields good noise and gain, but make the circuit suffer voltage headroom issue. A single PMOS load results in appropriate voltage headroom, but leads to deteriorated noise performance. The composite load of resistor and PMOS is adopted, which tradeoff performance among voltage headroom, noise and gain.

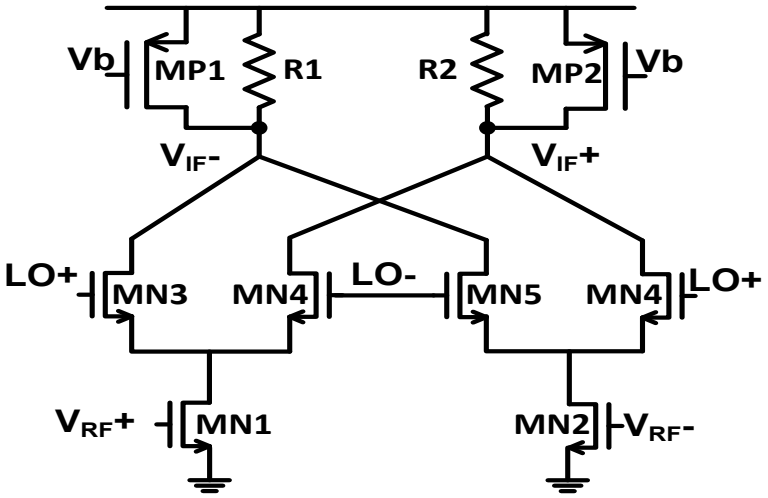

Figure 4.12: Mixer

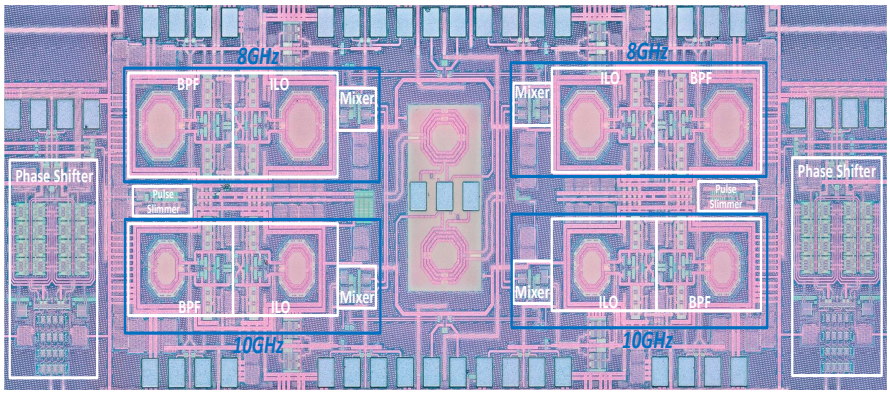

Figure 4.13: Chip micrograph

4.5 Measurements

The micrograph for the chip fabricated in TSMC's 65nm CMOS process is shown in Fig. 4.13. The active area of the chip is $2.7mm^2$. The BPFs and VCOs operate at 0.5V supply, and the phase shifters operate at 1.5V. All the other blocks are operated at 1V. The overall power consumption is 63.5mW.

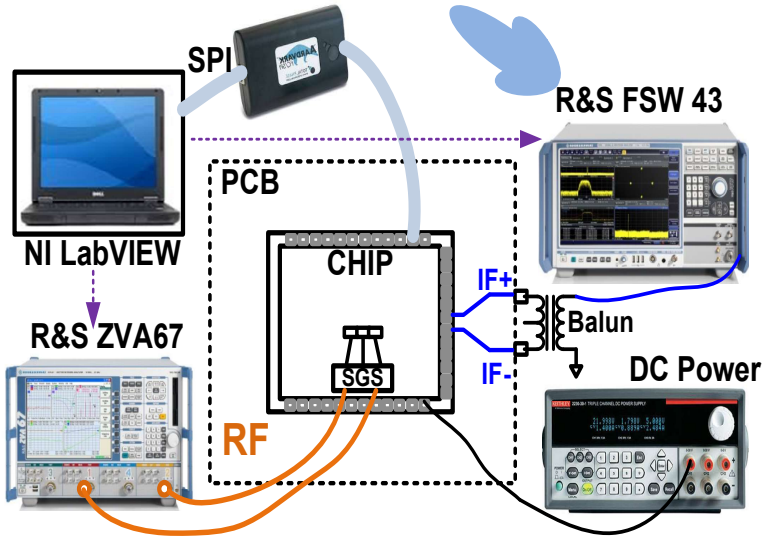

Figure 4.14: Measurement setup

For our measurement setup shown in Fig. 4.14, the two RF inputs are connected to a R&S ZVA67 network analyzer via SGS probes. A R&S SMW signal generator supplies the 2GHz LO signals. The outputs are connected to a R&S FSW43 spectrum analyzer via an off-chip balun. Additional on-chip GSSG PADs (via buffers) are used to characterize the ILO performance. A Total Phase AArdvark SPI host adaptor provides the necessary interface for the on-chip register setup. The entire measurement setup is controlled via Labview for accurate beam pattern generation. The measured return losses for the two RF inputs are better than -12dB over the frequency range of 7GHz to 11GHz.

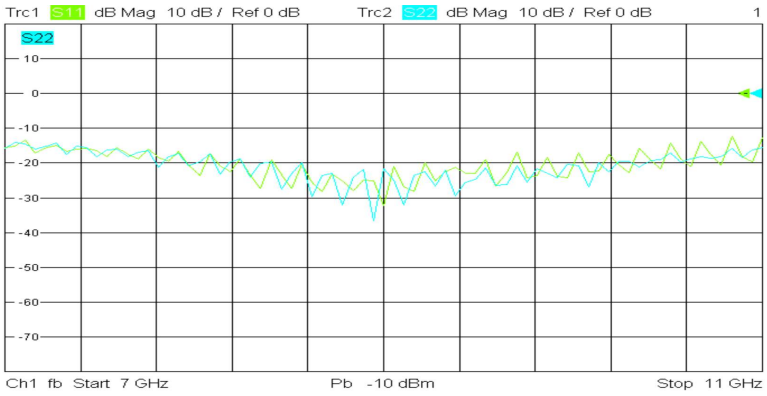

Figure 4.15: Measured return loss of two channels RF inputs

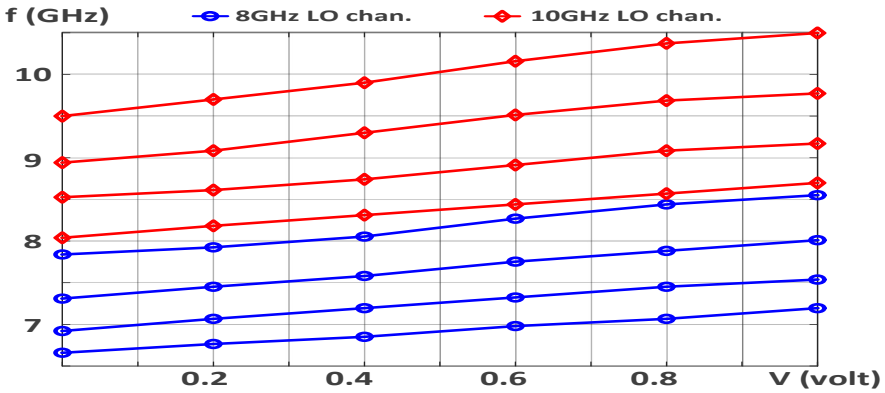

Figure 4.16: Measured frequency tuning range of 8 GHz and 10 GHz LO channels

GSSG PADs after the ILO test buffers were connected to a FSW43 Spectral Analyzer to evaluate LO performance. Two digital bits for the capacitor array and a varactor were used to adjust the ILO center frequency. The measured frequency tuning range for two oscillators are shown in Fig. 4.16. The oscillator center frequencies varied from 6.66 GHz to 8.551 GHz for the low frequency sub-band, and from 8.04 GHz to 10.498 GHz for the high frequency sub-band. The measured ILOs phase noise characteristic for the LO at 8 GHz and 10GHz are shown in Fig. 4.17a and Fig. 4.17b respectively. The measured phase noise is -120.6dBc/Hz @1MHz offset and the measured phase noise for the 10GHz LO at the same offset was -118.1dBc/Hz. Theory suggests a 1.94dB offset which is close to the measurements.

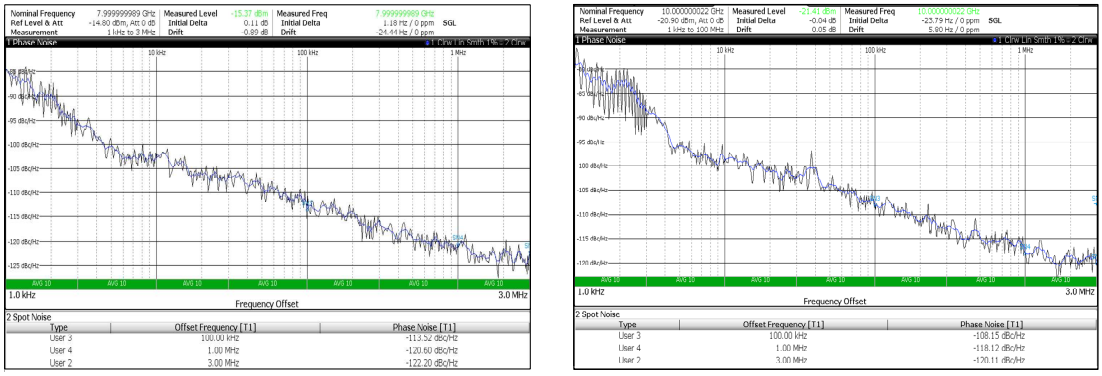

(a) (b)

Figure 4.17: Measured phase noise of (a) 8GHz, and (b) 10GHz ILO

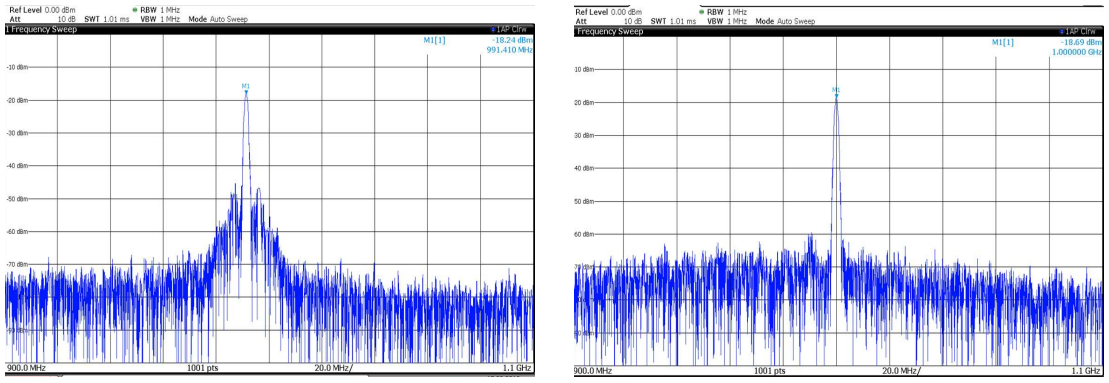

(a) (b)

Figure 4.18: Measured one tone (1GHz) baseband spectrum (a) without, and (b) with injection locking

Next, we measure the signals at baseband after down-conversion. Fig. 4.18 shows baseband spectrum without and with injection signal when RF is feed by 11GHz single tone and LO outputs approximate 10GHz. Without injection locking, the oscillator runs at about 991MHz frequency due to limited external control voltage resolution, which is very likely if the control voltage is driven by DAC. Also the close-in noise at about 1GHz is higher (The noise is expected from oscillator itself and control line). After

injection locking is enabled, the oscillator operates at exact 1GHz, and the close-in noise performance is significantly improved [60].

To accurately test wideband phase arrays the RF antenna inputs must use progressive time delays. We use a the R&S ZVA67 to generate our RF inputs. However, by default when the ZVA67 is set up in coherent mode the two signals that are generated have relative phases (instead of delays). We resolve this issue via programming the phases for each individual frequency. Specifically, for a spatial beam direction of θ corresponding to a phase difference of ϕ at 11GHz, the phase difference at 10GHz, 9GHz, 8GHz, and 7GHz are set to be $\frac{10}{11}\phi$, $\frac{9}{11}\phi$, $\frac{8}{11}\phi$ and $\frac{7}{11}\phi$ respectively. We use the same methodology to generate the equivalent phases for each beam direction and frequency.

The measured normalized array patterns for two different spatial angles are shown in Fig. 4.19. The different curves represent measurements for RF signals at 7GHz (cyan), 8GHz (black), 9GHz-(magenta), 9GHz+ (green), 10GHz (red) and 11GHz (blue). The first three are measured at the 8GHz sub-band, and the latter three are measured at the 10GHz sub-band. The left plot shows the measurements for a beam direction of -30^o and the right plot shows the measurements for a beam direction of 52^o. We can see that after channelization, i.e., reducing the fractional bandwidth, and automatic compensation for beam-squinting among sub-bands, the peaks of the beams are aligned at the desired spatial angles. In particular, the beams peaks at 8GHz and 10GHz are perfectly aligned and beams at 7GHz and 9GHz- are well aligned and the beams at 9GHz+ and 11GHz are well aligned as might be expected from Fig. 4.4.

Ref. No.	**Technology**	**Area (mm^2)**	**Channel No.**	**Delay/Phase Shifting**	**True Time Delay**	**Cent. Freq. (GHz)**	**Frac. BW (%)**	**Null-depth (dB)**	**Power/antenna (mW)**
[49]	CMOS 130nm	9.9	4	RF	Syn. T-line	8	175	-	138.75
[52]	CMOS 140nm	1	4	RF	Analog Delay	1.75	87.2	>20	112.5
[58]	CMOS 65nm	0.94	2	IF	Spectral Channel.[1a]	8	-	>19	13.7
[59]	BiCMOS 90nm	7.1	2 x 2^2	LO	No[3]	78	20	>17	168.1
[61]	CMOS 130nm	15.6	4	LO	No[3]	12	100	>12.5	86.8
[62]	CMOS 65nm	1.08	4	IF	No[3]	2.5	120	>25	23.1
This work	**CMOS 65nm**	**2.7**	**2 x 2^{2b}**	**LO**	**Spectral Channel.[1b]**	**9**	**44.4[4]**	**>23**	**31.75**

[1a] Beam-squinting not solved among bands. [1b] Beam-squinting solved among bands. [2a] 2 antenna x 2 antenna. [2b] 2 antenna x 2 spectral band.[3] Beam-squinting not considered. [4] Can be extended by more spectral bands.

Table 4.1: Performance comparison of wideband phased array

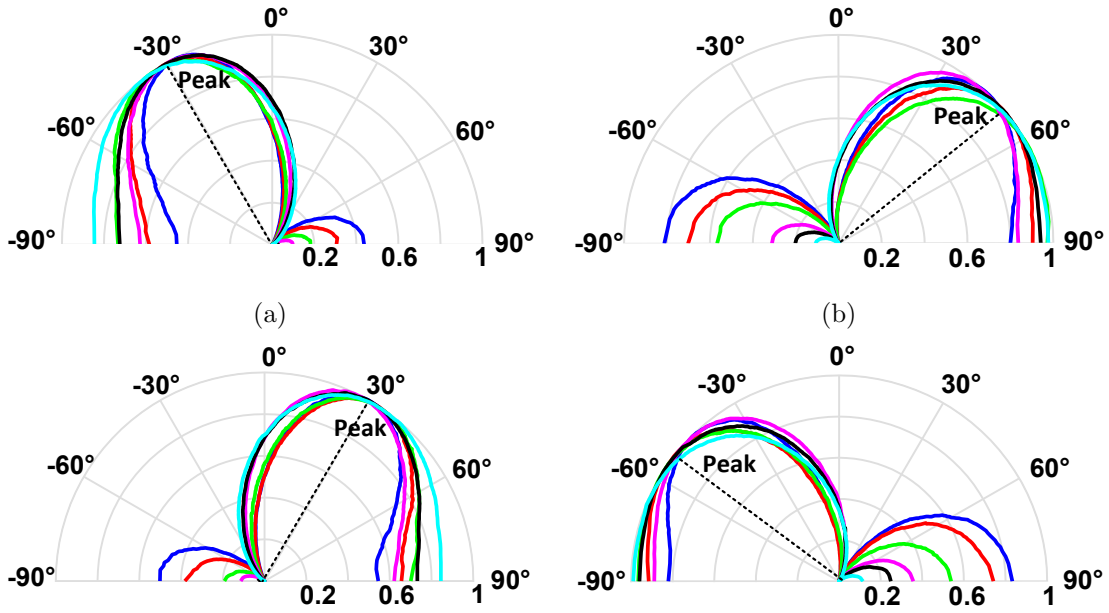

Figure 4.19: Measured normalized array patterns for the receiver at different frequencies (different colors) (a) -30^o, (b) 52^o, (c) 30^o and (d) 52^o

The measured null-depth is better than 23dB for all cases. Note, the nulls are not aligned and are a function of antenna spacing and frequency. The performance of the prototype is summarized and compared with other work in Table 4.1. Among the other designs that attempt to mitigate the beam-squinting issue, this work exhibits a smaller size in comparison to conventionally synthesized transmission line methods, and can work at a high frequency range in comparison to the analog delay approach [62]. The power consumption is lower than most of other delay/phase shifting methods except [58] and [62] which adopt IF phase shifting. Only [58] and this work feature simultaneous spectral channelization and beamforming, but [58] does not solve the beam squinting problem. This architecture reduces beam-squinting by using a combination of channelization and sub-band phase correction.

4.6 Conclusions

This paper presents a new 4GHz instantaneous bandwidth phased array receiver based on sub-harmonic injection locked oscillators with simultaneously spectral and spatial channelization. The combination of channelization and sub-harmonic injection locking synchronizes the center of the sub-bands so beam-squinting is reduced by the number of bands. The two-band prototype design realized in 65nm GP CMOS is centered at 9GHz, provides 4GHz instantaneous bandwidth, reduces beam-squinting by half, consumes 31.75mW/antenna and occupies $2.7mm^2$ of active area. Using frequency channelization and phase compensation for the two sub-bands reduces worst case beam-squinting by nearly half. Additional channelization can be used to reduce beam-squinting even further. The methodology introduced here allows for wideband phase arrays to have low beam-squinting without relying on true-time delay elements that are difficult to program and consume significant area. This work also provides the solution of LO based wideband phased array which has not been touched by prior publication. The simultaneous spectral and spatial filtering dictates less ADC dynamic range requirement and further reduces power. The injection locking scheme reduces the phase noise contribution from the oscillators, which avoid direct degradation on receiver performance, such as NF, linearity and bandwidth. The simultaneous spectral and spatial filtering dictates less ADC dynamic range requirement and further reduces power. The injection locking scheme reduces the phase noise contribution from the oscillators.

Chapter 5

Steerable FFT based multi-beam transmitter

5.1 Introduction

As channel state information (CSI) is available to transmitter, it's meaningful to create beamformig to improve wireless system performance. The power gain by beamforming can also be achieved in the transmitter side for wireless system link budget improvement. The CSI can be obtained in the following ways: In a time-division duplex (TDD) system, the transmitter can utilize channel reciprocity and measure the channel according to the opposite link. In a frequency-division duplex (FDD) system, the transmitter and use feedback information from the receiver to know the CSI.

Either conventional Butler matrix or FFT based multiple beamforming are suitable for the MIMO application in rich scattering environment, where the signals are all over the space, such as in urban city or the indoor room. However, this is not the case in the suburb, where the signal might only be from some directions. In addition, when the transmitter or/and receiver are physically moving, the beams could be away from the aligned positions to the signals. In these cases, the directions of the beams have to be changed to maximize the array gain, while each of the beams is independent of the others. Fig. 5.1 shows two scenarios to present the improvement due to steerability of beams. In Fig. 5.1a, the signals of arrival are misaligned with the peaks of the beams for fixed beams generation. In fig. 5.1b, the beams are pointing to desired

signals directions after beams steering, where the system performance is improved, i.e., the power gain are increased.

The work in this chapter solve these two problems. First, it extends the FFT based multiple beamforming introduced in chapter 2 to the transmitter design. Decimation-in-frequency (DIF) FFT architecture is adopted. Second, it presents a multi-beam steering method that can steer all the beams simultaneously while keeping each of the beams is independent of the others. It's very suitable for MIMO system where independent channels are desired.

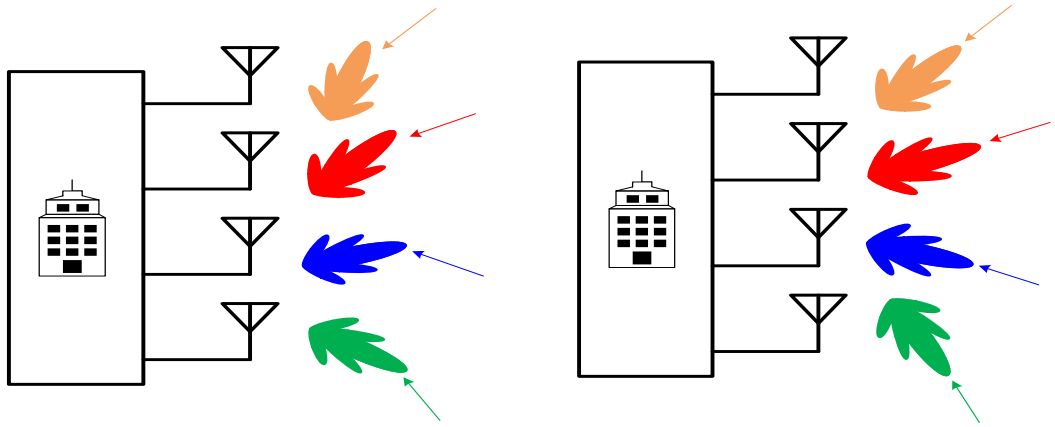

(a) Signal directions mis-aligned with the fixed beams

(b) Signal directions aligned with the steerable beams

Figure 5.1: (a) Fixed, and (b) Steerable independent multiple beams MIMO receiver

5.2 System

This section firstly presents the implementation concepts, and then presents our proposed architecture.

5.2.1 Replication and Combination

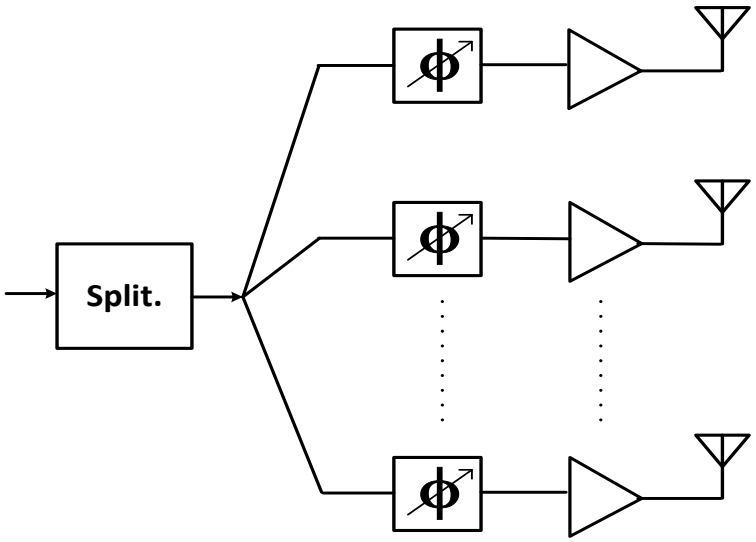

Figure 5.2: Phased array transmitter

Before moving forward, let's revisit conventional one-beam phased array transmitter in Fig. 5.2. It consists of one splitter and M phase shifters followed. The function of splitter is nothing but to generate the same signal for M paths. For active implementation, this can also be done by replicating the signals in voltage domain in CMOS technology, where the input impedance of source coupled differential pair exhibits large input impedance. Fig. 5.3 shows one example of "replication", where the differential output of the buffer or amplifier is connected to M source coupled differential inputs. In addition, in order to accomplish sharing of phase shifters among different paths, it's also expected to combine the signal before the phase shifting, which can be easily done in current domain by reusing pre-existng components in transmitter, as what we have done for receiver before.

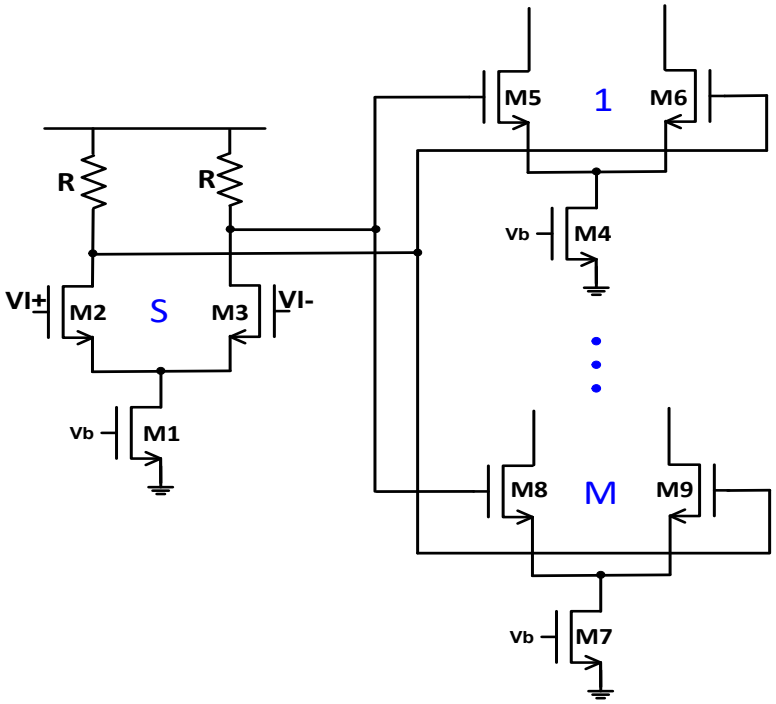

Figure 5.3: Active implementation of splitter

5.2.2 Transpose and DIF-FFT

Let's first look at the transmitter architecture of generating fixed multi-beams, where the concept of RF/analog FFT based multi-beam generation is adopted here. Because of duality between receiver and transmitter, the signal flow of decimation-in-time for receiver can be transposed to decimation-in-frequency (DIF) for transmitter. Fig. 5.4 shows the signal flows of 4-point and 8-point DIF-FFT architecture. We can see the modularity discussed in receiver is also inherited in transmitter after the transpose. The inputs and outputs relationship for 4-point DIF-FFT from X_i to Y_j, where i,j=1,2,3,4, can be expressed by Eqns (5.1)-(5.4).

$$X_1 = Y_1 e^{j0^\circ} + Y_2 e^{j0^\circ} + Y_3 e^{j0^\circ} + Y_4 e^{j0^\circ} \quad (5.1)$$

$$X_2 = Y_1 e^{j0^\circ} + Y_2 e^{j90^\circ} + Y_3 e^{j180^\circ} + Y_4 e^{j270^\circ} \quad (5.2)$$

$$X_3 = Y_1 e^{j0^\circ} + Y_2 e^{j180^\circ} + Y_3 e^{j0^\circ} + Y_4 e^{j180^\circ} \quad (5.3)$$

$$X_4 = Y_1 e^{j0^\circ} + Y_2 e^{j270^\circ} + Y_3 e^{j180^\circ} + Y_4 e^{j90^\circ} \quad (5.4)$$

The spatial angles change from $+30°$, $\pm 90°$ and $-30°$ as the receiver.

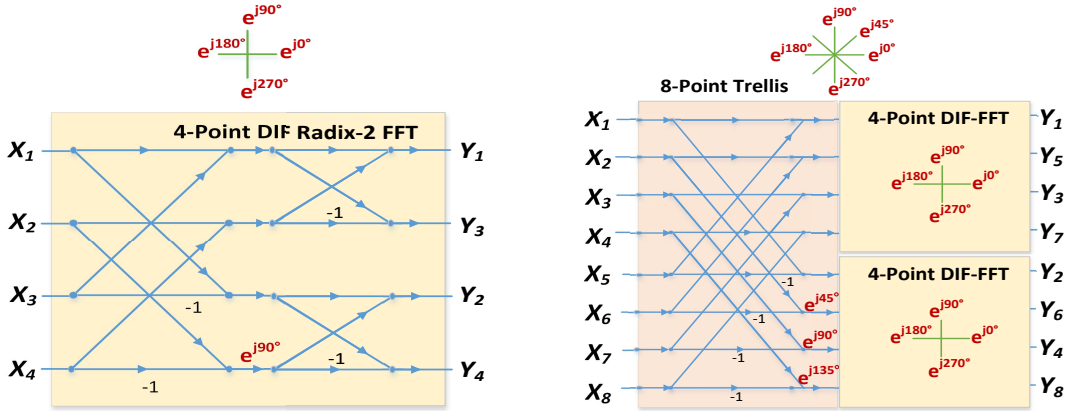

(a) (b)

Figure 5.4: (a) 4-point, and (b) 8-point DIF FFT

5.2.3 Steerability

We then add progressive phase shifter before the antenna for each path as shown in Fig. 5.5. In this architecture, the progressive phase difference from each input X_i to four outputs change to be $\phi + 90°(i-1)$, where $i = 1, 2, 3, 4$. The four eigen-beams with progressive phase difference of $0°$, $90°$, $180°$ and $270°$ are rotated into those of $0° + \phi$, $90° + \phi$, $180° + \phi$ and $270° + \phi$, while keeping the orthogonality. The relationship from X_i to Y'_j is given by

$$X_1 = Y'_1 e^{j\phi} + Y'_2 e^{j2\phi} + Y'_3 e^{j3\phi} + Y'_4 e^{j4\phi} \quad (5.5)$$

$$X_2 = Y'_1 e^{j(0°+\phi)} + Y'_2 e^{j(90°+2\phi)} + Y'_3 e^{j(180°+3\phi)} + Y'_4 e^{j(270°+4\phi)} \quad (5.6)$$

$$X_3 = Y'_1 e^{j(0°+\phi)} + Y'_2 e^{j(180°+2\phi)} + Y'_3 e^{j(0°+3\phi)} + Y'_4 e^{j(180°+4\phi)} \quad (5.7)$$

$$X_4 = Y'_1 e^{j(0°+\phi)} + Y'_2 e^{j(270°+2\phi)} + Y'_3 e^{j(180°+3\phi)} + Y'_4 e^{j(90°+4\phi)} \quad (5.8)$$

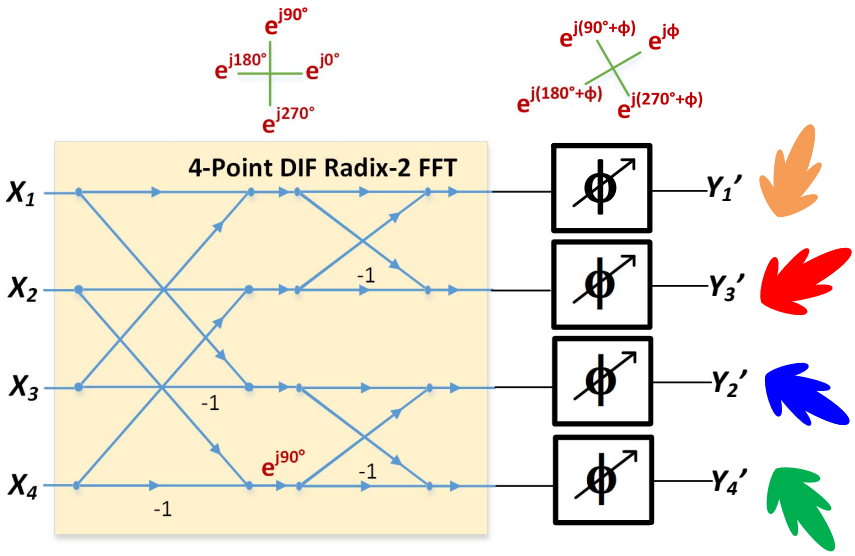

Figure 5.5: Steerable 4-point FFT

The associated four beam directions are changed to be arcsin $\frac{\phi}{180°}$, arcsin $\frac{\phi+90°}{180°}$, arcsin $\frac{\phi+180°}{180°}$ and arcsin $\frac{\phi+270°}{180°}$ after phase shifting. The peak of each one beam is at the locations of nulls of the other three, making the four beams are always independent of each other during steering. This is what are expected by MIMO,as indicated in chapter 3, that independent channels (or beams) are required to maximize the diversity gain and multiplexing gain. It should be noticed that our architecture use much less phase shifters to steer the beams compared to conventional way of phased array. For example, our architecture only needs four variable phase shifters to four beams steerability (Note: 4-point FFT is explicit-shiftless), but conventional phased array needs 16 phase shifters. Conventional phased array uses more phase shifters flexibly to steer each beam to arbitrary direction, which however, is unnecessary for from MIMO perspective. Our architecture, which is much more power-area efficient, can steer the independent multi-beams all over the space to satisfy the requirements by MIMO.

5.2.4 Proposed Architecture

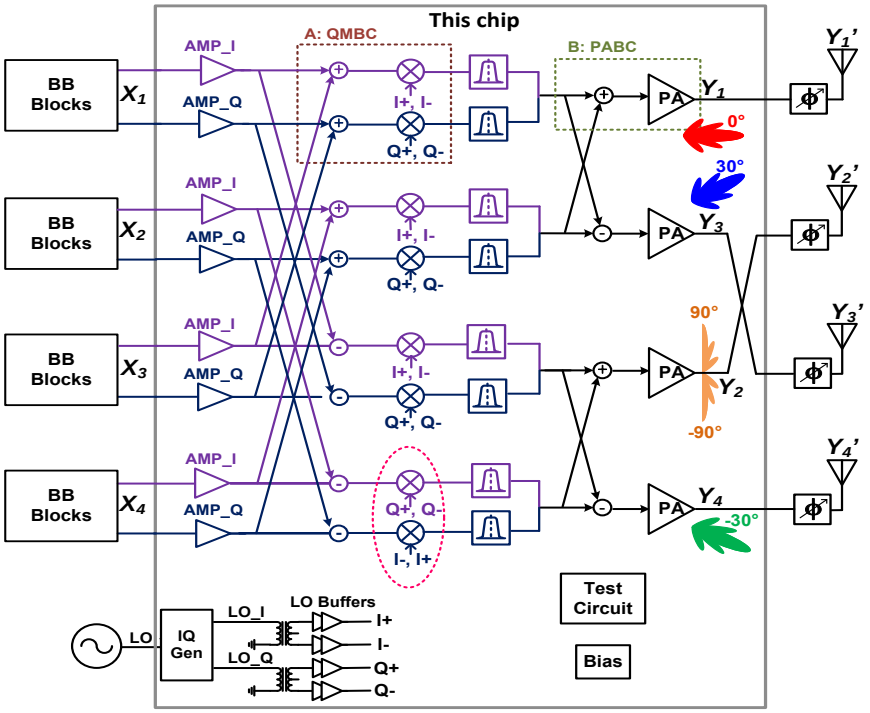

Figure 5.6: Proposed steerable FFT based four-channel four-beam transmitter

Fig. 5.6 exhibits our proposed steerable FFT based four-channel four beam transmitter, consisting of 4-point DIF-FFT and adjustable phase shifters as mentioned above. Similar as receiver architecture, the 4-point DIF-FFT is also implemented by reusing pre-existing transmitter components. Each baseband input is replicated into two paths in voltage domain, then these signals are pairwise $(1 : \pm 1)$ combined [added $(0°)$ or subtracted $(180°)$] in the current domain before up-conversion. In particular, at baseband X_1 and X_3 forms a pair. Each of the information X_1 and X_3 is replicated into two copies, and each copy from X_1 and X_3 are combined at the channels associated with X_1 and X_3. Similarly for the baseband pair of X_2 and X_4. The IF signals are then up-converted to RF before final stage signal replication and combination are done. The 4^{th} channel the I+I- and Q+Q- are replaced by Q+Q- and I-I+ which is a phase rotation of $90°$. The replications at RF are also implemented in voltage domain, and additions and subtractions are accomplished in the current domain.

The steerable phase shifters are implemented off-chip, which can be integrated in the future. Because of active implementation by reusing pre-existing transmitter components, each of the independent information from based band, X_i, where $i = 1, 2, 3, 4$, is replicated and phase shifted in four paths, arriving at Y_1, Y_2, Y_3 and Y_4. They are followed by phase shifters, resulting in Y_1', Y_2', Y_3' and Y_4'. The four beams at ports of either $Y_i s$ or $Y_i' s$ are independent respectively.

5.3 Circuit

This section overview the circuit for our proposed architecture.

5.3.1 Baseband amplifier

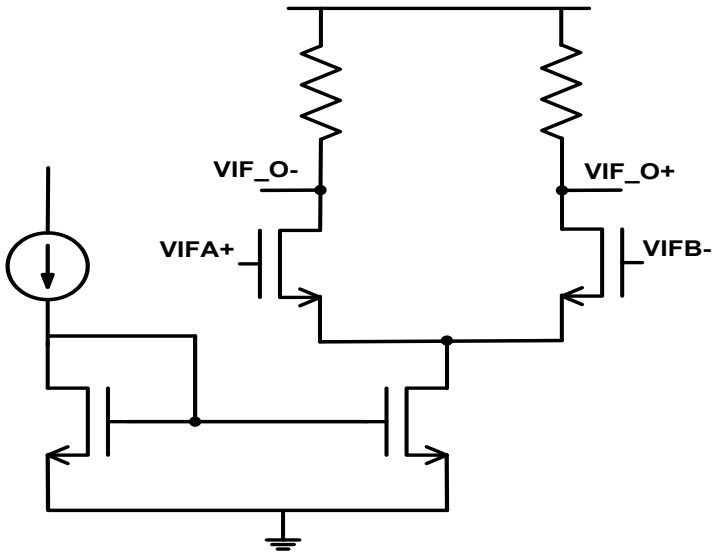

Figure 5.7: Baseband Amplifier

The baseband amplifier as shown in Fig. 5.7 is common source differential pair with resistor load. It provides gain for the transmitter path before mixer. The differential 50ohm resistors (not shown) are placed on-chip for testing. A large off-chip capacitor is connected to each input of the differential pair to feed in the signal.

5.3.2 Quadrature Up-conversion Mixer with Built-in Combination (QUMBC)

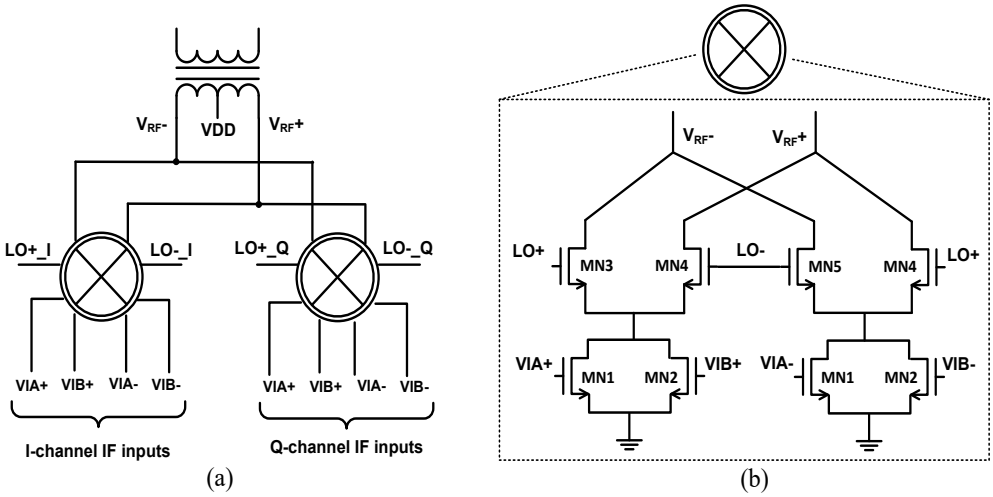

Figure 5.8: QUMBC

The Fig. 5.8 (a) shows the architecture of transformer based quadrature upconversion mixer with built-in combination. It consists of I and Q QUMBC core in Fig. 5.8 (b), and transformer at output. Each QUMBC core is constructed based on Gilbert mixer. Each tail is made up with two transistors in parallel, where the gates of two transistor are connected to different paths for $(1:1)$ combination. Similar as the receiver, the $(1:-1)$ combination can be achieved by swapping the differential inputs of another pair. The center tap of the primary is connected to power supply to feed power to QUMBC cores. It should be noticed that

5.3.3 Power Amplifier with Built-in Combination (PABC)

The PABC is based on two-stage transformer based two-stage class-AB power amplifier. The block diagram is shown in Fig. 5.9. It has driver stage, power stage, input matching network (MN), interstage MN and output MN.

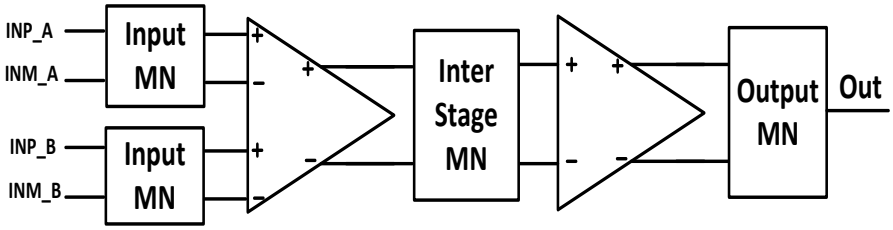

Figure 5.9: Block diagram of PABC

The power stage is to provide maximum power to the load. Class-AB mode is adopted to achieve good linearity and efficiency. Fig. 5.10 shows the circuit implementation. In order to increase the output power and/or reduce the output matching network loss, 1.8 supply voltage is feed through the center tap of the transformer into the power stage core. Thick oxide transistor are used for cascode to withstand high supply voltage and output swing, and thus provide high output power. The thin oxide transistor is used for common source stage to increase the trans-conductance g_m and characteristic frequency f_T.

The driver stage can increase overall gain, and drive large input capacitance of the power stage. The circuit in Fig. 5.10 is implemented as differential cascode. With 1 volt power supply feed through center tap of transformer, all transistors are core devices to achieve larger gain and higher characteristic frequency (f_T). Self biased configuration for cascode transistors alleviate the issue of oxide breakdown and hot carrier effect. High RC network at driver inputs provides proper DC bias, and feed in RF signals from QUMBC.

The output of the power stage are power matched to maximize the output power. C-C output matching network is decided based on load-pull simulation. The inter-stage matching network is implemented in the way of conjugate match to maximize the gain. A capacitor is connected in series to the power stage input to resonate out the inductance seen from the driver stage output.

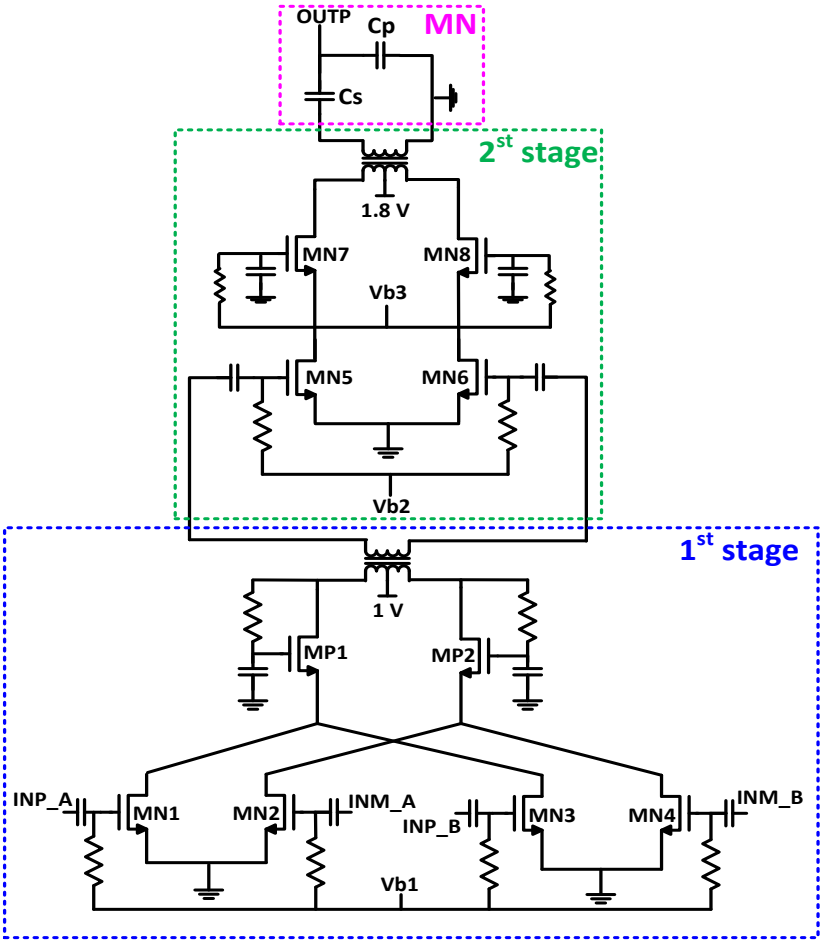

Figure 5.10: PABC

5.4 Floorplan and Layout

The chip dimension is $1.92mm \times 1.39mm = 2.67mm^2$, where each channel occupies $0.67mm^2$ on average. The chip size includes multiple phases LO routing, PAD, ESD and other auxiliary circuit. The floorplan inherits the concept of FFT based RX design.

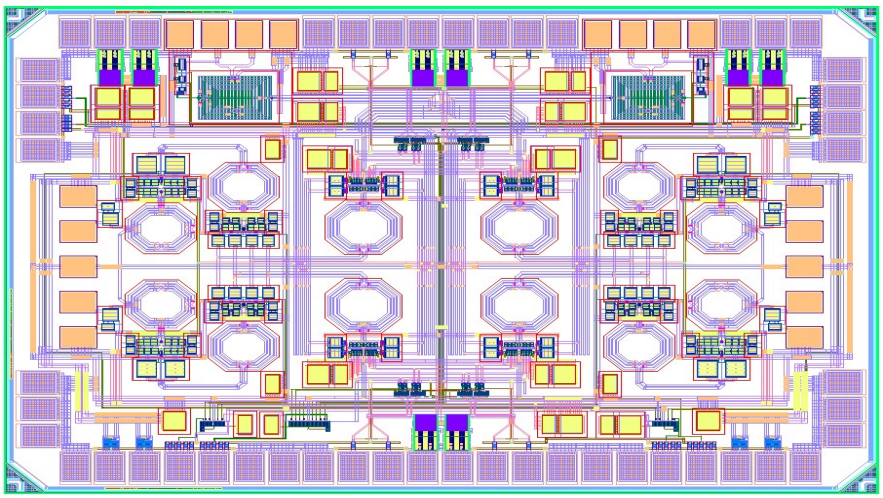

Figure 5.11: Layout of 4-channel 4-beam transmitter

5.5 Conclusion

This section presents steerable DIF-FFT based four-channel four-beam transmitter design. The way of simultaneous steerability with independent multiple beams make the architecture extremely suitable for MIMO applications. The system architecture is presented, and circuit details are elaborated.

Chapter 6

Research contributions

This thesis presents three innovative work to address existing problems of RF/analog beamforming. The designs include RF receiver, local oscillator and RF transmitter.

The first work is a RF/analog DIT-FFT based multi-channel multi-beam receiver. Different from conventional way of Butler matrix that is physically large and directly degrades receiver performance, the proposed architecture reuses pre-existing receiver components to generate simultaneously multiple beams. The partial spatial filtering property before final stage combination further improves the system linearity. The proposed architecture can be extended for more channels and more beams.

The second work is injection locked oscillator based channelized wideband phased array receiver. Instead of using true time delay, the proposed architecture reduces the beam squinting error within tolerance by channelization: the phase deltas among different harmonic outputs reduces the beam squinting by the number of the channels. The proposed architecture features simultaneous spectral and spatial filtering to reduce ADC dynamic range requirement. In addition, different from the conventional way of putting true time delay in signal path, this is the first wideband phased array that places delay/phase element in LO path, which only indirectly impact receiver performance.

The third work is a steerable DIF-FFT based multi-beam transmitter. The idea is placing one phase shifter at RF for each channel, and it can steer all beams simultaneously while keep their relative orthogonality. This architecture can be used to exploit the full spatial degree of freedom in portable environment.

As the data rate requirement goes up every year, wideband and multi-beam are the

popular ways to copy with the issue by exploiting more spectral and spatial degree of freedom. The architectures proposed in this thesis provide promisingly small size and low power solutions to resolve existing issues in wideband and multi-beam transceivers.

References

[1] B. P. Lathi and Zhi Ding. *Modern Digital and Analog Communication Systems*. Oxford, 2009.

[2] David Su. Wireless trends. [Online] http://www.maltiel-consulting.com/ISSCC-2013-Wirelessl-Trends.html.

[3] Da-Shan Shiu, Gerard J. Foschini, Michael J. Gans, and Joseph M. Kahn. Fading correlation and its effect on the capacity of multielement antenna systems. *IEEE Transactions on Communications*, 48:502 – 513, Mar. 2000.

[4] Robert H. Walden. Analog-to-digital converter survey and analysis. *IEEE Journal on Selected Areas in Communications*, 17:539 – 550, Apr. 1999.

[5] Rahim Bagheri, Ahmad Mirzaei, Saeed Chehrazi, Mohammad E. Heidari, Minjae Lee, Mohyee Mikhemar, Wai Tang, , and Asad A. Abidi. An 800-mhz6-ghz software-defined wireless receiver in 90-nm cmos. *IEEE Journal of Solid-State Circuits*, 41:2860 – 2876, Dec. 2006.

[6] Bodhisatwa Sadhu, Martin Sturm, Brian Sadler, and Ramesh Harjani. Analysis and design of a 5gs/s analog charge-domain fft for an sdr front-end in 65nm cmos. *IEEE Journal of Solid-State Circuits*, 48:39 – 42, May 2013.

[7] Hundo Shin and Ramesh Harjani. Low-power wideband analog channelization filter bank using passive polyphase-fft techniques. *IEEE Journal of Solid-State Circuits*, 52:1753 – 1767, July 2017.

[8] Pradeep Kotte Prakasam, Mandar Kulkarni, Xi Chen, Zhuizhuan Yu, Sebastian Hoyos, Jose Silva-Martinez, and Edgar Sanchez-Sinencio. Applications of multipath

transform-domain charge-sampling wide-band receivers. *IEEE Transactions on Circuits and Systems II: Express Briefs*, 55:309 – 313, Apr. 2008.

[9] Vineet Singh, Travis Forbes, Wei-Gi Ho, Jaegan Ko, and Ranjit Gharpurey. A 16-band channelizer employing harmonic rejection mixers with enhanced image rejection. In *IEEE Custom Integrated Circuits Conference*, pages 1 – 4, Sep. 2014.

[10] Constantine A. Balanis. *Antenna theory: analysis and design.* Wiley Interscience, 2005.

[11] Xiang Guan, Hossein Hashemi, and Ali Hajimiri. A fully integrated 24-ghz eight-element phased-array receiver in silicon. *IEEE Journal of Solid-State Circuits*, 39:2311 – 2320, Dec. 2004.

[12] James F. Buckwalter, Aydin Babakhani, Abbas Komijani, and Ali Hajimiri. An integrated subharmonic coupled-oscillator scheme for a 60-ghz phased-array transmitter. *IEEE Transactions on Microwave Theory and Techniques*, 54:4271 – 4280, Dec. 2006.

[13] Ta-Shun Chu, Jonathan Roderick, and Hossein Hashemi. A 4-channel UWB beamformer in 0.13m CMOS using a path-sharing true-time-delay architecture. In *IEEE International Solid State Circuits Conference*, pages 426 – 613, Feb. 2007.

[14] Arun Natarajan, Brian Floyd, and Ali Hajimiri. A bidirectional rf-combining 60ghz phased-array front-end. In *IEEE International Solid State Circuits Conference*, pages 202 – 597, Feb. 2007.

[15] R.B. Dome. Wideband audio phase-shift networks. 19:112–115, Dec. 1946.

[16] James Buckwalter and Ali Hajimiri. An active analog delay and the delay reference loop. In *IEEE Radio Frequency Integrated Circuits Symposium*, pages 17–20, Jun. 2004.

[17] Byung-Wook Min and Gabriel M. Rebeiz. Ka-band bicmos 4-bit phase shifter with integrated lna for phased array t/r modules. In *IEEE International Microwave Symposium*, pages 479 – 482, June 2007.

[18] Cameron T. Charles and David J. Allstot. A 2-ghz integrated cmos reflective-type phase shifter with 675 control range. In *IEEE International Symposium on Circuits and Systems*, May 2006.

[19] Hossein Zarei and David J. Allstot. A low-loss phase shifter in 180 nm cmos for multiple-antenna receivers. In *IEEE International Solid State Circuits Conference*, pages 392 – 534, Feb. 2004.

[20] Kwang-Jin Koh and Gabriel M. Rebeiz. 0.13-m CMOS phase shifters for X-, Ku-, and K-band phased arrays. *IEEE Journal of Solid-State Circuits*, 42:2535 – 2546, Nov. 2007.

[21] Hua Wang and Ali Hajimiri. A wideband cmos linear digital phase rotator. In *IEEE Custom Integrated Circuits Conference*, pages 671–674, Apr. 2007.

[22] David Tse and Pramod Viswanath. *Fundamentals of Wireless Communication.* Cambridge, 2005.

[23] Akbar M. Sayeed. Deconstructing multiantenna fading channels. *IEEE Transactions on Signal Processing*, 50:2563 – 2579, Nov. 2002.

[24] Ali Hajimiri, Hossein Hashemi, Arun Natarajan, Xiang Guan, and Abbas Komijani. Integrated phased array systems in silicon. *Proceedings of the IEEE*, 93:1637 – 1655, Sep. 2005.

[25] Qingrui Meng and Ramesh Harjani. An easily extendable FFT based four-channel, four-beam receiver with progressive partial spatial filtering in 65nm. In *IEEE European Solid-State Circuits Conference(ESSCIRC)*, pages 359–362, Sep. 2016.

[26] Salvador H. Talisa, Kenneth W. O'Haver, Thomas M. Comberiate, Matthew D. Sharp, and Oscar F. Somerlock. Benefits of digital phased array radars. *Proceedings of the IEEE*, 104:530 – 543, Mar. 2016.

[27] Sanggeun Jeon, Yu-Jiu Wang, Hua Wang, Florian Bohn, Arun Natarajan, Aydin Babakhani, and Ali Hajimiri. A scalable 6-to-18 GHz concurrent dual-band quadbeam phased-array receiver in CMOS. *IEEE Journal of Solid-State Circuits*, 58:2660–2673, Dec. 2008.

[28] Bon-Hyun Ku, Ozgur Inac, Michael Chang, and Gabriel M. Rebeiz. A 75-85GHz flip-chip phased array RFIC with simultaneous 8-transmit and 8-receive paths for automotive radar applications. In *IEEE Radio Frequency Integrated Circuits Symposium*, pages 1–4, June 2013.

[29] Jesse Butler and Ralph Lowe. Beam forming matrix simplifies design of electronically scanned antennas. *Electronic Design*, pages 170–173, Apr. 1961.

[30] Mohamed Elkhouly, Mao Yanfei, Chafik Meliani, Frank Ellinger, and J. Christoph Scheytt. A 220-245 GHz switched beam Butler matrix in 0.13 μm SiGe BiCMOS technology. In *IEEE Bipolar/BiCMOS Circuits and Technology Meeting*, pages 119–122, Sep. 2013.

[31] Harish Krishnaswamy and Hossein Hashemi. A 4-channel, 4-beam, 24-26GHz, spatio-temporal RAKE radar transceiver in 90nm CMOS for vehicular radar applications. In *IEEE International Solid State Circuits Conference*, pages 214–215, Feb. 2010.

[32] Amro Tork and Arun Natarajan. Reconfigurable X-Band 4x4 Butler array in 32nm CMOS SOI for angle-reject arrays. In *IEEE MTT-S International Microwave Symposium*, pages 1–4, May 2016.

[33] M. Bona, L. Manholm, J.P. Starski, and B. Svensson. Low-loss compact Butler matrix for a microstrip antenna. *IEEE Transactions on Microwave Theory and Techniques*, 50:2069–2075, Sep. 2002.

[34] Mourad Nedil, Tayeb A. Denidni, and Larbi Talbi. Novel butler matrix using CPW multilayer technology. *IEEE Transactions on Microwave Theory and Techniques*, 54:499 – 507, Jan. 2006.

[35] Berke Cetinoneri, Yusuf A. Atesal, Jeong-Geun Kim, and Gabriel M. Rebeiz. CMOS 4x4 and 8x8 Butler matrices. In *IEEE International Microwave Symposium*, pages 69–72, May 2010.

[36] Berke Cetinoneri, Yusuf A. Atesal, and Gabriel M. Rebeiz. An 8x8 Butler matrix in 0.13-μm CMOS for 5-6-GHz multibeam applications. *IEEE Transactions on Microwave Theory and Techniques*, 59:295301, Feb. 2011.

[37] Ting-Yueh Chin, Sheng-Fuh Chang, Chia-Chan Chang, and Jen-Chieh Wu. A 24-GHz CMOS Butler matrix MMIC for multi-beam smart antenna systems. In *IEEE Radio Frequency Integrated Circuits Symposium*, pages 633–636, Jun. 2008.

[38] Chia-Chan Chang, Ting-Yueh Chin, Jen-Chieh Wu, and Sheng-Fuh Chang. Novel design of a 2.5-GHz fully integrated CMOS Butler matrix for smart-antenna systems. *IEEE Transactions on Microwave Theory and Techniques*, 56:1757–1763, Aug. 2008.

[39] Taiyun Chi Jong Seok Park and Hua Wang. An ultra-broadband compact mm-wave Butler matrix in CMOS for array-based MIMO systems. In *IEEE Custom Integrated Circuits Conference*, Sep. 2013.

[40] Fei Wang and Hua Wang. A broadband compact low-loss 4x4 Butler matrix in CMOS with stacked transformer based quadrature couplers. In *IEEE MTT-S International Microwave Symposium*, pages 1–4, May 2016.

[41] Thomas H. Cormen, Charles E. Leiserson, Ronald L. Rivest, and Clifford Stein. *Introduction to Algorithms*. The MIT Press, 2009.

[42] J. Paul Shelton. Fast Fourier transforms and Butler matrices. *Proceedings of The IEEE*, 56:350, Mar. 1968.

[43] Francois Rivet, Yann Deval, Jean-Baptiste Begueret, Dominique Dallet, and Philippe Cathelin andDidier Belot. The experimental demonstration of a SASP-based full software radio receiver. *IEEE Journal of Solid-State Circuits*, 45:979–988, Apr. 2010.

[44] Bodhisatwa Sadhu, Martin Sturm, Brian M. Sadler, and Ramesh Harjani. Analysis and design of a 5 GS/s analog charge-domain FFT for an SDR front-end in 65 nm CMOS. *IEEE Journal of Solid-State Circuits*, 48:1199–1211, Apr. 2013.

[45] Robert J. Mailloux. *Phased Array Antenna Handbook*. Artech House, 2005.

[46] John R. Long. Monolithic transformers for silicon RF IC design. *IEEE Journal of Solid-State Circuits*, 35:1368 – 1382, Sep. 2000.

[47] B. Razavi. *RF Microelectronics*. Prentice Hall, 2012.

[48] Harish Krishnaswamy. *Architecture and integrated circuits for RF and mm-wave multiple-antenna systems on silicon*. PhD thesis, University of Southern California, May 2009.

[49] Ta-Shun Chu, Jonathan Roderick, and Hossein Hashemi. A 4-channel UWB beamformer in 0.13-μm CMOS using a path-sharing true-time-delay architecture. In *IEEE International Solid-State Circuits Conference*, pages 426–613, Feb. 2007.

[50] Yahya Tousi and Alberto Valdes-Garcia. A Ka-band digitally-controlled phase shifter with sub-degree phase precision. In *IEEE Radio Frequency Integrated Circuits Symposium*, pages 356–359, May 2016.

[51] James Buckwalter and Ali Hajimir. An active analog delay and the delay reference loop. In *IEEE Radio Frequency Integrated Circuits Symposium*, pages 17–20, June 2004.

[52] Seyed Kasra Garakoui, Eric A. M. Klumperink, Bram Nauta, and Frank F. E Van Vliet. A 1-to-2.5 GHz phased-array IC based on gm-RC all-pass time-delay cells. In *IEEE International Solid-State Circuits Conference*, pages 80–82, Feb. 2012.

[53] Hao Li; Chris M. Thomas; Gert Cauwenberghs; Lawrence E. Larson. A BiCMOS 50 MHz input bandwidth, 1-to-16 channelizer optimized for low power analog signal classification. In *IEEE Bipolar/BiCMOS Circuits and Technology Meeting*, pages 76–79, Sep 2014.

[54] Mohammad Elbadry, Bodhisatwa Sadhu, Joe X. Qiu, and Ramesh Harjani. Dual-channel injection-locked quadrature LO generation for a 4-GHz instantaneous bandwidth receiver at 21-GHz center frequency. *IEEE Transactions on Microwave Theory and Techniques*, 61:1186 – 1199, Mar. 2013.

[55] Amir Ghaffari, Eric A. M. Klumperink, Frank van Vliet, and Bram Nauta. A 4-element phased-array system with simultaneous spatial- and frequency-domain filtering at the antenna inputs. In *IEEE Journal of Solid-State Circuits*, pages 1303 – 1316, Apr. 2014.

[56] Naoki Oshima, Masaki Kitsunezuka, Kenta Tsukamoto, and Kazuaki Kunihiro. A 30-MHz-to-3-GHz CMOS array receiver with frequency and spatial interference filtering for adaptive antenna systems. In *IEEE Radio Frequency Integrated Circuits Symposium*, pages 326–329, May 2016.

[57] J. Fink and F. K. Jondral. Comparison of OFDM radar and chirp sequence radar. In *2015 16th International Radar Symposium (IRS)*, pages 315–320, June 2015.

[58] Sachin Kalia, Satwik A. Patnaik, Bodhisatwa Sadhu, Martin Sturm, Mohammad Elbadry, and Ramesh Harjani. Multi-beam spatio-spectral beamforming receiver for wideband phased arrays. *IEEE Transactions on Circuits and Systems I*, 60:2018 – 2029, Aug. 2013.

[59] Najme Ebrahimi, Po-Yi Wu, Mahdi Bagheri, and James F. Buckwalter. A 71-86GHz phased array transceiver using wideband injection-locked oscillator phase shifters. *IEEE Transactions on Microwave Theory and Techniques*, 65:346 – 361, Feb. 2017.

[60] Sachin Kalia, Mohammad Elbadry, Bodhisatwa Sadhu, Satwik Patnaik, Joe Qiu, and Ramesh Harjani. A simple, unified phase noise model for injection-locked oscillators. In *IEEE Radio Frequency Integrated Circuits Symposium*, pages 1–4, June 2011.

[61] Sanggeun Jeon, Yu-Jiu Wang, Hua Wang, Florian Bohn, Arun Natarajan, Aydin Babakhani, and Ali Hajimiri. A scalable 6-to-18 GHz concurrent dual-band quad-beam phased-array receiver in CMOS. In *IEEE Journal of Solid-State Circuits*, pages 2660 – 2673, Dec. 2008.

[62] Michiel C. M. Soer, Eric A. M. Klumperink, Bram Nauta, and Frank E. van Vliet. A 1.0-to-4.0GHz 65nm CMOS four-element beamforming receiver using a switched-capacitor vector modulator with approximate sine weighting via charge redistribution. In *IEEE International Solid State Circuits Conference*, pages 64 – 66, Apr. 2011.